JAERI-M
88-201

PROGRESS REPORT ON SAFETY RESEARCH OF HIGH-LEVEL WASTE MANAGEMENT FOR THE PERIOD APRIL 1987 TO MARCH 1988

October 1988

(Eds.) Haruto NAKAMURA and Shingo TASHIRO

日本原子力研究所
Japan Atomic Energy Research Institute

JAERI-Mレポートは，日本原子力研究所が不定期に公刊している研究報告書です。
入手の問合わせは，日本原子力研究所技術情報部情報資料課（〒319－11茨城県那珂郡東海村）あて，お申しこしください。なお，このほかに財団法人原子力弘済会資料センター（〒319-11茨城県那珂郡東海村日本原子力研究所内）で複写による実費頒布をおこなっております。

JAERI-M reports are issued irregularly.
Inquiries about availability of the reports should be addressed to Information Division, Department of Technical Information, Japan Atomic Energy Research Institute, Tokai-mura, Naka-gun, Ibaraki-ken 319-11, Japan.

編集兼発行　日本原子力研究所
印　　刷　日立高速印刷株式会社

JAERI-M 88-201

Progress Report on Safety Research of High-Level Waste Management for the Period April 1987 to March 1988

(Eds.) Haruto NAKAMURA and Shingo TASHIRO

Department of Environmental Safety Research
Tokai Research Establishment
Japan Atomic Energy Research Institute
Tokai-mura, Naka-gun, Ibaraki-ken

(Received September 20, 1988)

Researches on high-level waste management at the High Level Waste Management Laboratory and the Waste Safety Testing Facility Operation Division of the Japan Atomic Energy Research Institute in the fiscal year of 1987 are reviewed in the three sections of the report.

The topics are as follows:

1) On performance and durability of waste forms and engineered barrier materials, accelerated alpha radiation stability of glass form and Synroc has been investigated and stress corrosion cracking of canister materials was examined under simulated conditions.

2) Sorption of ^{237}Np on granite samples and behavior of iron during weathering of granites were studied with respect to safety evaluation for geological disposal.

3) Actual waste was transported from the Tokai Reprocessing Plant and hot operation using the actual waste was initiated at WASTEF.

Keywords: High-level radioactive wastes, Glass, Synroc, Radiation Effect, Leaching, Neptinium 238, Plutonium 238, Curium 244, Stress Corrosion, Granites, Natural Analogue, Safety Analysis, Hot Cells

JAERI－M 88－201

高レベル廃棄物処理処分の安全性研究に関する昭和62年度報告書

日本原子力研究所東海研究所環境安全研究部
（編）　中村　治人・田代　晋吾

（1988年9月20日受理）

原研の高レベル研及びＷＡＳＴＥＦ管理室で昭和62年度に実施した高レベル廃棄物処理処分に関する研究を3章に分けてまとめたものである。

そのトピックスは次の通り。

1）固化体及び人工バリア材の性能と耐久性については，ガラス固化体とシンロックのα加速試験が実施され，キャニスタ材の応力腐食割れが模擬的条件下で調べられている。

2）地層処分の安全性評価については，^{237}Npの花崗岩への吸着及び花崗岩風化中の鉄の挙動が研究された。

3）ＷＡＳＴＥＦでは，東海再処理工場から運搬した実廃棄物を用いたホット試験が開始された。

東海研究所：〒319-11 茨城県那珂郡東海村白方字白根2－4

Contents

Introduction 1
1. Waste Forms and Engineered Barrier Materials 2
1.1 Glass form 3
(1) Continuous-flow leach tests of simulated high-level waste glass 3
(2) Leaching behavior of ^{238}Pu from the nuclear waste glass 7
(3) Accelerated alpha radiation stability test (AARST) under beta and gamma irradiation 11
(4) He release behavior from Cm-doped glass specimen 14
(5) Alpha- and gamma-radioactivity measurements of neptunium-237 in leachants for waste glass leach tests 17
(6) Removal of fluorine from Teflon(R) RFA containers by the MCC cleaning procedure 20
1.2 SYNROC 25
(1) Identification of the surface precipitates produced in hydrothermal dissolution of SYNROC 25
(2) Fabrication of curium-doped SYNROC 32
1.3 Container 39
(1) Slow Strain Rate Stress-corrosion Test under gamma-ray irradiation for container materials 39
(2) Experiment to evaluate integrity of high-level waste canister in the high-pressure water tank 45
2. Safety Evaluation for Geological Disposal 50
2.1 Nuclide migration and retardation in rocks 51
(1) Porosities and diffusion coefficients of iodide anion in rocks 51
(2) Sorption of ^{237}Np on thin sections of granite 55
(3) Behavior of iron during weathering of a granitic rock 61
(4) Field test (Borehole radar investigation) 64
(5) Consideration of radionuclides migration model based on field studies at Chalk River 67
2.2 Natural analogue 69
(1) Infrared microspectroscopy of minerals as a tool for analyzing water-rock interactions 69

2.3 Safety assessment 76
(1) Development safety assessment scenario for geological disposal 76
(2) Model for safety assessment 79
3. Hot Operation at WASTEF 82
(1) Transport of actual high-level liquid waste to WASTEF 83
(2) Test plan with actual wastes 86

目　　次

まえがき …… 1
1. 廃棄物固化体と工学バリア材料 …… 2
1.1 ガラス固化体 …… 3
(1) 模擬高レベル廃棄物ガラス固化体の低流速浸出試験 …… 3
(2) 核廃棄物からのＰｕの浸出挙動 …… 7
(3) β，γ線照射下でのアルファ加速試験 …… 11
(4) Ｃｍ添加ガラス試料からのHe 浸出挙動 …… 14
(5) 廃棄物ガラス固化体浸出液中のNp－237のα，β放射能測定 …… 17
(6) ＭＣＣ洗浄法によるテフロン®ＲＦＡ容器からの残留ふっ素の除去 …… 20
1.2 シンロック …… 25
(1) シンロックの熱水溶解で形成された表面析出物の同定 …… 25
(2) Ｃｍ添加シンロックの製作 …… 32
1.3 容器 …… 39
(1) 容器材のγ線照射下の低歪速度応力腐蝕割れ試験 …… 39
(2) 高圧下における高レベル廃棄物模擬キャニスター健全性評価試験 …… 45
2. 地層処分の安全性評価 …… 50
2.1 岩石中の核種移行と遅延 …… 51
(1) 岩石中の間隙率とよう素の拡散係数 …… 51
(2) 花崗岩薄片へのＮｐ－237の収着 …… 55
(3) 花崗岩の風化過程における鉄の挙動 …… 61
(4) フィールド試験（ボアホールレーダー実験） …… 64
(5) チョークリバーにおける核種移行フィールド試験結果の考察 …… 67
2.2 ナチュラルアナログ …… 69
(1) 顕微赤外分光法による岩石－水反応の解析 …… 69
2.3 安全評価モデル …… 76
(1) 地層処分評価シナリオの開発 …… 76
(2) 安全評価モデル …… 79
3. ＷＡＳＴＥＦにおけるホット運転 …… 82
(1) 高レベル実廃液のＷＡＳＴＥＦへの輸送 …… 83
(2) 実廃液試験計画 …… 86

Introduction

S. Tashiro

In regard to the management of high level radioactive wastes Japan has made rapid progress on the industrial scale activities in the past year. The Power Reactor and Nuclear Fuel Development Corporation (PNC) finished the safety examination of the pilot plant for the vitrification of HLW generated at the Tokai reprocessing plant and started the construction. The safety examination advisory committee of the Government started discussions on the specifications of returnable wastes from oversea reprocessing plants. The Japan Nuclear Fuel Service Co., Ltd. (JNFS) has actually designed a storage facility for the returnable HLW packages and a vitrification plant attached to a commercial reprocessing plant to be located at the Shimokita site.

The Japan Atomic Energy Research Institute (JAERI) has contributed to the industrial scale activities mainly from a safety aspect as well as has compiled basic data for the long term safe management.

This report summarizes the status and the results of studies performed the fiscal year 1987 in the High Level Radioactive Waste Management Laboratory and the WASTEF (Waste Safety Testing Facility) Operation Division of the Department of Environmental Safety Research, JAERI.

The report is devided into three chapters; waste forms and engineered barrier materials, safety evaluation for geological disposal, hot operation at WASTEF.

The first chapter describes studies on glass forms and Synroc, and also gives a result of SSC examination of canister materials in disposal conditions.

The second chapter includes reports on behavior of ^{237}Np and iron in rock mass, bore hole radar techniques for fracture location, natural analogue and safety assessment methodology.

Regarding WASTEF work, items supporting the hot examinations are reported in the third chapter.

The relative annual reports have been previously pressed in the following numbers; JAERI-M 82-145, 83-076, 84-133, 85-090, 86-131 and 87-131.

1. Waste Forms and Engineered Barrier Materials

T. Banba

In this chapter, the studies on glass waste forms, Synroc waste forms, and canisters are described. Examinations of glass waste form have been carried out in order to obtain the data on leachability and radiation durability. In the leaching experiments, the effect of leachant flow rate on the leachability, and leaching behavior of plutonium were examined. In the radiation durability tests using ^{244}Cm-doped glass, The radiation effects on the properties of waste glass under β-γ irradiation condition, and the release behavior of helium were discussed. The technique of radioactivity measurement of leached ^{237}Np and the cleaning technique of Teflon leach container were also introduced.

Cooperation between Japan and Australia on development of Synroc waste forms has progressed favorably. In the past year, the leaching tests of Synroc were carried out under the hydrothermal conditions and then the precipitates on the surface of specimen were examined. And the ^{244}Cm-doped Synroc was prepared for an accelerated α-radiation stability test.

In the safety evaluation tests of canister, The stress corrosion cracking (SCC) in simulated basalt groundwater under γ-ray irradiation condition was examined. And the effect of external static pressure by using the high-pressure water tank was discussed.

1.1 Glass form

(1) Continuous-flow leach tests of simulated high-level waste glass

H. Kamizono

Continuous-flow leach tests were carried out on simulated high-level waste glass in synthetic Grande Ronde basalt groundwater at 90°C for up to 200 days. The composition of the glass and the groundwater used in this study are given in Tables 1 and 2, respectively. Linear flow rate, which was defined as volume flow rate (m^3/day) divided by specimen surface area (m^2), was adjusted at four successive orders ranging from 5.5×10^{-6} to 5.5×10^{-3} m/day by using a MCC-4 type leaching apparatus [1]. This apparatus was improved in three ways as follows:

(i) The shape of the leach containers was designed to provide a high glass-surface-area to leachant-volume ratio of 1000 m^2/m^3. This required fifty pineapple-sliced glass specimens.

(ii) The leach containers and the connected leachant-inlets and -outlets were made of stainless steel capable of enduring gamma irradiation dose of more than 10^5R, which would be one possible experimental condition in the future work.

(iii) The movable parts of the apparatus which had to be handled throughout the experiments were designed to be remote-controlled so that leach tests could be operated under a high gamma irradiation field in the hot cell.

Here, only preliminary results obtained without gamma irradiation will be described, as reference data comparable with those from future experiments with irradiation. Figure 1 shows the relationship between the leach rates of silicon and the linear flow rates at a fixed leach time of 100 days. The solid line in the figure was obtained based on the assumption in which the leach rate of silicon (L(g/m^2day)) was expressed as,

$$L = S \times F, \qquad \cdots(1)$$

where S (g/m^3) is the apparent saturation concentration of silicon in leachant, and F (m/day) the linear flow rate. This assumption holds true if the leachant around the specimen has been nearly saturated by silicon leached out from the specimens before being replaced by freshly pumped leachant.

It should be mentioned that the leach rate of silicon approaches its maximum value of 10^{-1} g/m^{2}day when the linear flow rate is more than 10^{-3} m/day, which is calculated from a transformation of equation 1,

$$F = L/S. \qquad \ldots(2)$$

The results concluded that leach rate of silicon increased in proportion to linear flow rate up to 10^{-3} m/day when the leachant had completed its apparent saturation by silicon. Above the critical linear flow rate of 10^{-3} m/day, leach rate of silicon tended to be a constant value of about 10^{-1} g/m^{2}day.

As the next step, we plan to use about 1300 Ci of Cs-137 as a gamma emitter near the leach containers. It is expected that the gamma irradiation will change the leachant chemistry in such a way that nitric acid formed by the irradiation results in a stronger leachant acidity, thereby affecting leaching behavior. We will also carry out some experiments in the future by using radioactive glass incorporating actual high-level waste elements as the goal of the present series of experiments.

Ref. [1] T. Sagawa, JAERI-M 87-131

Table 1 Composition of the simulated high-level waste glass

Component	Content (wt%)	Reagent used
SiO_2	45.20	SiO_2
B_2O_3	13.90	$Na_2B_4O_7$
Al_2O_3	4.90	$Al(OH)_3$
Na_2O	9.80	Na_2CO_3
CaO	4.00	$CaCO_3$
Li_2O	2.00	Li_2CO_3
ZnO	2.50	ZnO
SeO_2	0.02	SeO_2
Rb_2O	0.12	$RbNO_3$
SrO	0.34	$Sr(NO_3)_2$
Y_2O_3	0.20	$Y(NO_3)_3 \cdot 6H_2O$
ZrO_2	1.65	$ZrO(NO_3)_2 \cdot 2H_2O$
MoO_3	1.74	$H_2MoO_4 \cdot H_2O$
MnO_2	0.21	$Mn(NO_3)_2 \cdot 6H_2O$
RuO_2	0.92	$RuCl_3 \cdot 3H_2O$
Ag_2O	0.03	$AgNO_3$
CdO	0.03	$Cd(NO_3)_2 \cdot 4H_2O$
SnO_2	0.02	$SnCl_4 \cdot 5H_2O$
Sb_2O_3	0.004	$SbCl_3$
TeO_2	0.23	TeO_2
Cs_2O	0.98	$CsNO_3$
BaO	0.63	$Ba(NO_3)_2$
La_2O_3	0.51	$La(NO_3)_3 \cdot 6H_2O$
CeO_2	1.91	$Ce(NO_3)_3 \cdot 6H_2O$
Pr_6O_{11}	0.50	$Pr(NO_3)_3 \cdot 6H_2O$
Nd_2O_3	1.65	$Nd(NO_3)_3 \cdot 6H_2O$
Sm_2O_3	0.33	$Sm(NO_3)_3 \cdot 6H_2O$
Eu_2O_3	0.06	$Eu(NO_3)_3 \cdot 6H_2O$
Gd_2O_3	0.04	$Gd(NO_3)_3 \cdot 6H_2O$
P_2O_5	0.30	H_3PO_4
Fe_2O_3	0.70	$Fe(NO_3)_3 \cdot 9H_2O$
Fe_2O_3	2.20	Fe_2O_3
Cr_2O_3	0.50	$Cr(NO_3)_3 \cdot 9H_2O$
NiO	0.40	$Ni(NO_3)_2 \cdot 6H_2O$
ZrO_2	1.00	ZrO_2
Ru	0.12	Ru
Rh	0.15	Rh
Pd	0.43	Pd
Total	100.00	

Table 2 Composition of the synthetic Grande Ronde basalt groundwater

Element	mg/ℓ
Na	355.0
K	4.34
Ca	2.77
Mg	0.00429
Si	30.1
F	27.3
Cl	306.0
SO_4	172.0

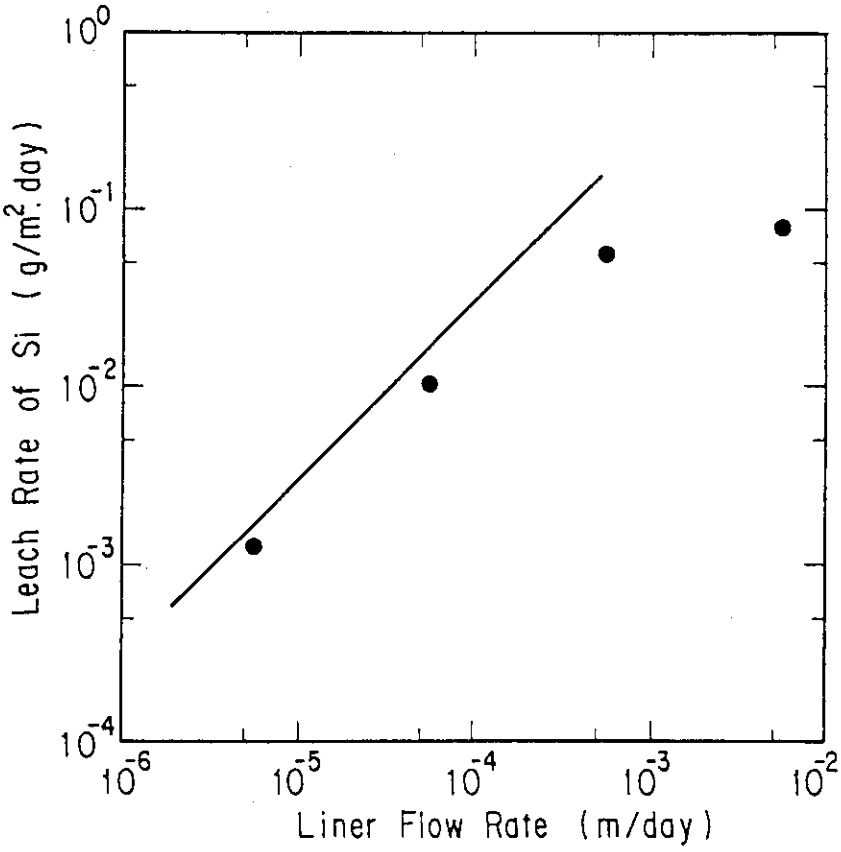

Fig. 1 Relationship between leach rates of Si and liner flow rates.

(2) Leaching behavior of ^{238}Pu from the nuclear waste glass

T. Banba

The leachability of nuclear waste glasses has been investigated for the reason that a waste form is the first protective material from the release of radionuclides in the repository, and that we need to predict the radionuclide release rates from waste forms[1,2]. In this report, the leaching behavior of plutonium, which has a potential long term environmental hazard because of its long half-life, is investigated.

Experimental

ISO type static leach tests[3] were done using the ^{238}Pu-doped simulated nuclear waste glass. The dopant level was 1.35 wt% PuO_2 (^{238}Pu: 6.7×10^9 Bq/g-glass). The composition of waste glass is shown in Table 1. Five specimens (14 mm^{ϕ} x 8 mm^{t}) were prepared by cutting and polishing. The experimental conditions are as follows:

1) Leach tests with deionized water are carried out.
2) The ratio of surface area to leachant volume (SA/V) is determined to be 0.1 cm^{-1}.
3) The Teflon leach container is used.
4) The test temperatures are chosen to be 25°C and 90°C.
5) After certain intervals the specimen is withdrawn from the leach container and immediately transferred to a new leach container filled with fresh leachant. The leachant and container are changed at the first-, second-, fourth-, eighth-, sixteenth-, thirtysecond-, and sixtyfourth-day after starting the leach test.

Aliquots of 100 μl leachate were dried on cleaned stainless steel planchets and ^{238}Pu concentrations were determined through a combination of gas flow proportional counting and surface barrier spectrometry techniques.

The pH of leachate was measured with a pH meter (TOA Electronics Ltd, Model HM-10K). All leachates had the value of pH range between 5.8 and 6.4.

Results and Discussion

The release of ^{238}Pu from the ^{238}Pu-doped simulated nuclear waste glass is illustrated in Figure 1 and 2. Figure 1 shows the normalized elemental mass losses (g/m^2) for ^{238}Pu plotted as a function of time for test temperatures of 25°C and 90°C, and Figure 2 shows the normalized leach rate (g/m^2day) for ^{238}Pu versus time for both temperatures. ^{238}Pu has the value of normalized elemental mass loss with asymptotically approaching 0.5 g/m^2 for 25°C, and 1 g/m^2 for 90°C after 64 days. Namely, it appears that the leach rate of ^{238}Pu reaches a constant value of 0.002 g/m^2day after 64 days (Figure 2).

Figure 2 indicates that the effect of temperature on the normalized leach rate for ^{238}Pu is very small. The factor of Pu leach rate between 25°C and 90°C is 4.8 at 8 days which is the largest value during this experiment, and then it decreases with the increasing leach time. These factors are less than that of the other elements, e.g., the leach rate of Cs increases by factor of 35 between 40°C and 90°C[4]. One of reasons for the small temperature-dependence of ^{238}Pu leach rate will be explained as follows: Plutonium is more concentrated in the alteration layer than in bulk glass[5]. This implies that Pu is blocked from diffusing into solution by the alteration layers. As the growth rate of the alteration layer increases with the rising in temperature, it is considered that the protective effect of the layer on the release of Pu becomes larger at higher temperature. Consequently, the temperature-dependence of Pu leach rate becomes smaller than the other elements such as Cs.

References

1) T. Murakami and T. Banba; Nucl. Technol., **67**, 419 (1984)
2) T. Banba and T. Murakami; Nucl. Technol., **70**, 243 (1985)
3) "Long-term Leach Testing of Radioactive Waste Solidification Products", ISO/DIS-6961, International Organization for Standardization (1979)
4) J.E. Mendel; PNL-5157, p1-35 (1984)
5) J.K. Bates, et al.; Mat. Res. Soc. Symp. Proc., Vol.15, 183 (1983)

Table 1 Composition of Simulated High-Level Waste Glass

Component	Content (wt%)	Component	Content (wt%)
Additive		Waste	
SiO_2	45.2	TeO_2	0.23
B_2O_3	13.9	Cs_2O	0.98
Al_2O_3	4.9	BaO	0.62
CaO	4.0	La_2O_3	0.45
Na_2O	9.8	CeO_2	0.90
ZnO	2.5	Pr_6O_{11}	0.44
Li_2O	2.0	Nd_2O_3	1.48
		Sm_2O_3	0.29
Waste		Eu_2O_3	0.06
Rb_2O	0.12	Gd_2O_3	0.03
SrO	0.34	SeO_2	0.02
Y_2O_3	0.18	RuO_2	0.95
ZrO_2	2.64	Fe_2O_3	2.90
MoO_3	1.73	NiO	0.40
MnO_2	0.26	Cr_2O_3	0.50
Ag_2O	0.03	P_2O_5	0.30
CdO	0.03		
SnO_2	0.02	PuO_2	1.35
Sb_2O_3	0.004		

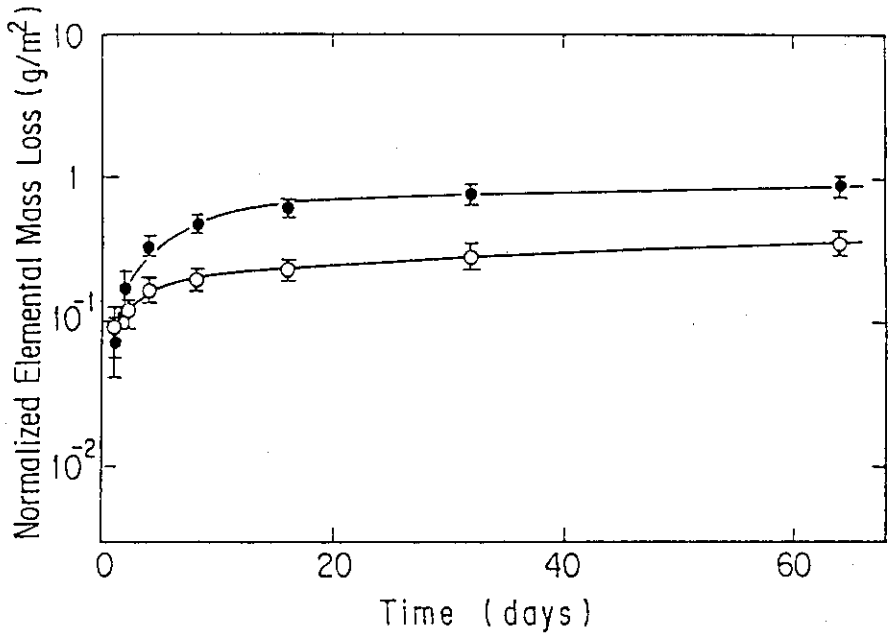

Fig. 1 The normalized elemental mass losses for ^{238}Pu plotted as a function of leach time for testing temperature of 25°C (○) and 90°C (●). Error bars show the standard deviation of each plot.

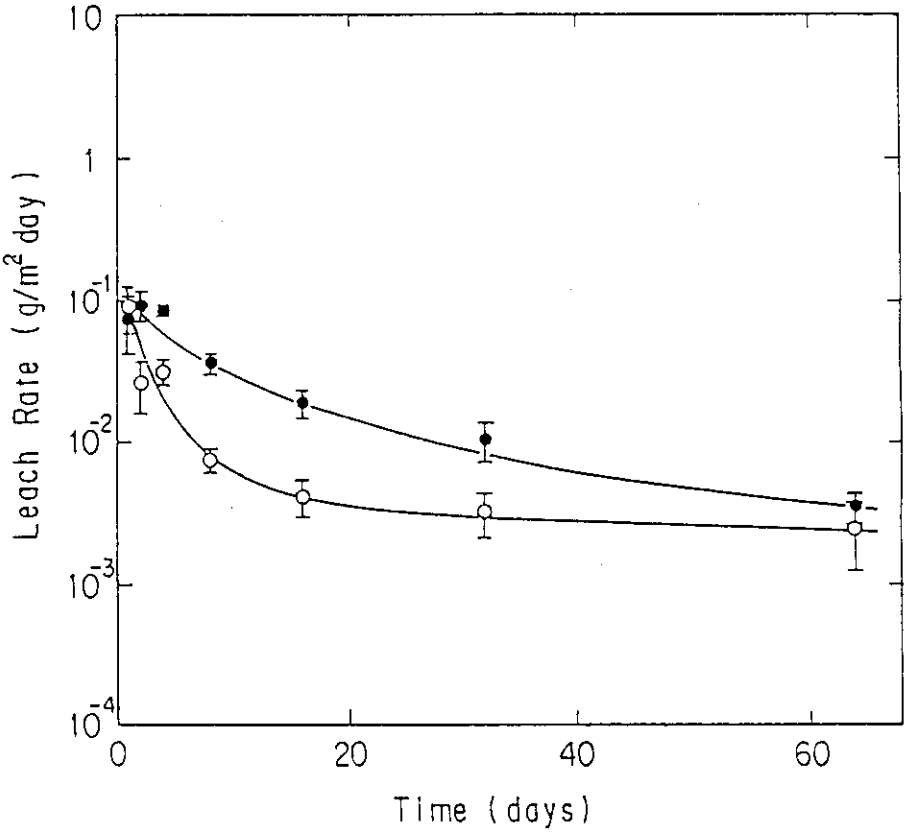

Fig. 2 The normalized leach rates for ^{238}Pu plotted as a function of leach time for 25°C (○) and 90°C (●). Error bars show the standard deviation of each plot.

(3) Accelerated Alpha Radiation Stability Test (AARST) under Beta and Gamma Irradiation

S. Matsumoto and S. Tashiro

Following a previous test on alpha radiation stability of vitrified froms, a new series of the test was initiated using 75 Ci of ^{244}Cm under beta and gamma irradiation at WASTEF. During the test some similar conditions have been established to the test specimen as in the long term duration of actual waste forms. Total alpha disintegration density in the specimen will reach finally to 7.76×10^{18} alpha disintegration/cm^3, and then the nuclide transmutation of curium 244 to plutonium 240 will be about 7 % and the third is absorption dose; 3.5×10^8 rad for gamma radiation and 6.3×10^7 for beta radiation. Test specimens of disk shape have been stored for a given duration upto 2 years and then measured or observed on the alteration in density, leachability, fine structure, helium behavior etc.

At the moment the test has been proceeded the 5,000 year equivalent. The test procedure is shown in Fig. 1 and the results are shown in Fig. 2. The test will finally finish in the coming June at 10,000 year simulation.

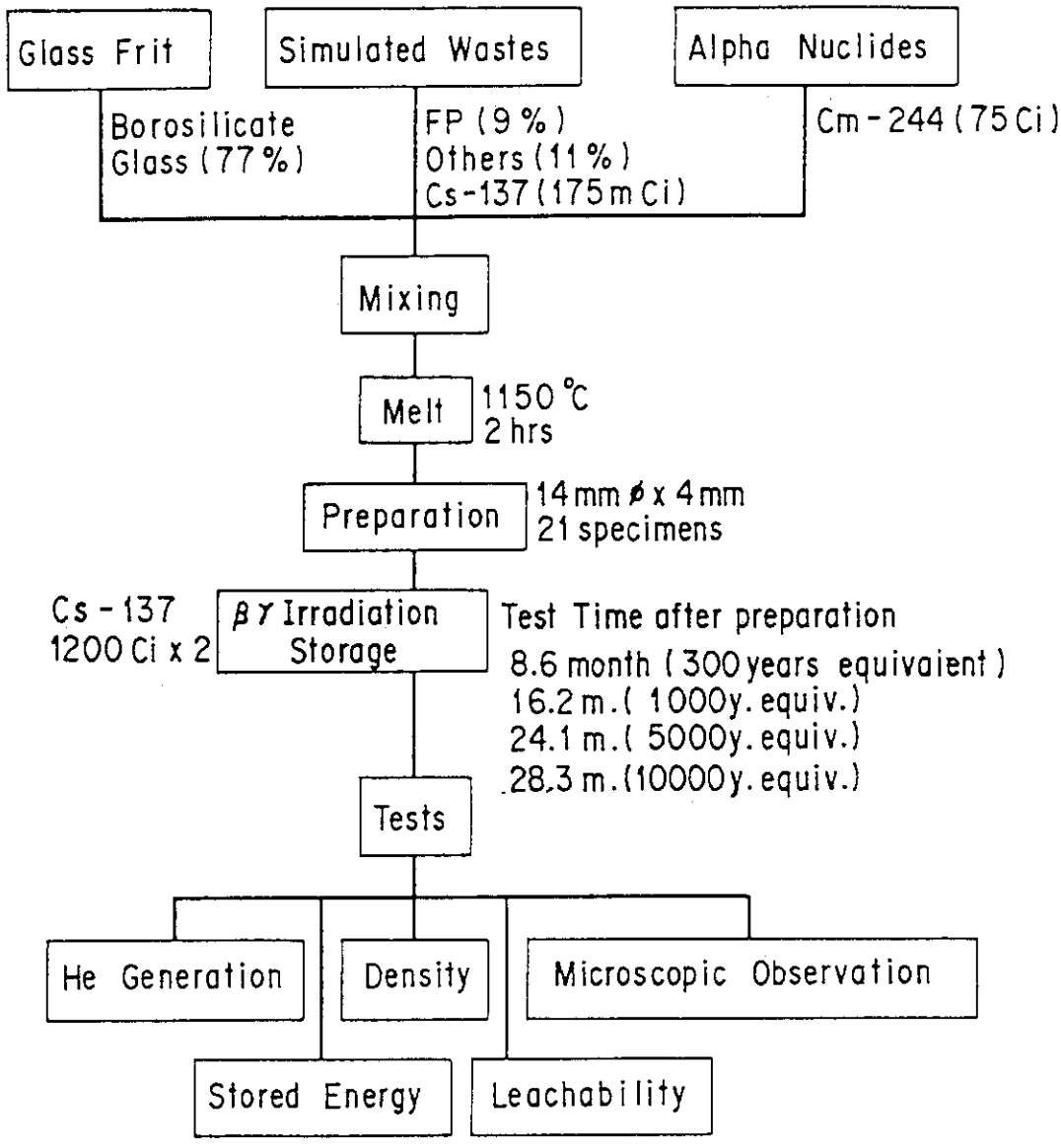

Fig. 1 Block diagram of the test method for accelerated alpha radiation stability under βγ irradiation of vitrified forms.

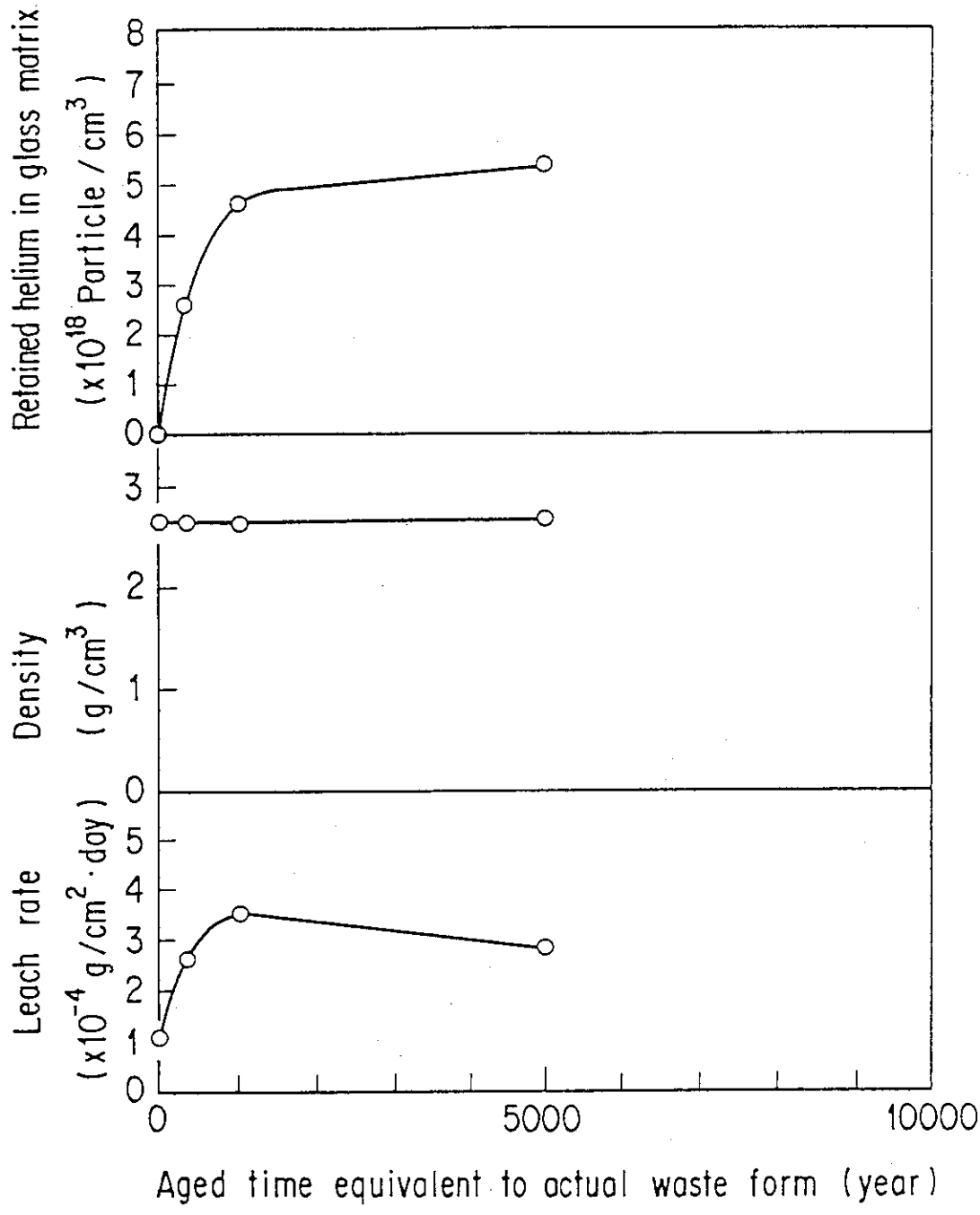

Fig. 2 Results of an accelerated alpha radiation stability test under Beta and Gamma Irradiation of vitrified forms.

(4) He release behavior from Cm-doped glass specimen

K. Morikawa

[Introduction]

Alpha decays of actinides generate the excessive helium in high level radioactive waste glass. This helium may affect characteristics of the waste glass.

In this study ^{244}Cm-doped simulated waste glass which was prepared for an accelerated alpha radiation stability test was used as specimen aged four years after the doping.

[Experimental]

The glass specimen irradiated to 6.1×10^{18} alpha disintegration/g was reformed into the sized of 3mmϕ × 0.5mm, 3mmϕ × 1.0mm, and 3mmϕ × 2.0mm. The test was carried out in a vacuum system in the No.5 hot cell of WASTEF. An outline of the equipment is shown in Fig. 1. Each specimen was put on the alumina stand and heated at a given temperature of 260 ~ 540°C. It usually took about ten minutes before the specimen reached the given temperature. Released gas was lead to a reserve tank and the concentration was measured with a mass spectrometer.

The release of helium from the specimen obeys the Fick's second law.

$$\frac{\partial C}{\partial t} = D \left\{ \frac{\partial^2 C}{\partial r^2} + \frac{1}{r}\frac{\partial C}{\partial r} + \frac{\partial^2 C}{\partial z^2} \right\} , \qquad (1)$$

where D is a diffusion coefficient of helium in the specimen, and C is concentration of helium in the specimen. A solution of Eq.(1) is given using the following initial conditions and boundary conditions,

Initial conditions $C=C_0$ at $t=0$, $0<4<a$, $0<z<L$,

Boundary conditions $C=0$ at $t>0$, $r=a$, $z=0,L$,

where C_0 is a initial concentration of helium in the specimen, a is radius of the specimen, and L is thickness of the specimen. The solution gives fractional release (M_t/M_∞) of helium as,

$$\frac{M_t}{M_\infty} = 1 - \frac{32}{\pi^2 a^2} \sum_{k=0}^{\infty} \sum_{n=1}^{\infty} \left[\frac{1}{(2k+1)^2 \alpha_n^{\,2}} \times \exp\left\{-D(\alpha_n^{\,2} + (2k+1)^2 \pi^2 / L^2) t\right\}\right] , \qquad (2)$$

where M_t is the amount of released helium from the specimen at the time t, M_∞ is the total amount of helium in the specimen, and α_n is a positive zero

point of Bessel function of zero dimension, $J_0(a,\alpha_n)=0$. Thus, the diffusion coefficient of helium in the specimen can be lead by fitting this equation to the obtained data.

[Result and discussion]

The obtained data and a curve given by fitting the Eq.(2) to the data are shown in Fig. 2. This curve is good fitness to the obtained data for early time. But when fractional release (M_t/M_∞) excess 0.8, it is bad. It is suspected that helium is trapped with radiation defects and bubbles, so helium release was late from natural diffusion. Again, Eq.(2) was fitted to this region of data, and a new diffusion coefficient was given. A diffusion coefficient of untrapped region was named D(u), and a diffusion coefficient of trapped region was named D(t).

Arrehnius plot of both the D(u) and D(t) of several temperatures is shown Fig. 3. Each coefficient is shown by the follow equations,

$$D(u) = 1.80 \times 10^{3} \exp(-12.7 \text{ kcal/RT}) \quad cm^2/s \ ,$$

and

$$D(t) = 0.176 \exp(-19.9 \text{ kcal/RT}) \quad cm^2/s \ .$$

It suppose that the reason of difference of activation energies is trapping of helium to radiation defects and bubbles.

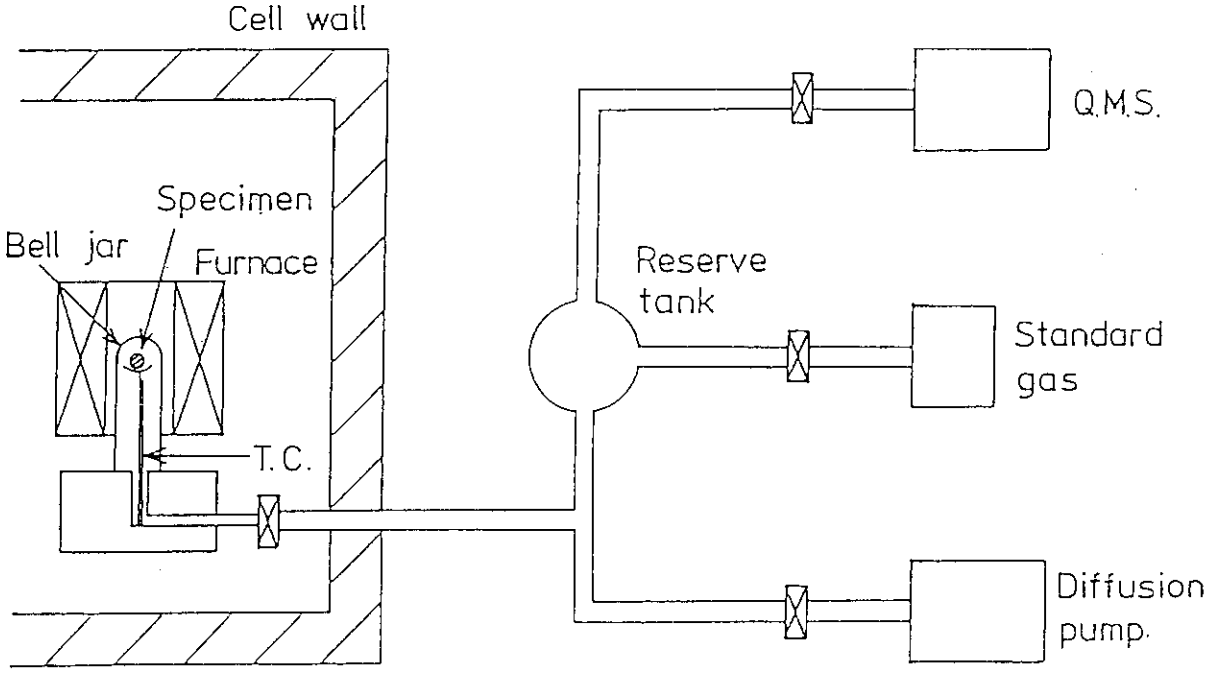

Fig. 1 The outline of the equipment

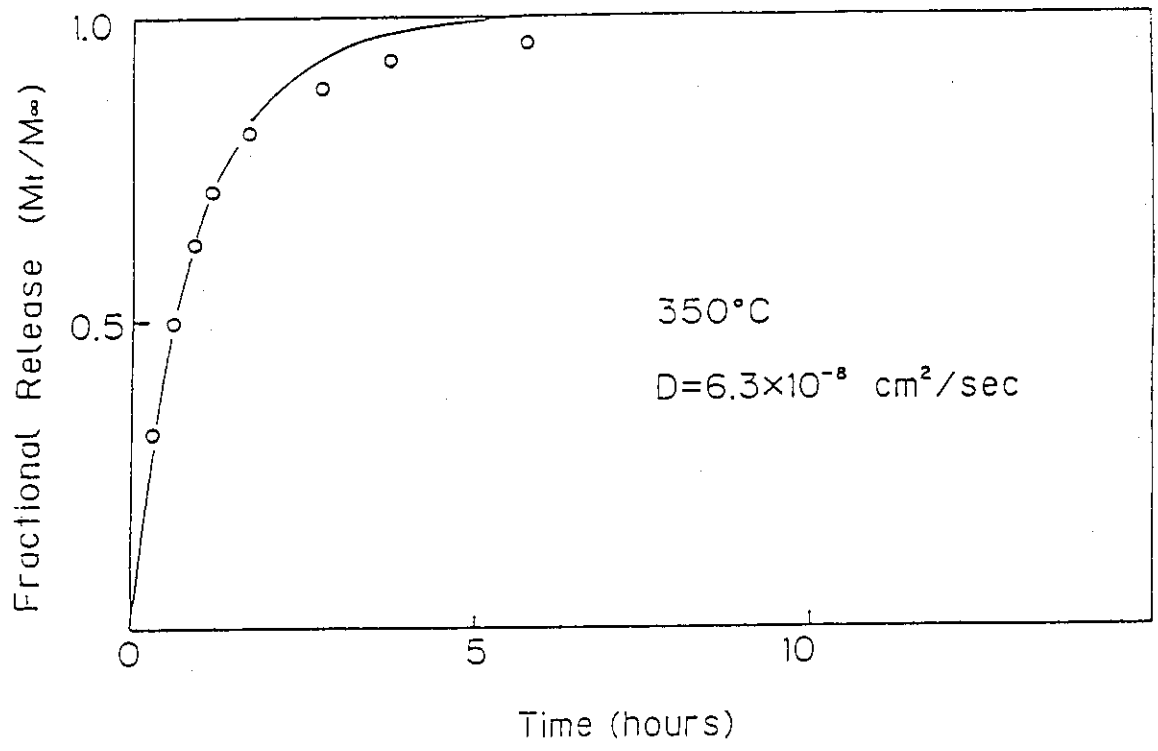

Fig. 2 Obtained data and a fitting curve at 350°C

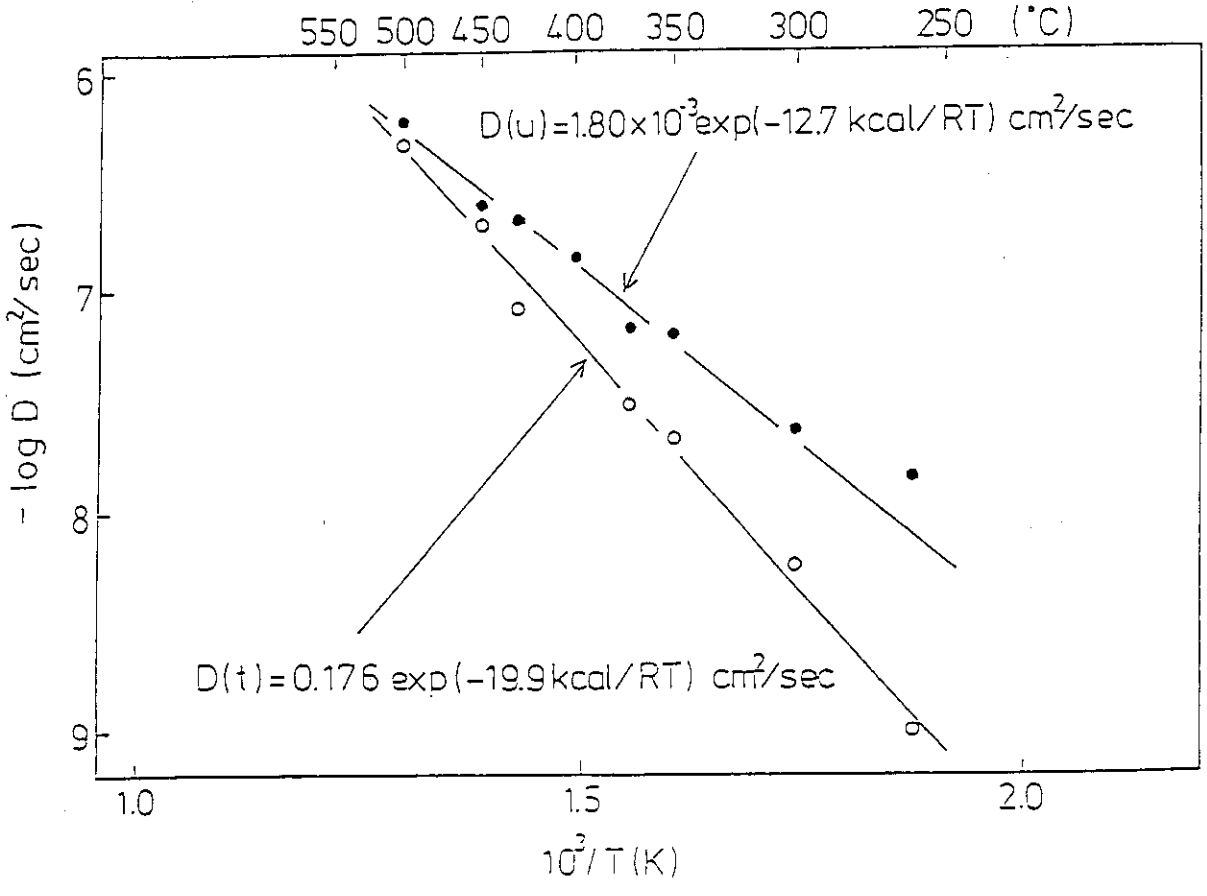

Fig. 3 Arrhenius plot of the obtained data

(5) Alpha- and gamma-radioactivity measurements of neptunium-237 in leachants for waste glass leach tests

S. Nakayama and T. Banba

Introduction

Concentrations of actinides contained in glass leachates obtained from waste glass leach tests are generally calculated from their alpha radioactivities. An aliquot of the leachate is dried on a stainless steel pan, and alpha particles emitted from the smaple are counted with a proportional counter or a silicon surface barrier detector. This method is not favorable when the ionic strength of the leachate is high, because the energy of alpha particles are more or less absorbed by the dried salts formed on the pan and a part of alpha particles are not detected. The energy absorption makes precise radioactivity measurement difficult.

At JAERI a leach test for neptunium-237 (^{237}Np)-doped simulated waste glass has been carried out with synthetic basalt groundwater[1] as a leachant. The above-mentioned problem in radiometric determination is serious in this leach test because (1) a large volume of the glass leachate is required for measurement due to the low specific activity of ^{237}Np and (2) the leachate (synthetic basalt grounwater) forms a much amount of salt when dried, which is likely to effectively inhibit detection of alpha particles. On the other hand, gamma-ray detection seems applicable for ^{237}Np determination because the yields of gamma emission from ^{237}Np are measurably high: 14.0 % for 29.3 keV and 12.6 % for 86.5 keV of gamma rays. However, long-time measurement is needed due to low detection efficiency of gamma-ray detectors.

The objectives of this preliminary experiment are as follows; (1) to know the effect of the energy absorption of alpha particles in the dried groundwater leachant on the alpha-radioactivity measurement and to study if it is practically possible to correct the so measured alpha radioactivity to obtain an exact value of radioactivity, and (2) to study if it is practical to measure radioactivity by long-time gamma-ray detection for small amount of leachants (0.5 ml).

Results

Figures 1(a), (b) and (c) show the alpha spectra of ^{237}Np emitted from a standard source (Amersham), dried deionized water and dried synthetic basalt groundwater leachant spiked with ^{237}Np, respectively. In Fig. 1(c),

peak tailing can be seen resulting from the absorption of energies of alpha particles. A part of alpha particles is not detected in appropriate energy channels and not counted. Hence, the proportionality cannot hold between detected counts and concentration of spiked ^{237}Np. This tendency is shown in Fig. 2 by blank circles. In practice, it seems impossible to estimate alpha radioactivities from this result with sufficient accuracy. The typical period for alpha-radioactivity measurement with 2π gas-flow proportional counter was 5 to 10 minutes. Samples prepared for the above alpha-radioactivity measurement were also used for gamma-radioactivity measurement with the low-energy photon spectroscopy equipped with high-purity germanium detector. The measurement period required was a half to one day. The measured gamma radioactivities are shwon in Fig. 2 by blank triangles. A solid line in this figure represents the measured alpha radioactivities for ^{237}Np-spiked deionized water, for which little energy absorption in dried salt is observed as expected by Fig. 1(b). Comparison of the measured gamma radioactivities with the solid line shows that gamma-radioactivity measurement is practically applicable with sufficient accuracy though it takes a long period for measurement.

Conclusion

The measurement of alpha radioactivities was not appropriate to determine the concentration of ^{237}Np contained in the synthetic basalt groundwater. The salt formed by drying the groundwater absorbed energies of alpha particles so that alpha particles were not detect correctly. The gamma-radioactivity measurement was, though it took long time, practically applicable for ^{237}Np determination in both the deionized water and the groundwater.

Reference

1) Jones, T.E.: "Reference Material Chemistry - Synthetic Groundwater Formulation", RHO-BW-ST-37P (1982).

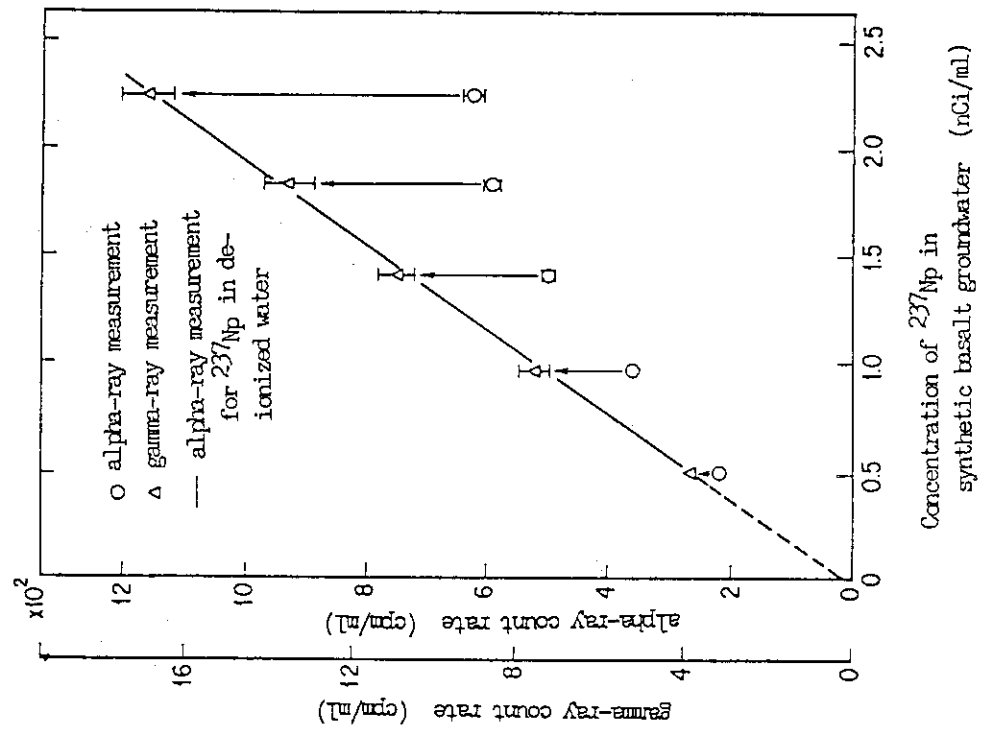

Fig. 2 Concentration of ^{237}Np in synthetic basalt groundwater versus their alpha-ray and gamma-ray count rates. Alpha-ray counting was made with a 2π gas-flow proportional counter and gamma-ray counting with a high-purity germanium detector.

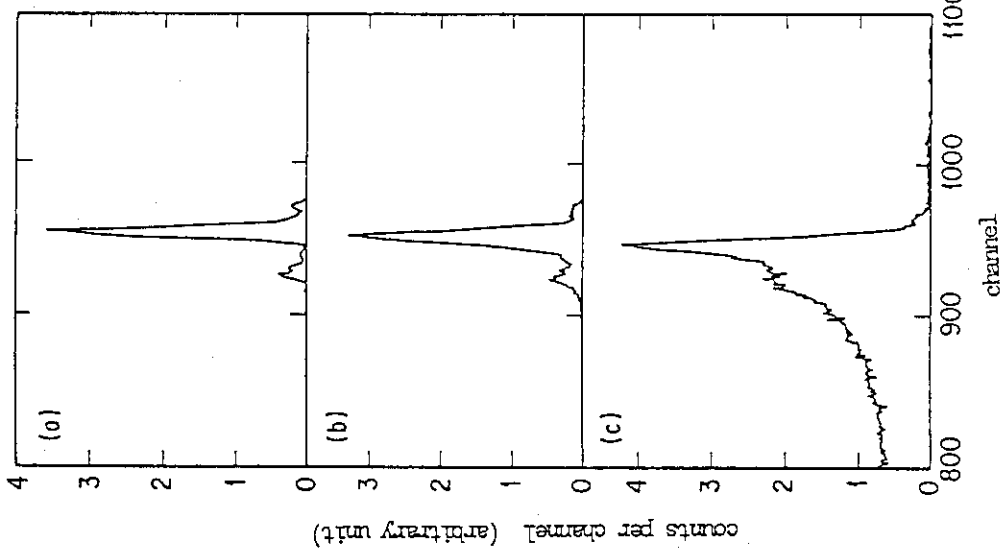

Fig. 1 Alpha-ray spectra of ^{237}Np by silicon surface barrier detector. (a) standard source (Amersham), (b) ^{237}Np-spiked deionized water (0.5ml) dried on a stainless steel pan, (c) ^{237}Np-spiked synthetic basalt groundwater (0.5ml) dried on a stainless steel pan.

(6) Removal of fluorine from Teflon® PFA containers by the MCC cleaning procedure

S. Nakayama

Introduction

In WASTEF a leach test has been carried out for a ^{237}Np-doped waste glass since June 1987. Before the leach test it was found that the pH of purified water stored in Teflon® PFA (Polytetrafluoroethylene-Perfluoroalkylvinylether) containers at 90°C decreased from 5.7 to about 4 during the first 3 days. The Teflon PFA containers have been recommended to use as leach containers by the MCC (Materials Characterization Center) -1 Static Leach Test Method[1], and before the test the containers used were cleaned following the procedure described by the MCC manual. Water used was found to have no measurable impurities.

From the pH 4 water about 1 ppm of fluorine ion was detected by using an ion chromatography. The two facts, the decrease in pH and the increase in fluorine ion concentration, imply that hydrogen fluoride HF remained in the Teflon PFA containers. An aqueous solution of HF is hydrofluoric acid. This acid is known to dissolve silicate such as glass. Then the HF released from Teflon PFA containers to leachant may affect the leaching of glass.

The objectives of the present experiments are (1) to find convenient ways of cleaning in addition to the MCC cleaning procedure in order to remove HF from the Teflon PFA containers to the level that the pH decrease is not observed, and (2) to study whether HF remained in Teflon PFA containers affects the weight loss of a simulated waste glass.

Experiments and results

Removal of fluorine by the MCC cleaning procedure

The MCC cleaning procedure described in Ref.1) consists of following eight steps:

1) Heat new containers at 200°C for one week.
2) Soak for 1 h in 6MHNO_3-0.2MHF.
3) Rinse with 3 container volumes of high-purity H_2O.
4) Soak in 6MHNO_3 for 4 h at 50°C.
5) Soak for 30 min in >60°C high-purity H_2O.
6) Soak for at least 8 h in fresh high-purity H_2O.
7) Boil for 30 min in fresh high-purity H_2O.

8) Rinse with successive container volumes of high-purity H_2O until the pH of two successive rinse solutions is within 0.5 pH unit of the original high-purity H_2O. A minimum of three rinses is required.

In order to study the extent of removal of fluorine from Teflon PFA containers by the above procedure, new Teflon PFA containers were prepared as the following three kinds, to which different steps of the cleaning procedure were subjected.

Container A: Supersonically cleaned in tap water for 10 min and rinsed with purified water. (The purified water used in these experiments was provided by Kyouei Seiyaku Company, Chiba, Japan.)

Container B: In addition to the procedure for the Container A, step 1) of the MCC cleaning procedure (heating at 200°C for one week) was made.

Container C: Steps 1) to 8) were completed.

About 40 cc of purified water were put in the containers A, B and C. They were kept at 90°C in an oven. At desired time those containers were taken out from the oven and cooled to room temperature. The pH and the fluorine ion concentrations of waters were measured. (This procedure is called a cleaning test in this report.) The measurement of the fluorine ion concentration was made with an ion chromatography (Shodex IC) equipped with an anion-exchange column (Shodex IC I-524A).

Figure 1(a) shows the pH for samples A, B and C. The pH values of all these three samples rapidly decrease in one day. The extent of the pH decrease is in order of A > B > C, which agrees the extent of cleaning. Even in the sample C, for which the MCC cleaning procedure was completed, the pH decreased to about 4. Figure 1(b) also shows the pH for samples A, B and C. This result was obtained by the procedure in which after each pH measurement the containers were rinsed with purified water and fresh purified water were put into the containers. This procedure allows to detect smaller pH changes. Figure 1(b) shows that it took about 60 days for the pH to recover to that of purified water.

Figure 2 shows the hydrogen ion concentration $[H^+]$ and fluorine ion concentration $[F^-]$ for samples A, B and C. The $[H^+]$ were calculated from the measured pH values plotted in Figure 1(a). As shown in Figure 2, $[F^-]$ and $[H^+]$ change in a similar manner. Quantitatively $[F^-]$ seems nearly equal to $[H^+]$ throughout the studied period. This fact leads to an assumption that the impurity remained in Teflon PFA and causing the pH decrease is

hydrogen fluoride HF.

In order to study effects of heating on removal of HF, heating duration was extended to 2 to 4 weeks and the cleaning tests were carried out. As shown in Table 1, more than 3 week heating is effective to remove HF from Teflon PFA containers, but not sufficient.

The effect of the hydrofluoric acid concentration on glass leaching

A glass leach test was carried out with hydrofluoric acid of different concentrations as a leachant. The $[F^-]$ in the leachant were adjusted to 0, 2.1 and 23 ppm. These values cover the range of $[F^-]$ corresponding to that of [HF] released from Teflon PFA containers. Cylindrical specimen of simulated waste glass (5 mm D×30 mm L) were leached at 90°C for 14 days. The SA/V ratio was 0.17 cm^{-1}. The measured weight loss was listed in Table 2.

The pH of glass leachates increases as the leaching progresses. Also in this leach test, the final pH values (9.0 to 9.3) were much higher than initial pH values (3 to 6). Since the final pH values were almost identical, there would be no effect of pH on glass leaching at this time. The effect of pH would appear at shorter leach time if any, where the pH values were different from sample to sample. The result shown in Table 2 means that under the considered leaching condition there is little effect of hydrofluolic acid on glass leaching.

Conclusion

Hydrogen fluoride HF seems to remain in new Teflon PFA containers even after the MCC cleaning procedure. To remove the HF more than about 2 month soaking of the containers in purified water at 90°C is required following the MCC cleaning procedure. It is also effective to extend the heating (200°C) duration to three weeks or longer. These two procedures should be added to the MCC cleaning procedure.

A 14-day glass leach test at 90°C was made to study whether HF of concentrations as high as those remaining in the Teflon PFA containers affect the glass leaching. The weight loss was measured. Little effect was observed under the considered condition.

Reference

1) Materials Characterization Center: "Nuclear Waste Materials Handbook", Test Methods, MCC-1P Static Leach Test Methods, Revision 1 (1983).

Table 1 Effect of heating duration on pH of rinse solutions[a)]

heating duration (week)	pH after cleaning test	pH after a cleaning test and the MCC cleaning procedure
1	4.57	—
	4.70	—
	4.11	—
2	4.96	—
	5.00	—
3	5.4	5.02
	6.0	4.87
4	6.9	5.13
	6.8	4.85

a) Heating temperature was 200°C. A cleaning test was made at 90°C for one week.

Table 2 Weight loss of simulated waste glass in different concentrations of hydrofluoric acid[a)]

fluorine ion concentration (ppm)	pH initial	pH final	weight loss (%)
0	5.7	9.31	0.45
2.1[b)]	4.01	9.23	0.31
23[b)]	3.22	9.04	0.41

a) Leach test was made at 90°C for 14 days.
b) These values were measured with the ion chromatography.

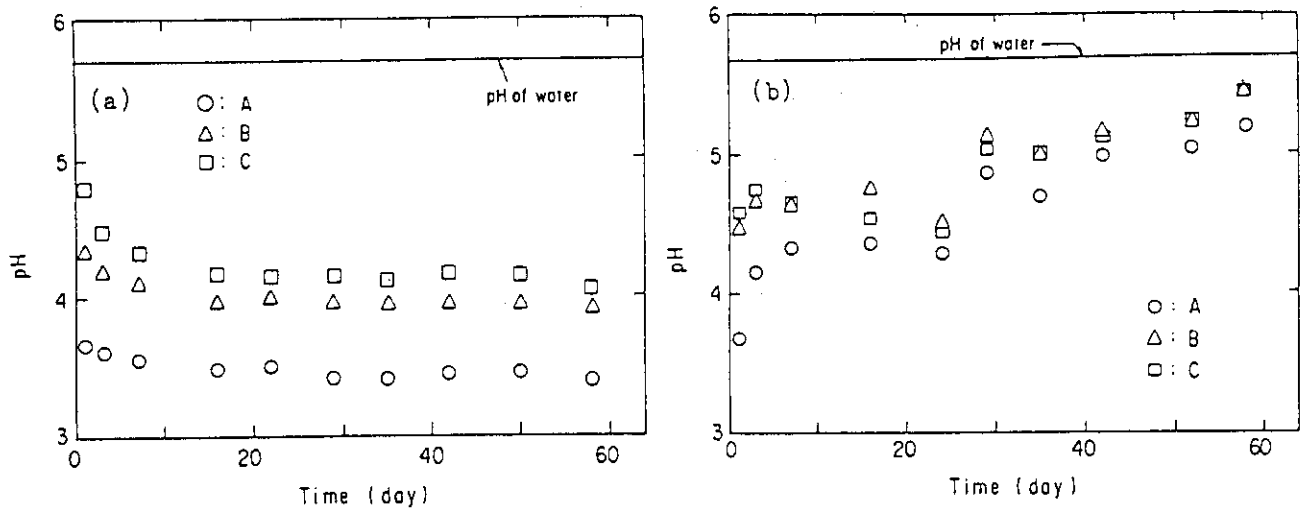

Fig. 1 (a) pH of rinse solutions for samples A, B and C. (b) Same as (a), but after each pH measurement the containers were rinsed with purified water and fresh purified water was put into the containers. A: supersonically cleaned, B: supersonically cleaned and heated at 200°C for 1 week, C: cleaned by the MCC cleaning procedure.

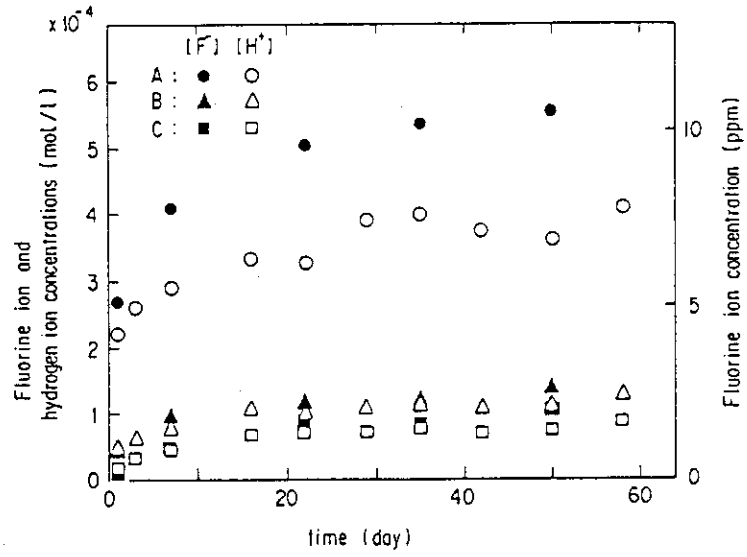

Fig. 2 Hydrogen ion concentration and fluorine ion concentration for samples A, B and C. Supersonically cleaned, B: Supersonically cleaned and heated at 200°C for 1 week, C: cleaned by the MCC cleaning procedure.

1.2 SYNROC

(1) Identification of the surface precipitates produced in hydrothermal dissolution of SYNROC

H. Mitamura and T. Murakami

Introduction

High level nuclear waste (HLW) is to be solidified and then isolated from biosphere over one million years since it contains a lot of hazardous long-lived radionuclides. SYNROC is a titanate ceramic designed for the immobilization of HLW elements which are incorporated as dilute solid solutions in three main constituent minerals, namely hollandite ($BaAl_2Ti_6O_{16}$), perovskite ($CaTiO_3$) and zirconolite ($CaZrTi_2O_7$). After a geological disposal of the HLW form, release of the radionuclides can occur due to percolating ground water. Many studies have been carried out using various kinds of leaching methods to elucidate the release mechanisms and to assess long-term release rates of the radionuclides from the waste form. From the results of these studies, surface layers and/or precipitates are considered to greatly influence the release rates of some hazardous long-lived radionuclides. In the present study, we examined surface precipitates under hydrothermal condition which is assumed to accelerate the growth of the surface products.

Experimental

An ANSTO SYNROC (SFG 556) containing 10 wt% of nonradioactive simulated HLW was sliced into two millimeter-thick sections. A part of the sections were polished with diamond paste of 0.25 μm before leaching. The test was carried out using deionized water at 190 ^{o}C for 28 days in accordance with the Materials Characterization Center (MCC)-2 method. After leaching, test vessels were naturally cooled to room temperature and then the samples were dried after a rinse with deionized water. Leached samples were subjected to observation of scanning electron microscopy (SEM) equipped with energy dispersive X-ray analyzer. A part of the surface products were collected and dispersed on a microgrid for observation of analytical transmission electron microscopy (ATEM).

Results

Figure 1 shows a SEM image of the SYNROC sample after the leaching test. In this figure, granular precipitates below 0.3 μm are distributed all over the surface. Needle-like precipitates up to 60 μm are also scattered on the granular surface products. Figures 2.① and 2.②-2.⑧, respectively, display a SEM image and X-ray mapping images. These figures show that the needle-like precipitates contain neodymium and cerium. It is not clear in these figures whether phosphor is included in the needle-like precipitates or not because the X-ray peaks of zirconium-L and phosphor-K occur at almost the same enrgy range.

ATEM revealed that the needle-like precipitates consisted of neodymium (Nd), cerium (Ce), calcium (Ca) and phosphor (P) (Fig.3). Electron diffractometry elucidated that these precipitates had a monazite structure and that they were extended along the c-axis. Secondary electron images using ATEM clarified that the needle-like precipitates were rectangular prisms in shape. On the other hand, ATEM also revealed that the granular surface products consisted of titanium (Ti).

Discussion

A chemical form of the needle-like precipitates is considered to be (Nd, Ce, Ca)PO_4 based on the results of SEM, ATEM and electron diffractometry. Kastrissios et al.[1] have reported that a perovskite phase is more soluble than the other main constituent mineral phases and dissolves congruently under hydrothermal conditions similar to the present study. ATEM revealed that perovskite grains contained rare earth elements such as neodymium (Fig. 4). Rare earth elements in the needle-like precipitates is considered to originate from those in perovskite grains. On the other hand, phosphor was rarely detected in perovskite grains in the present study. This element must be derived from the other soluble SYNROC phases.

Figure 2 indicates that needle-like precipitates are concentrated in a region rich in ruthenium and iron. In this region, the granular precipitates are distributed widely. Since most of these surface products is supposed to originate from the perovskite grains, rare

earth elements in these grains may be consumed for growth of the needle-like precipitates. Therefore, the other soluble SYNROC phases in the ruthenium- and iorn-rich region need to be considered as source for the eqivalent amount of phosphor, but it is still unknown.

Monazite usually contains uranium and/or thorium in natural minerals and has long-term stability in terms of radiation damage and chemical durability[2]. This phase is considered to be desirable as the host phase for actinide elements in HLW. A part of these elements are incorporated in perovskite phase in SYNROC. Although a perovskite phase has lower chemical durability than the other main constituent phases, actinide elements dissolved are again incorporated in the monazite-structure precipitates in which actinide elements are hardly dissolved. This phenomenon may be favorable for confinement of HLW elements.

References

[1] KASTRISSIOS, T., STEPHENSON, M., TURNER, P. S. and WHITE T. J., "Hydrothermal dissolution of perovskite: Implications for Synroc formulation," J. Am. Ceram. Soc., 70[7] (1987) c144-c146.

[2] ABRAHAM, M. M., BOATNER, L. A., BEALL, G. W., FINCH, C. B., FLORAN, R. J., HURAY, P. G. and RAPPAZ M., "A review of research on analogs of monazite for the isolation of actinide waste," CONF-8005107, U.S. Department of Energy, Technical Information Center, Oak Ridge, TN (1981).

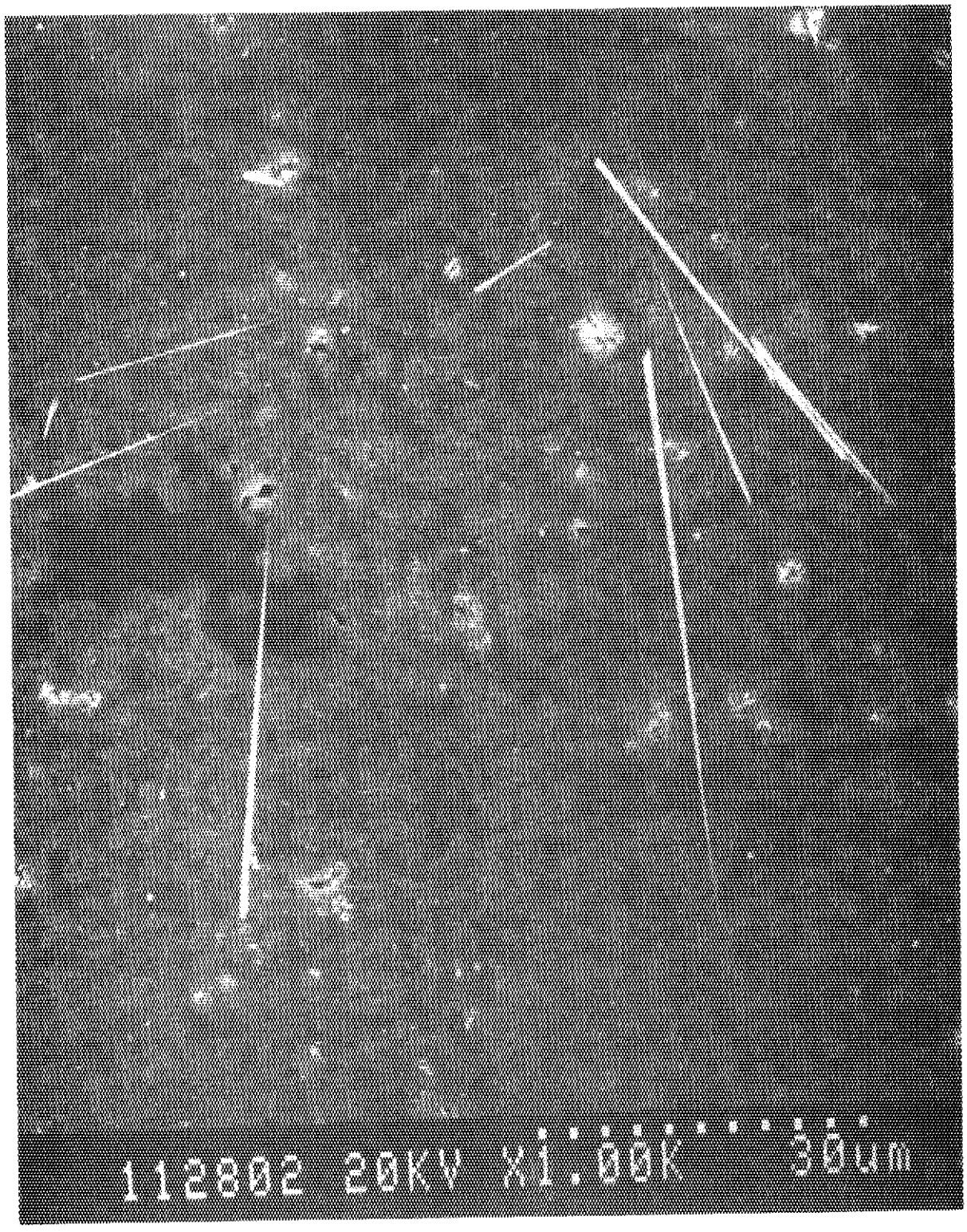

Fig. 1 Scanning electron micrograph of SYNROC surface after leaching at 190°C for 28 days.

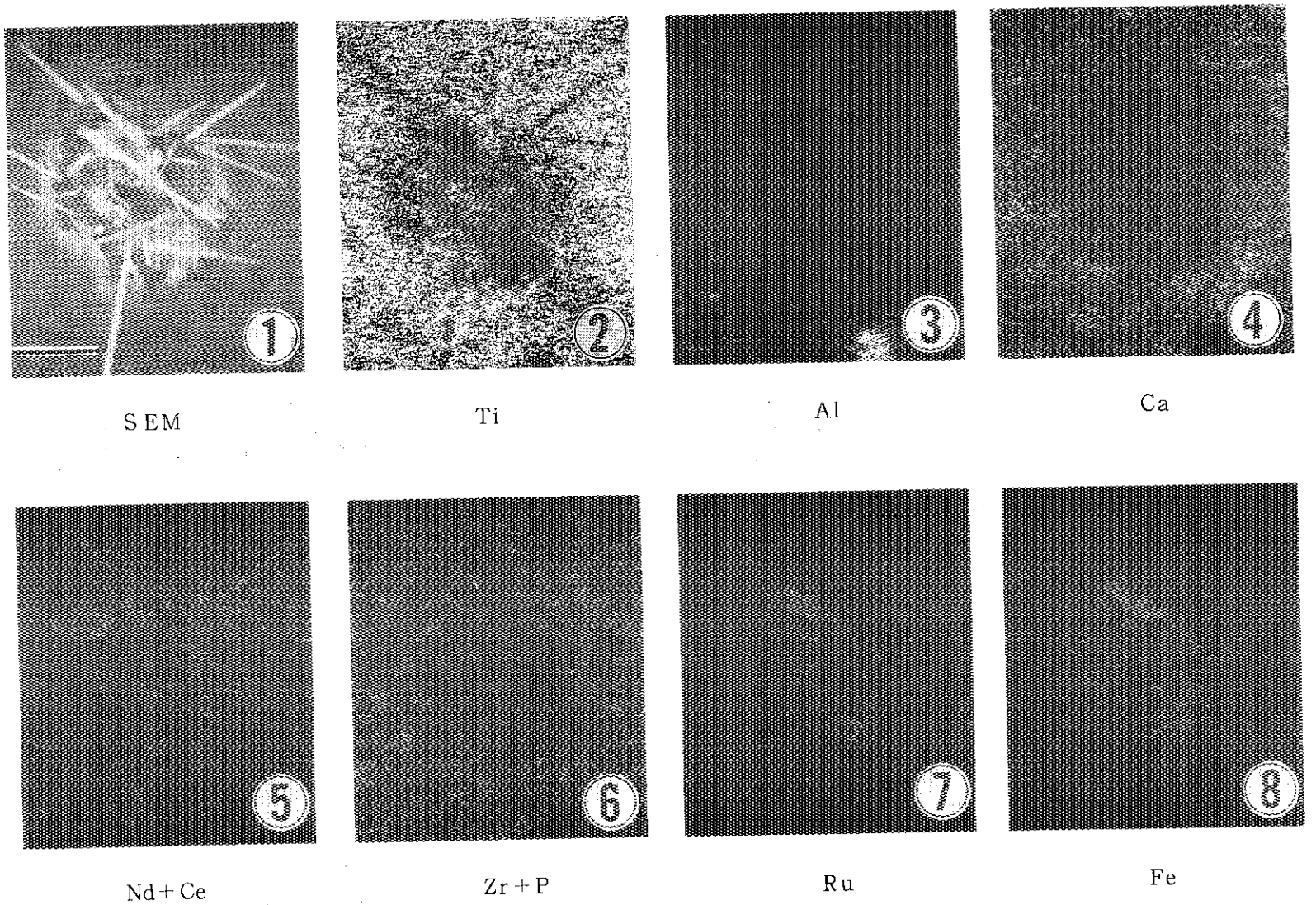

Fig. 2 Scanning electron micrograph (Fig. 2.1) of SYNROC surface after leaching at 190°C for 28 days and its X-ray mapping images for Ti, Al, Ca, Nd+Ce, Zr+P, Ru and Fe (Fig. 2.2 - 2.8, respectively). A black bar in Fig. 2.1 is 5 μm.

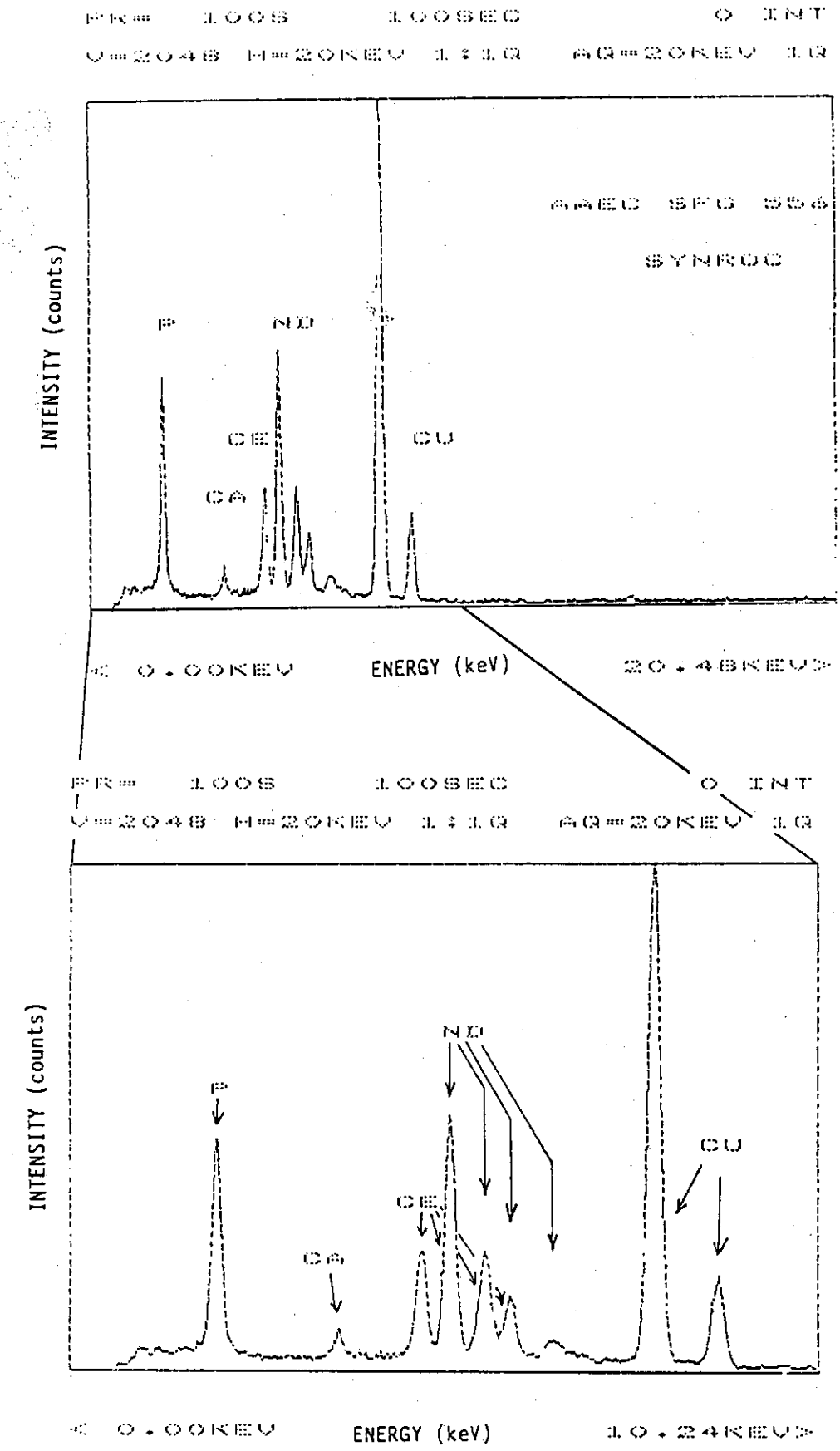

Fig. 3 Typical energy dispersive X-ray spectrum of needle-like precipitates using analytical transmission electron microscopy.

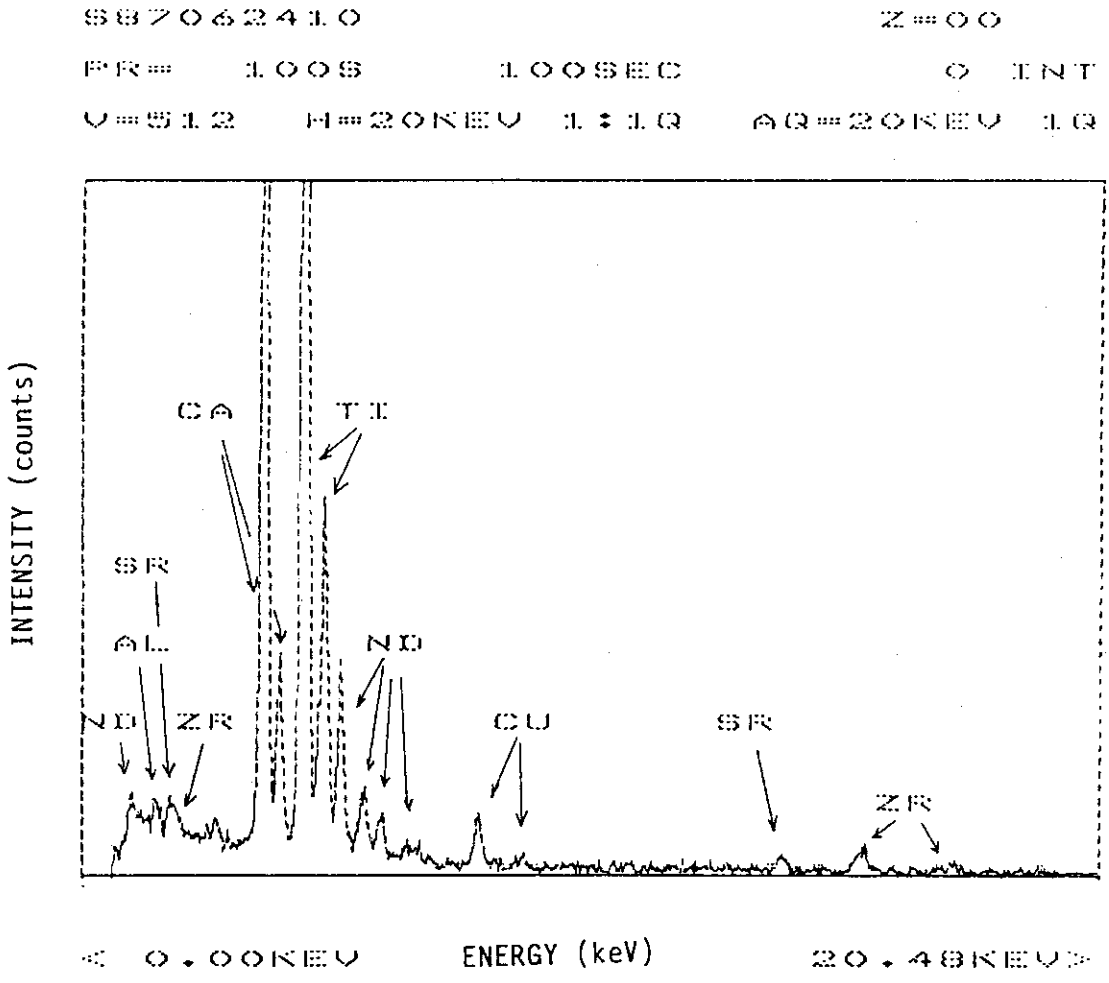

Fig. 4 Typical energy dispersive X-ray spectrum of perovskite grains in as-prepared SYNROC.

(2) Fabrication of curium-doped SYNROC

S. Matsumoto and H. Mitamura

Introduction

Alpha decay of actinide elements in nuclear waste forms results in the formation of two particles: a recoil nucleus and an alpha particle. In the waste forms, the former particle has a short range of ∿ 10 nm and produces several thousand atomic displacements, while the latter particle has a range of ∿20 μm and produces several hundred atomic displacements [1]. It is generally assumed that radiation damage in the waste forms results primarily from atomic displacements. In Synroc, the actinide elements can be incorporated mainly in perovskite and zirconolite phases. Consequently, two alpha damage mechanisms are supposed to exist in Synroc including actinide elements: synergistic damage due to recoil nuclei and alpha particles in the actinide containing phases, and alpha particle damage in the actinide free phases.

An accelerated alpha radiation stability test was planned at WASTEF using curium-244 under a co-operative program between JAERI and ANSTO. In order to carry out the test, a set of hot cell apparatuses was installed in the hot cell of WASTEF, which mainly consists of a calciner and a hot press (see Figs. 2 and 4 in Ref. 2). The Synroc blocks containing curium-244 were prepared using the apparatuses in the first week of December, 1987 and then the test was initiated.

Fabrication of Curium-doped Synroc

1) Curium Source

The curium source (as dioxides) was enclosed in two small capsules which were shipped from the Oak Ridge National Laboratory (ORNL), USA. The total amount of the curium source collected from the capsules was 1.48 g which corresponds to the total alpha activity of 1.90 TBq (51.3 Ci) and the ^{244}Cm activity of 1.89 TBq (51.1 Ci) as of the beginning date of Synroc fabrication (Table 1). These activities have been calculated using a mass assay in shipping data sheets of ORNL. In this calculation, long-lived nuclides (half life: more than 8×10^3 years) were regarded as stable ones, and the elemental

impurities were neglected since the total amount of the impurities was less than 1.5 wt%.

2) Substitution of Curium Source

In order to estimate the accumulated alpha disintegration density of an actual Synroc in a disposal time and assign it to that of the curium-doped Synroc in a storage period, the following assumptions are adopted:

[1] It is assumed that the actual Synroc contains 10 wt% of an as-calculated HLW which will be termed "JW".

[2] The 10^5-year disposal time is supposed as a maximum accelerated term in the present alpha radiation stability test.

[3] The curium content is fixed so as to complete the test in two years.

These assumptions demand that the curium source of 1.48 g should be incorporated in 91.7 g of the curium-doped Synroc. Therefore, the content of the curium source in the Synroc becomes 1.61 wt%.

Next, it is assumed that 10 wt% of a simulated HLW named JW-A is loaded in a Synroc before curium-doping. As our curium source is used without further purification, it contains the approximately same amount of the plutonium element which is daughters of the curium nuclides. The total amount of curium and plutonium elements are substituted for all of actnides and rare earth elements of higher mass numbers in the JW-A waste on a mole basis. Table 2 shows the composition of a simulated JW-A waste which is partly substituted by the curium source. From this substitution, the curium-doped Synroc is to have 10.59, 87.42 and 1.99 wt% of the simulated JW-A waste, precursor and titanium metal, respectively (Table 3).

3) Fabrication Process

Table III shows the composition of the Synroc precursor which was prepared by a hydroxide-route process. Figure 1 shows the preparation process of the curium-doped Synroc. At the beginning, the precursor and the simulated JW-A waste only excluding the curium source were made up in a cold laboratory. This waste was not subjected to pH adjustment with nitric acid because an adequate amount of nitric acid

was added to the simulated JW-A waste as the solvent of the curium source mentioned below.

In the hot cell, the curium source of 1.48 g was dissolved in concentrated nitric acid (41.7 g) with some drops of hydrofluoric acid (0.11 g) on a hotplate at 60 ^{o}C. This curium solution was dark green. Although the weight of the curium soulution was measured, its volume was not done as the curium source was dissolved in a glass beaker to facilitate the remote handling. The curium solution was divided with a balance into three equal parts to mix with the Synroc slurry consisting of the precursor and the simulated JW-A waste because the capacity of the calciner was not sufficient to treat at a time. The pH of each mixture was adjusted to about 9 with ammonium hydroxide before introduction into the calciner. The each mixture was dried at 70 ^{o}C for more than 24 h and calcined at 750 ^{o}C for 2 h.

For one of the three batches of the calcined powder, the pour and tap densities were measured using a graduated polyethylene cylinder, a funnel and a spatula by remote handling. The capacity of the cylinder was 50 cm^3 and the minimum graduated scale was 0.5 cm^3. The calcine powder of 44 cm^3 was poured into the cylinder to measure the pour density. The 1 cm-high tapping was repeated until it caused no change in powder volume.

Adequate amounts of the calcined powder were collected from the three batches to mix with titanium metal powder ($<$ 44 μm) in the blender at a time. This mixture enables us to make four Synroc blocks of 20 mm in diameter and 10 mm in thickness. On the other hand, the residue of the calcined powder has been stored in teflon containers.

The runs of hot pressing at 1200 ^{o}C and 29 MPa for 2 h were carried out four times. The graphite mould was renewed at each run to guarantee a safe and reproducible operation during hot pressing. The Synroc blocks were ground to remove the surface skins contacting the graphite moulds. The periphery of each block was polished with #600 of grids and the flat surfaces were done with 6 um of diamond paste. After polishing, the densities of the four Synroc blocks will be measured using water displacement method.

Results up to date

The curium-doped Synroc which consisted of the simulated JW-A waste (the curium source), the precursor and titanium metal of 10.59 (1.61), 87.42 and 1.99 wt%, respectively, was prepared for the alpha radiation stability test using the calciner and the hot press in the hot cell. The Synroc slurry containing 1.48 g of the curium source (total alpha activity: 1.90 TBq) was calcined at 750 ^{o}C for 2h with very little powder carryover. The calcined product had the pour and the tap densities of 0.5 and 0.85 g.cm^{-3}, respectively. The mixture of a part of the calcined product, and titanium metal powder was hot pressed four times at 1200 ^{o}C and 29 MPa for 2 h. This process made the four Synroc blocks of 20 mm in diameter and 10 mm in thickness.

References

[1] W. J. WEBER and F. P. ROBERTS, "A review of radiation effects in solid nuclear waste forms", Nucl. Technol. **60**, 178(1983).

[2] S. MATSUMOTO, "In-cell Synroc solidification apparatus" in JAERI-M 87-131 (Eds. H. NAKAMURA & S. TASHIRO), Japan Atomic Energy Research Institute, Tokai (1987).

Table 1 Estimated assay* of 1.48 g of the curium source

Component	Content (g)	Activity (TBq)
$^{244}CmO_2$	0.714	1.89
$^{245}CmO_2$	0.011	-**
$^{246}CmO_2$	0.060	-
$^{247}CmO_2$	0.001	-
$^{248}CmO_2$	0.001	-
$^{240}PuO_2$	0.692	0.01
$^{236}UO_2$	0.001	-
[Total]	1.480	1.90

*: Values as of November 1, 1987. These are calculated on the basis of shipping data of the Oak Ridge National Laboratory, USA.

**: Symbol indicates that activity is less than 0.001 TBq.

Table 3 Composition of curium-doped Synroc

Component		Content (wt%)
Precursor		
TiO_2		62.24
CaO		9.70
ZrO_2		5.95
BaO		4.81
Al_2O_3		4.72
	[Subtotal]	87.42
Titanium (metal)		1.99
Simulated JW-A waste (oxide)		10.59
	[Grand total]	100.00

Table 2 Composition of simulated JW-A waste[1]

Component	Content (wt%)	Component	Content (wt%)
(Fission Products)		La_2O_3	2.48
SeO_2	0.10	CeO_2	4.95
Rb_2O	0.60	Pr_6O_{11}	2.43
SrO	1.66	Nd_2O_3[2]	2.24
Y_2O_3	0.98	Sm_2O_3	-
ZrO_2	8.05	Eu_2O_3	-
MoO_3	8.49	Gd_2O_3	- } 15.24
MnO_2	1.26	(U and Actinides)	as (CmO_2
RuO_2	4.78	CeO_2[3]	- +PuO_2)
Rh_2O_3	0.99	(Process Chemicals)	
PdO	2.61	Na_2O	15.60
Ag_2O	0.14	P_2O_5	1.58
CdO	0.15	(Corrosion Products)	
SnO_2	0.09	Fe_2O_3	13.05
Sb_2O_3	0.02	Cr_2O_3	1.89
TeO_2	1.11	NiO	1.65
Cs_2O	4.79	[Total]	100.00
BaO	3.07		

(1): Substitution of a JW-A waste by the curium source is carried out on a mole basis.

(2): Part of neodymium is also replaced by the curium source.

(3): Cerium was substituted for uranium, neptunium, plutonium, americium and curium in the JW-A waste.

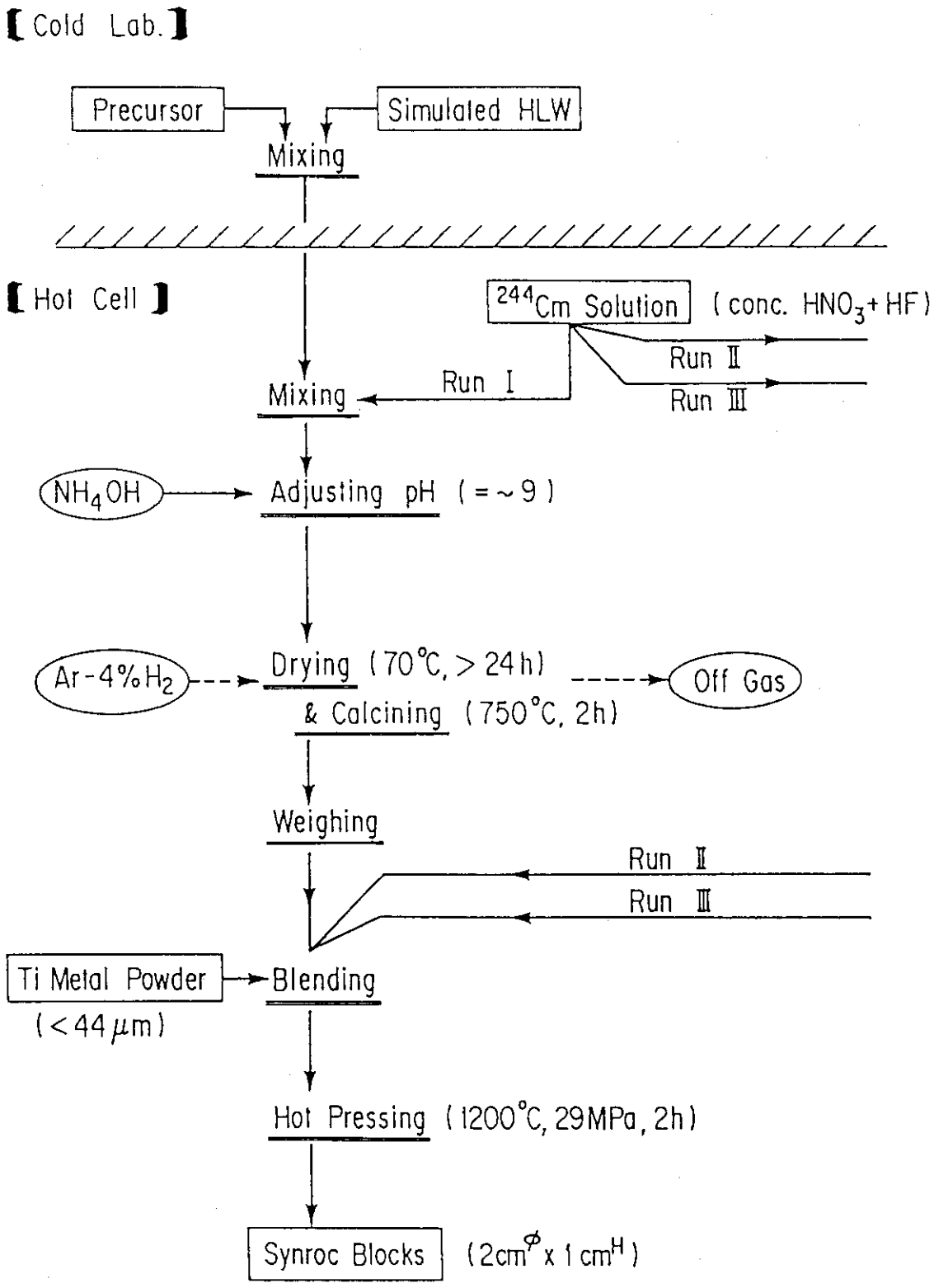

Fig. 1 Fabrication Process of curium-doped Synroc

1.3 Container

(1) Slow Strain Rate Stress-corrosion Test under gamma-ray irradiation for container materials

S. Muraoka

[Introduction]

Currently at JAERI there is an effort to evaluate the candidate material as a prime corrosion resistant material for high-level waste containers which will be emplaced in deep geologic repository. Preliminary data indicate that local corrosion such as stress corrosion cracking (SCC) is likely to present a problem with respect to failure of a container. Little information is available on possible localized corrosion failure mechanisms under gamma-ray irradiation condition. The assessment of localized corrosion mechanisms is essential for the prediction of the life time of the containers. This report outlines initial results on SCC in a simulated basalt ground water solution under gamma-ray irradiation.

[Experimental]

Slow strain rate test were performed using the tensile machine as shown in Fig. 1 in the hot cave with a Co-60 source. All tests were carried out in simulated basalt groundwater and its synthetic composition is shown in Table 1. The specimens of Type 304 stainless steel and 1020 low carbon steel were used in this investigation. The compositions are presented in Table 2 along with the condition of heat treatment. The temperature tested was 90°C. Gamma-ray irradiation dose rate was 2.8×10^4 R/hr at the test specimen. The test lasted for periods of 22 to 260 hours until failure for specimens.

[Results and Discussion]

Fig. 2 shows the stress-strain curves of Type 304 stainless steel and 1020 carbon steel under gamma-ray and non-irradiation respectively. To evaluate the susceptibility of SCC we applied the concept of SCC susceptibility index developed by Okada[1]. The material susceptible to SCC shows the decrease of rupture strain due to crack propergation.

The proposed index of susceptibility to SCC is expressed as follows:

$$I_{scc} = \frac{P_b(\varepsilon_b+1)}{P_o(\varepsilon_o+1)}$$

where P_b is maximum load (tested in basalt ground water)

ε_b is maximum tensile strain at the maximum load (tested in basalt ground water)

P_o is maximum load (tested in oil)

ε_o is maximum tensile strain at the maximum load (tested in oil).

I_{scc} value becomes smaller according to the SCC susceptibility. In the case of non-susceptibility to SCC the values shows unit. To obtain the data of P_o and ε_o, SCC tests were carried out in the oil at 90°C under the non-irradiation condition. The results are summarized in Table 3. I_{scc} value of low carbon steel shows nearly unit. This suggests carbon steel is not susceptible to SCC in the experimental condition. On the other hand Type 304 stainless steel shows I_{scc} value of smaller than 1.

The result shows the enhancement of SCC susceptibility by gamma-ray irradiation.

Reference

(1) H. Okada, Y. Hoshi, S. Abe and S. Yamamoto; J. Inst. Metals 38 (1974) 646

Table 1 Composition of synthetic basalt groundwater.

Chemical Species	mg/l
Na^{+}	393
K^{+}	4.14
Ca^{2+}	0.26
Mg^{2+}	0.009
F^{-}	38.7
Cl^{-}	389
SO_4^{2-}	160

Table 2 Chemical composition and heat treatment of test materials.

Alloy	Composition (%)								
	C	Si	Mn	P	S	Cu	Ni	Cr	Fe
Carbon Steel	0.20	0.25	0.40	0.016	0.017	0.13	0.05	0.08	Bal
SUS 304ss	0.06	0.29	1.37	0.034	0.022	--	8.09	18.21	Bal

Heat Treatment

700°Cx100min heating⟶Air cooling⟶

500°Cx24hr Air cooling⟶Air cooling

Table 3 Result of stress corrosion cracking test.

Steel	Environment		P (Kg)	ε	I scc
	Solution	γ -ray			
Carbon Steel 1020	Basalt water	Yes	211	0.202	1.06
	Basalt water	No	216	0.207	1.09
	Oil	No	204	0.168	—
Typ304 Stainless Steel	Basalt water	Yes	213	0.230	0.60
	Basalt water	No	247	0.492	0.84
	Oil	No	257	0.707	—

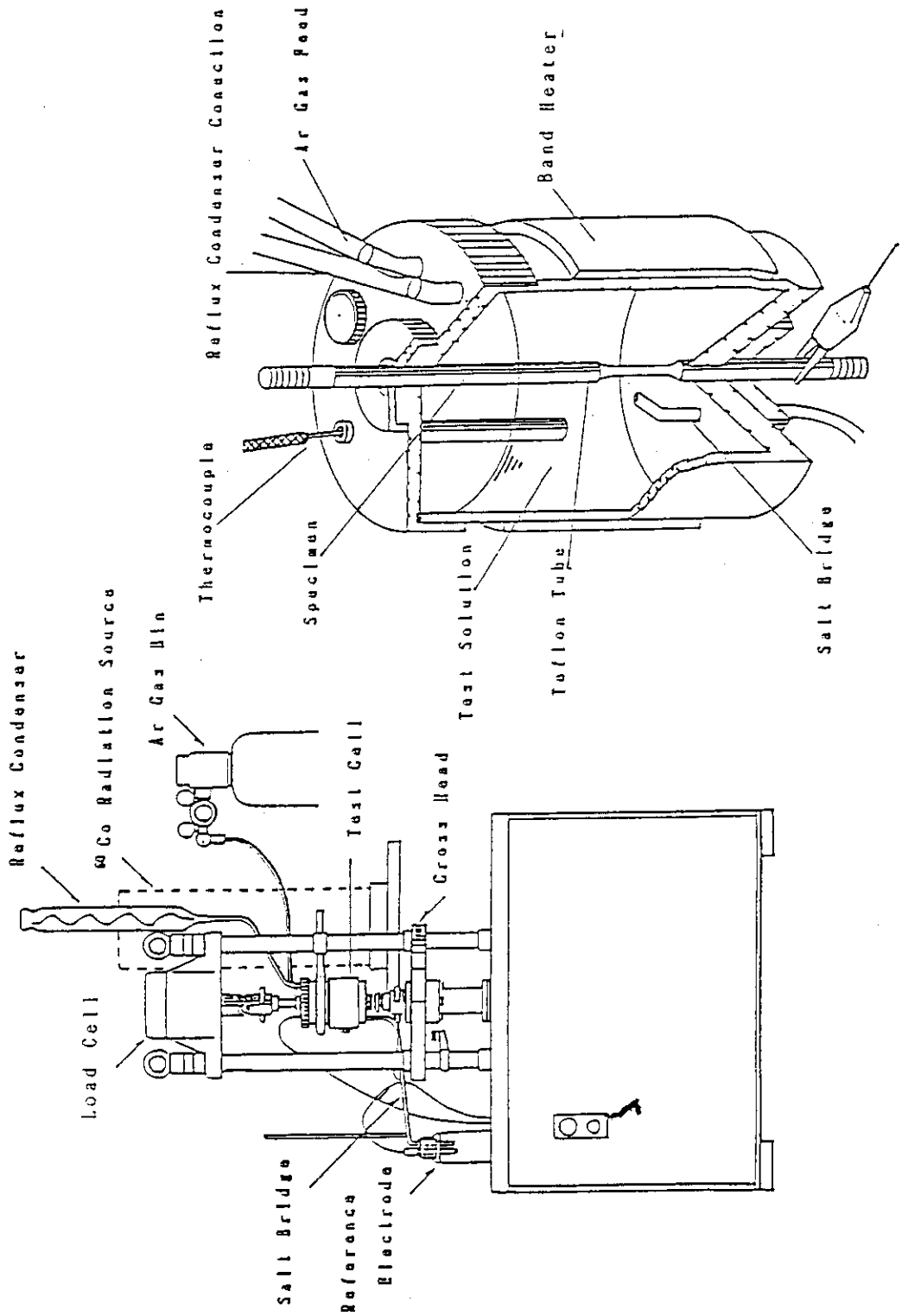

Fig. 1 Slow strain rate test equipment.

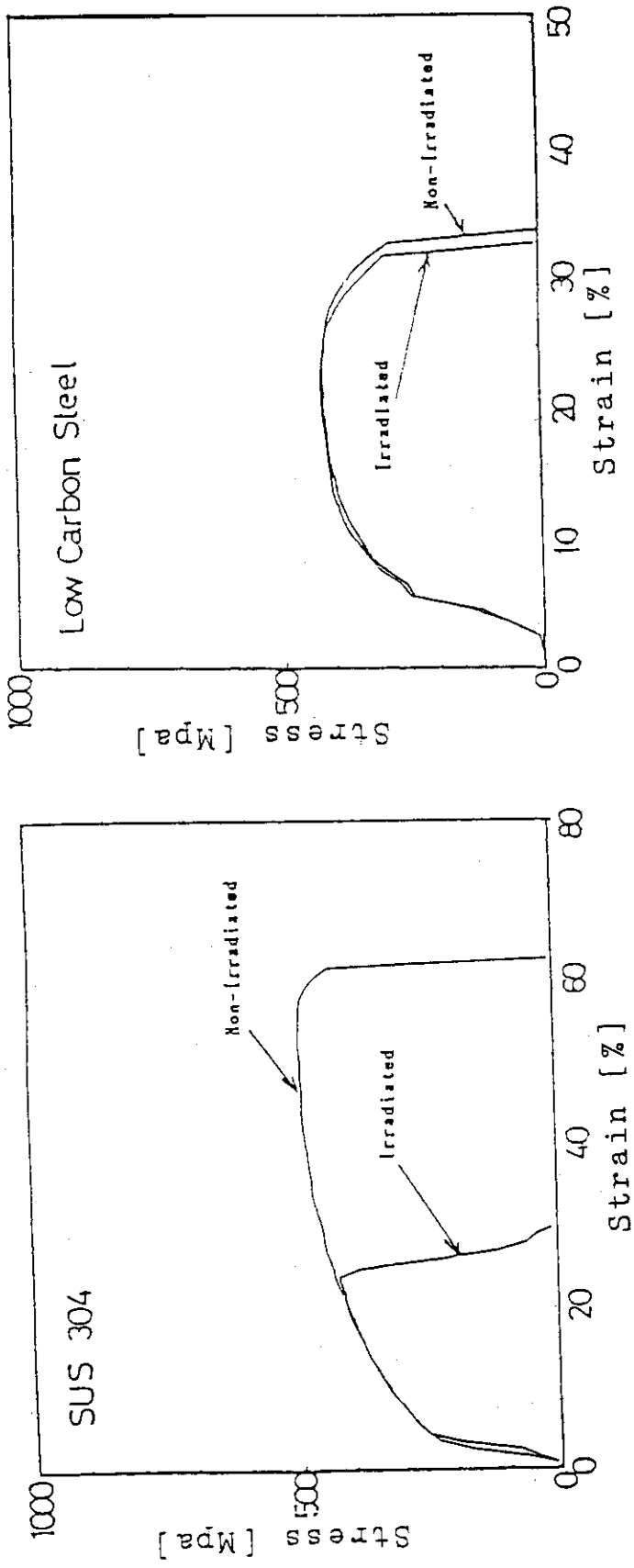

Fig. 2 Stress-strain curves of Type 304 stainless steel and 1020 carbon steel.

(2) Experiment to evaluate integrity of high-level waste canister in the high-pressure water tank

T. SUZUKI

Introduction

The effect of external static pressure on the high-level waste canister was examined by using the high-pressure water tank.

The purpose of this test is to evaluate the integrity of a canister throughout the canister handling and disposal.

In this test, the deformation of simulated high-level waste canister was observed by increasing the hydraulic pressure gradually.

Experimental

The tested canister was made of Type 304 stainless steel and was in the form of typical canister as shown in Fig. 1. In the canister, the concrete was filled to simulate the vitrified waste, and 16 strain gages (triaxial 0°, 45°, 90° crossing or biaxial 0°, 90° crossing gage) were provided on its outer surface axisymmetrically as shown in Fig. 2, to measure strain changes due to the hydraulic pressure increase.

The deformation of the canister was proved to be axisymmetric by analyzing the strain data from one radial of strain gages (gage No. ①, ②, ③, ④ as shown in Fig. 2).

A couple of principal stresses can be calculated as follows:

$$\varepsilon_1 = \frac{\varepsilon_o+\varepsilon_{90}}{2} + \sqrt{\left(\frac{\varepsilon_o+\varepsilon_{90}}{2}-\varepsilon_{45}\right)^2+\left(\frac{\varepsilon_o-\varepsilon_{90}}{2}\right)^2}\ , \tag{1}$$

$$\varepsilon_2 = \frac{\varepsilon_o-\varepsilon_{90}}{2} \sqrt{\left(\frac{\varepsilon_o+\varepsilon_{90}}{2}-\varepsilon_{45}\right)^2+\left(\frac{\varepsilon_o-\varepsilon_{90}}{2}\right)^2}\ , \tag{2}$$

$$\sigma_1 = E \cdot \frac{\varepsilon_1+\nu\cdot\varepsilon_2}{1-\nu^2}\ , \tag{3}$$

$$\sigma_2 = E \cdot \frac{\varepsilon_2+\nu\cdot\varepsilon_1}{1-\nu^2}\ , \tag{4}$$

where $\varepsilon_1, \varepsilon_2$: principal strain (-)

$\varepsilon_o, \varepsilon_{45}, \varepsilon_{90}$: observed strain (-)

σ_1, σ_2 : principal stress (kgf/mm^2)

E : modulus of elasticity (kgf/mm^2)

ν : Poisson's ratio (-).

According to Mises-Henkey theory of the biaxial stress condition, materials yield when its stress condition satisfies the next equation:

$$\sigma_1^2 - \sigma_1 \cdot \sigma_2 + \sigma_2^2 = \sigma_s^2 \ , \qquad (5)$$

where σ_s : uniaxial tensile strength (kgf/mm^2).

σ_s and E were determined previously to be 14.6 kgf/mm^2 and 18114 kgf/mm^2, respectively, from another uniaxial tensile strength tests, and ν was assumed to be 0.24 that equals to the average value of Type 304 stainless steel.

Calculated values of Σ ($= \sigma_1^2 - \sigma_1 \cdot \sigma_2 + \sigma_2^2$) versus hydraulic pressures are plotted in Fig. 3, and the yielded hydraulic pressures were determined by the intercept of the curve and the line of $\Sigma = \sigma_s^2 = 14.6^2 = 213.2$.

Results

The result shows that the plenum of tested canister was yielded by hydraulic pressure from 0.37 Mpa to 1.32 Mpa gradually and axisymmetrically. Meanwhile, as shown in Fig. 4, a sudden hydraulic pressure decrease was observed in the course of increasing hydraulic pressure at the point A due to the large and radical deformation at the hydraulic pressure of 1.46 Mpa. Fig. 5 shows the outer shape of the canister after the test.

It was confirmed that the plenum is the most weak part of the canister. It should be noted that large and radical deformation caused the residual stress and then it can cause stress corrosion cracking (SCC) after the deep underground disposal.

The plenum should be protected to prevent the defomation and the occurrence of SCC.

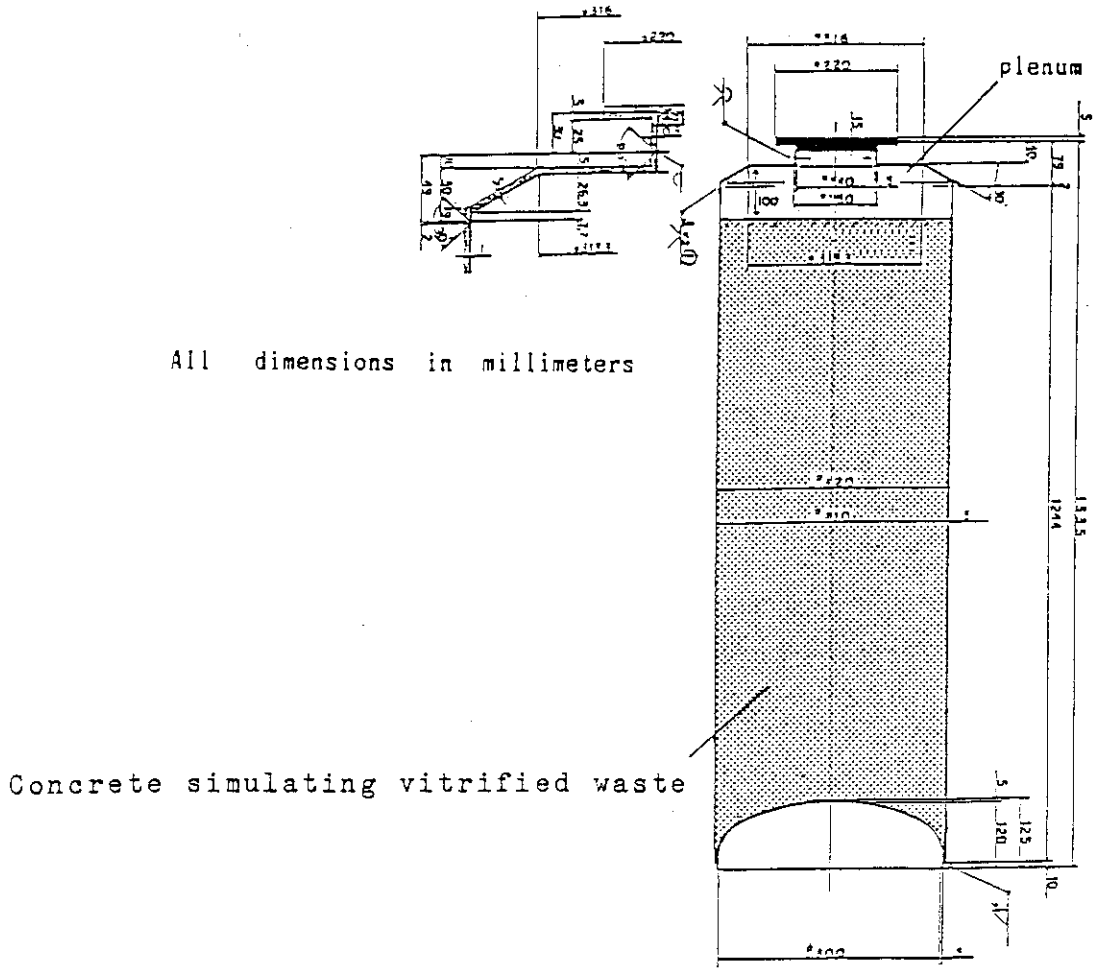

Fig. 1 General view of simulated canister

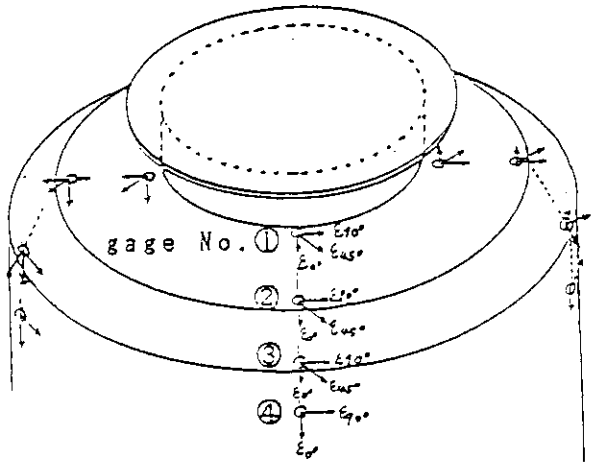

Fig. 2 Schematic distribution and designation of the strain gages and the strain directions

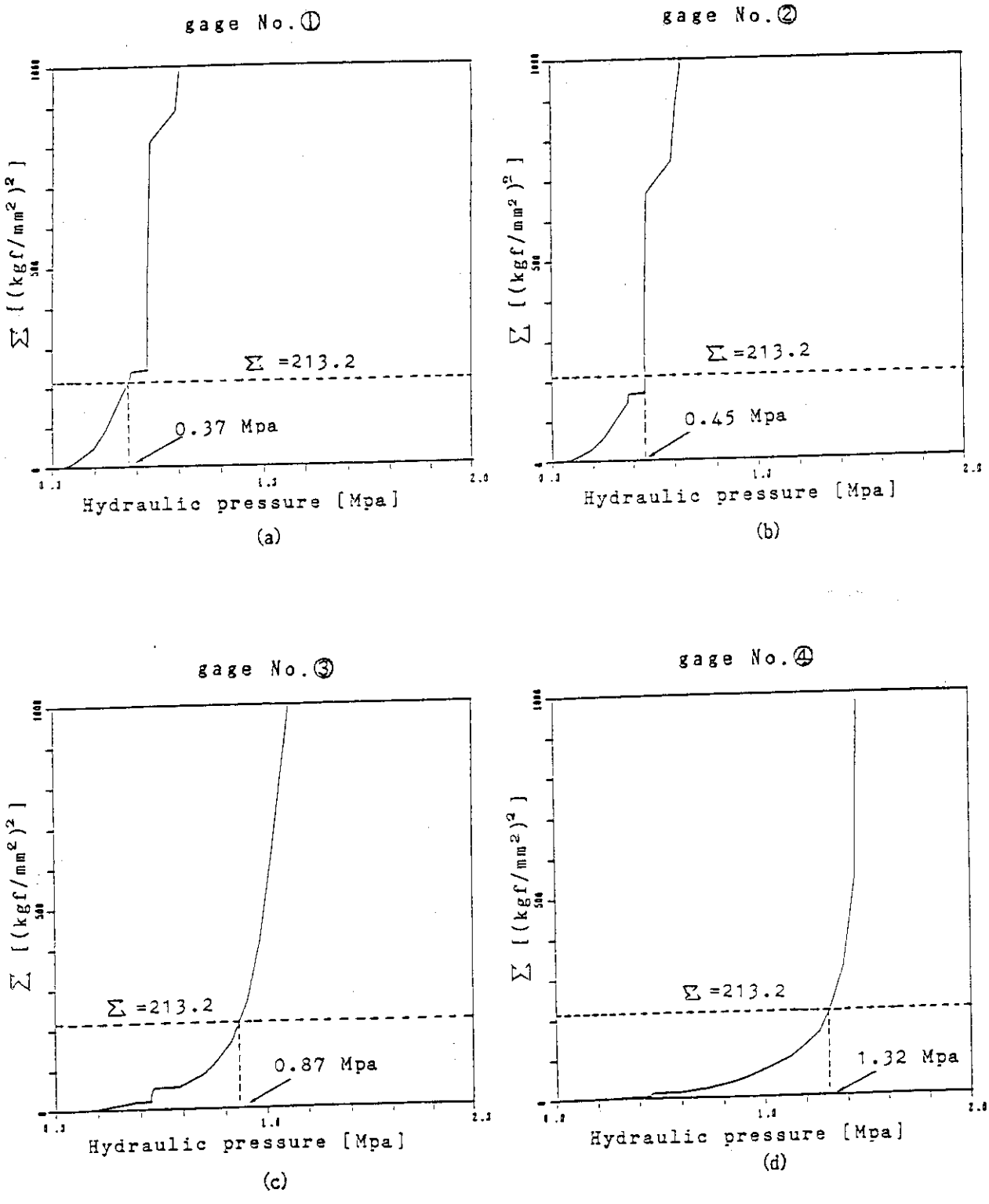

Fig. 3 Σ-hydraulic pressure curve and yield pressure

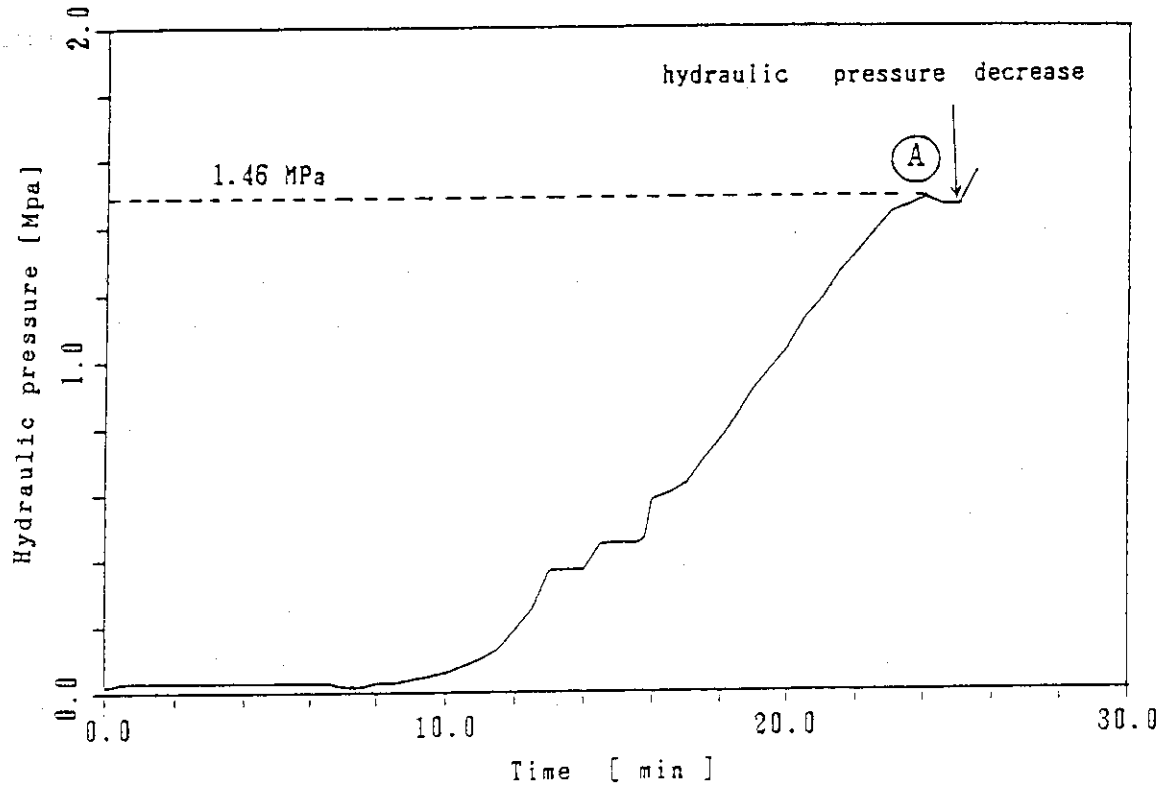

Fig. 4 Hydraulic pressure versus time.

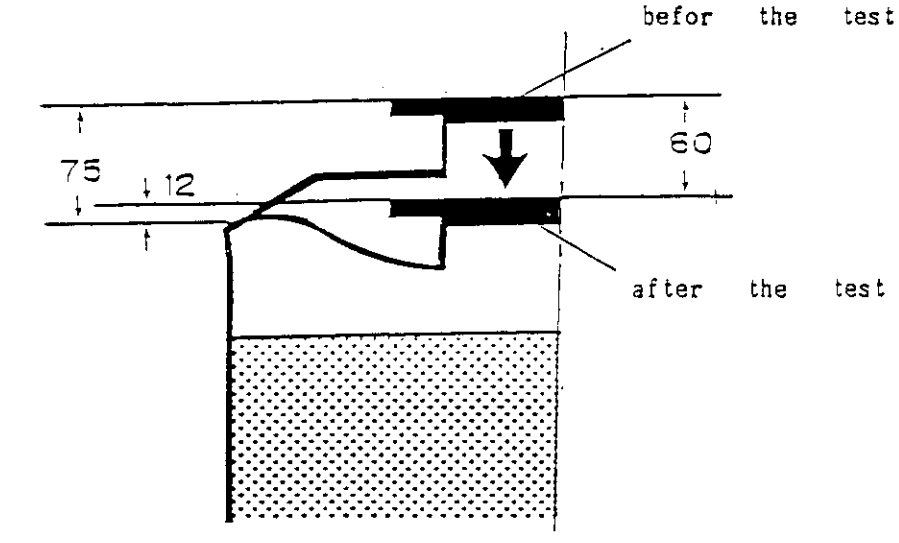

All dimensions in millimeters.

Fig. 5 Schematic representation of the canister after the test.

2. Safety Evaluation for Geological Disposal

S. Muraoka

An extensive R and D has been carried out for the long term assessment of the geological disposal of high-level waste. The research activities for the present period are as follows;

Diffusion of non-sorbing iodide ions in granite and tuff was studied.

Sorption of ^{237}Np on rock samples was studied by autoradiographic method using thin granitic rocks.

Behavior of iron during weathering has been examined by analysing the naturally weathered rock.

In-situ bore hole radar measurement techniques have been developed to investigate the locations of fracture zone in granitic rock mass.

CRNL information was reviewed for nuclide migration modeling.

As a natural analogue study, infrared microspectroscopy was applied to minerals in order to analyse a hydrated surface layer to get information of water-rock interactions.

The computer code LEACH2DF was developed to quantify the disolution of nuclide waste glass and HYDROCOIN level-3 problems were tuckled by using 2D-SEEP and 3D-SEEP.

Safety assessment scenario was discussed for preclosure and postclosure phase respectively.

2.1 Nuclide migration and retardation in rocks

(1) Porosities and diffusion coefficients of iodide anion in rocks

H. Kita

Introduction

In the case of diffusion of non-sorbing radionuclides in rocks having no major fractures, diffusivities of the radionuclides can be correlated closely with porosities of rock matrixes. Measurements of porosity and diffusion coefficients were conducted on samples of granites from Inada, tuffs from Izu and schists from Iwaki. Based on the results, the correlation between the porosity and the diffusion coefficient has been studied.

Experimental

A. Porosity measurement

The rock pieces (ϕ40 × 100 mm) are put into a vacuum chamber filled with water. After 72 hours the pieces are weighed in water (the water saturation weight in water; W1). The surfaces of the pieces are wiped off with wet cloths. The pieces are then weighed in the air (the water saturation weight in the air; W2). After keeping the pieces at 110°C in a drying oven for 24 hours, they are cooled in a vacuum desiccator. The dry pieces are weighed (the dry weight; W3). The value of porosity can be calculated based on measured three different weights.

$$\text{porosity} = (W2-W3)/(W2-W1)$$

B. Diffusion experiment

The diffusion experiments were conducted on rock samples (ϕ = 25 mm, L = 5 mm), using 1M KI solution as a source of iodide anion(I^-). The method was in principle the same as that has been used previously by KITA et. al. (1987)[1] and by other investigators (see, for examples, SKAGIUS and NERETNIEKS, 1986[2]). For schist samples, two types of sample are prepared, one is set in the diffusion cell having schistosity parallel to the diffusion direction, another having schistosity perpendicular to the diffusion direction.

Results and discussion

The concentrations of iodide anion which has diffused through rock samples are plotted on a normal diagram as a function of time. The curves

can be fitted to straight lines by the asymptotic solution of the diffusion equation:

$$C_2 = (D_e\ C_1\ A\ /\ V\ L)\ t - A\ L\ C_1\ /\ 6\ V\ ,$$

where D_e is the effective diffusion coefficient, C_1 the concentration in the reservoir, C_2 the concentration in the measurement cell (with $C_2 \ll C_1$), A the cross-sectional area of the rock sample, L the sample thickness, V the volume of distilled water in the measurement cell and t the time. The rock capacity factor α is defined here by

$$\alpha = \varepsilon + \rho\ Rd$$

with the porosity ε, the density of rock ρ and the distribution ratio Rd. D_e can be obtained from the slope of the fitted straight line (KITA et. al., 1987[1]; SKAGIUS and NERETNIEKS, 1986[2]).

Correlation between porosities and effective diffusion coefficients of iodide in granites and gneisses from Sweden, which have been obtained by SKAGIUS and NERETNIEKS (1986)[2] are plotted on a logarithmic diagram in Fig. 1. The straight line in Fig. 1 is a fitted line of their data by a least-squares method. Results on the present study are also plotted on the same diagram. The points for the granite and tuff samples obtained in this study are located roughly on the extension of this fitted line. The effective diffusion coefficient at the zero point of log porosity given by the further extended line is 6.4×10^{-10} m^2/s. This value is close to the reported value about 2×10^{-9} m^2/s of diffusion coefficient of iodide anion in water (WADDEN and KATSUBE, 1983[3]).

However, for schist samples there is a large difference in effective diffusion coefficients between two types of sample in spite of the same porosity. This difference can be readily understood by the fact that diffusion of iodide anion will be much easier along the linear structure of rocks (schistosity) than perpendicular to it.

The empirical logarithm-linear correlation is useful to estimate diffusion coefficients of the iodide anion in homogeneous porous rocks such as tuffs. However, in the case of rocks having oriented structures such as schistosity, a careful consideration should be paid to the structure of rocks as well as the porosity.

References

(1) KITA, H., IWAI, T. and NAKASHIMA, S. (1987): Diffusion of ions in rock pore water, Collected papers presented at the Annual Meeting of the Japan Society of Engineering Geology, Oct. 1987, pp.45-48.

(2) SKAGIUS, K. and NERETNIEKS, I. (1986): Porosities and diffusivities of some nonsorbing species in crystalline rocks, Water Resource Research, Vol. 22, No. 3, pp.389-398.

(3) WADDEN, M.M. and KATSUBE, T.J. (1982): Radionuclide diffusion rates in igneous crystalline rocks, Chem. Geol., Vol. 36, pp.191-214.

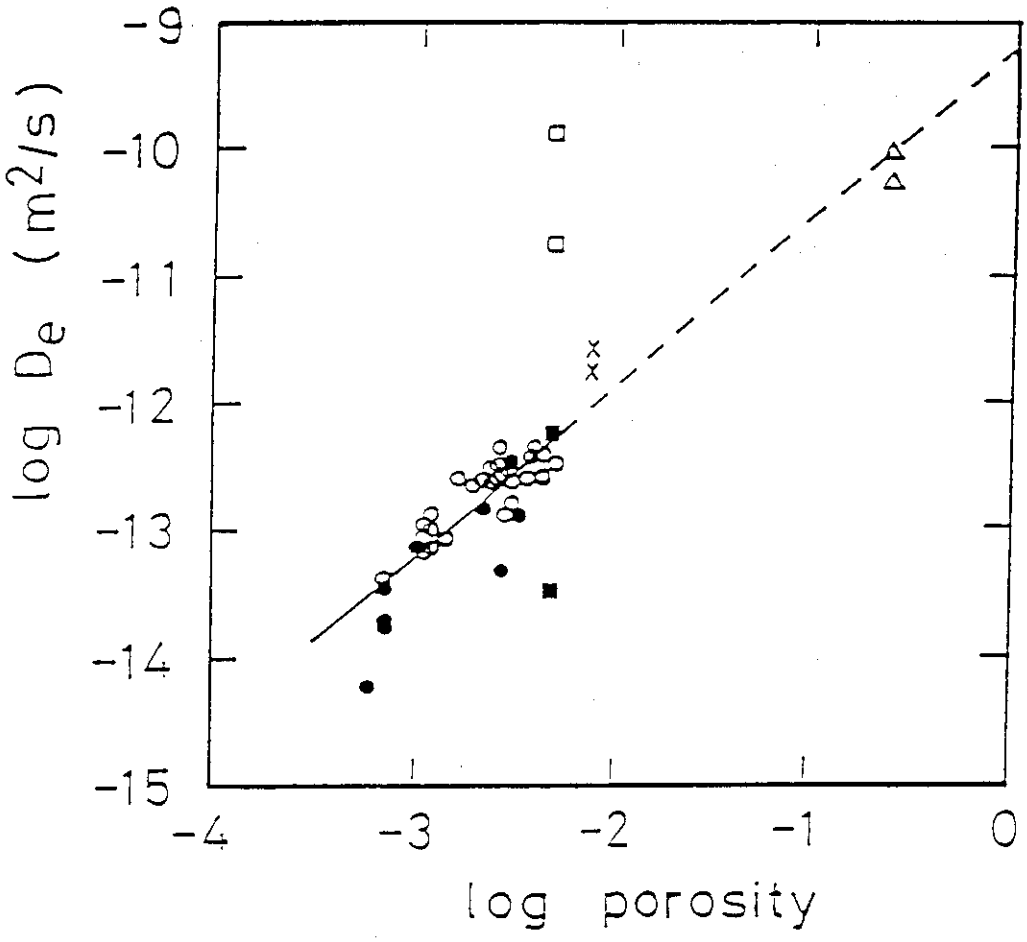

Fig. 1 Correlation between the effective diffusion coefficient and the porosity.
○: granite from Sweden; ●: gneiss from Sweden (SKAGIUS and NERETNIEKS, 1986), ×: granite from Inada; △: tuff from Izu; □: schist from Iwaki whose schistosity is parallel to the diffusion direction; ■: schist from Iwaki whose schistosity is perpendicular to the diffusion direction (this study).

(2) Sorption of ^{237}Np on thin sections of granite

M. KUMATA

Introduction

In order to evaluate natural barriers to radionuclide migration in groundwater, radionuclide sorption properties of various rocks have been studied. The rock samples studied are complex polymineralic materials, and variations in mineral composition of rocks can lead to large differences in sorptive properties between rocks. These complexities can lead to difficulties in the interpretation of the laboratory sorption measurements.

Several qualitative autoradiographic experiments on rock thin sections were carried out to identify the specific phases in granite which were responsible for the sorption of ^{237}Np, one of the long-lived radionuclides.

Experimental

The granite used in this study was Inada granite. Thin sections of the granite, about 25 × 25 mm square and about 30 micron thick, were prepared with a surface ground to a 1/2 micron finish. The thin sections were observed under a polarization-microscope and analysed petrographically. The areas of the thin sections to come in contact with the radionuclide-tagged solutions were delineated with a black hydrophobic ink, which prevents the radioactive solutions from spreading beyond the marked area.

Natural groundwater was used in the sorption studies. The composition of the groundwater is shown in Table 1. A radionuclide solution including about 18 μCi was added to 500 ml pre-filtered groundwater (through a 0.45-micron Millipore) and left to equilibrate with air for about one month. 0.7 ml of the spiked groundwater was dropped on the thin sections. These thin sections were placed in plastic chambers. The chambers were filled with deionized water to provide a humid atmosphere.

After a 48-hr contact period, aliquots of the spiked groundwater solutions were removed. Then the surface of the thin sections were rinsed with deionized water. The remainder of the solution was removed with filter papers and the thin sections were dried in air.

Two types of solid state nuclear track detector were used in this study. They were CR-39 (Solar Optical Japan Co.) and Kodak CN-85. CR-39 is a plastic plate about 5 mm thick. Kodak CN-85 is a thin cellulose nitrate film. These detectors can be exposed under ordinary room light. The detectors were exposed to the "cold" thin sections for one week to determine

if any natural activity was associated with individual mineral grains. However no natural activity was detected.

The exposure consisted of placing the thin section with the detector for an appropriate period of time. To prevent transfer of sorbed radionuclide from the thin sections to the detectors, the thin sections were wrapped up with a mylar film. After exposure, the detectors were developed according to the manufacturer's instructions.

Results and Disscussion

Photomacrographs of a granite thin section are shown in Fig. 1. However photomacrographs of the thin section are close-up photographs, and these two photographs indicate different information. Fig. 1(a) is originally a coloured photograph. This photograph emphasizes locations of biotite. On the other hand, Fig. 1(b) is originally positive. In this photograph, grain boundaries and microcracks of minerals are optically emphasized.

Autoradiographs of ^{237}Np sorbed on the granite thin section are shown in Fig. 2. The low magnification photograph of the autoradiograph (Fig. 2(a)) is positive, so the bright areas in the photograph indicate the locations of the sorbed radionuclides. The high magnification photograph is negative, so the dark spots indicate each alpha track. Autoradiographs of ^{237}Np indicate preferential sorption on the biotites in comparison with the feldspars and quartzs.

In the solutions employed for these studies, the Np is expected to exist as the NpO_2^+ cation. Generally, it is known that biotite contain Fe(II) in the crystal structure. It suggested that the mechanism of sorption most likely involves reduction of NpO_2^+ to the much less soluble Np(IV) by Fe(II). One possibe sorbed Np state is NpO_2 solid phase reduced by the following reaction.

$$NpO_2^+ + Fe^{++} \rightarrow NpO_2 + Fe^{+++}$$

There is some background sorption on the quartz and feldspar. This background sorption might be connected with the electric double layer on the surface of these minerals.

Further, there are many bright lines in Fig. 2(a). These lines correspond to the grain boundaries of quartz. Fig. 3 is a secondary electron image showing grain boundaries among quartz grains. It suggests

that ^{237}Np is trapped in the grain boundaries ditches. If radionuclides migrate through intact rock, grain boundaries are most important as a path for the grain boundary diffusion. However, further examinations are necessary and the autoradiograph method is expected to be a useful technique for the study of grain boundary diffusion.

Table 1 Chemical composition of groundwater (ppm*)

DO	pH	COND.	NH_4	Na	K	Ca	Mg	Fe**	Mn**	Cr**
9.31	8.4	125	<0.1	19.2	0.7	5.5	<0.1	<0.1	<0.1	<0.1
Ni	Al	HCO_3	SO_4	Cl	NO_3	PO_4		Si**	Si***	BOD
<0.1	<0.1	47	8.3	4.7	0.7	<0.5		7.0	6.9	<5

* except pH and cond.
** total
*** dissolved

(a)

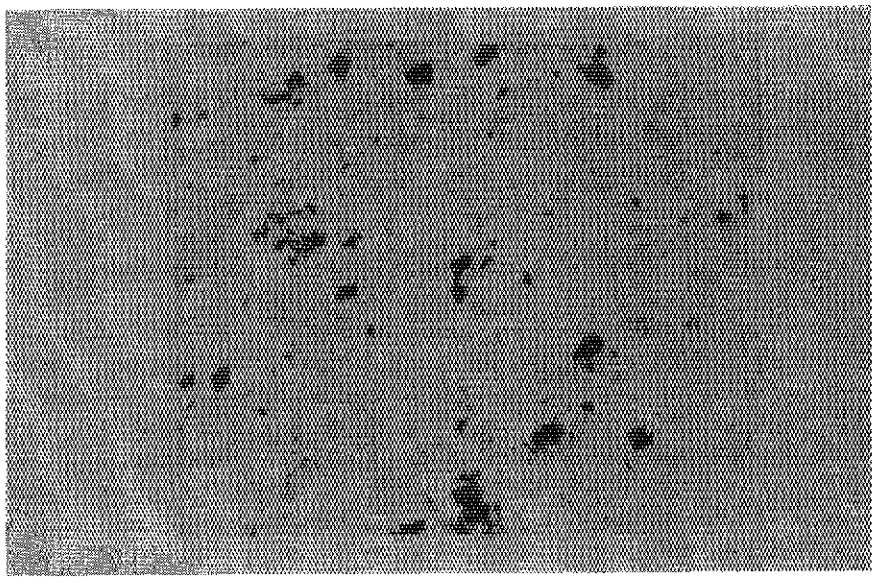

(b)

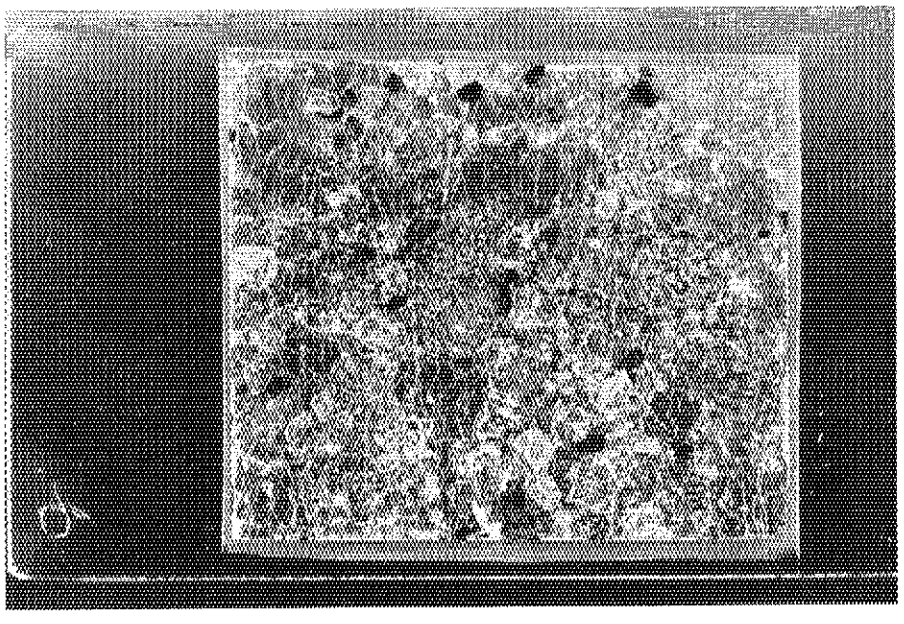

Fig. 1 Photomacrographs of the thin section of granite.
(a) originally coloured photo; indicate the location of biotite
(b) positive photo; emphasized grain boundaries and microcracks

(a)

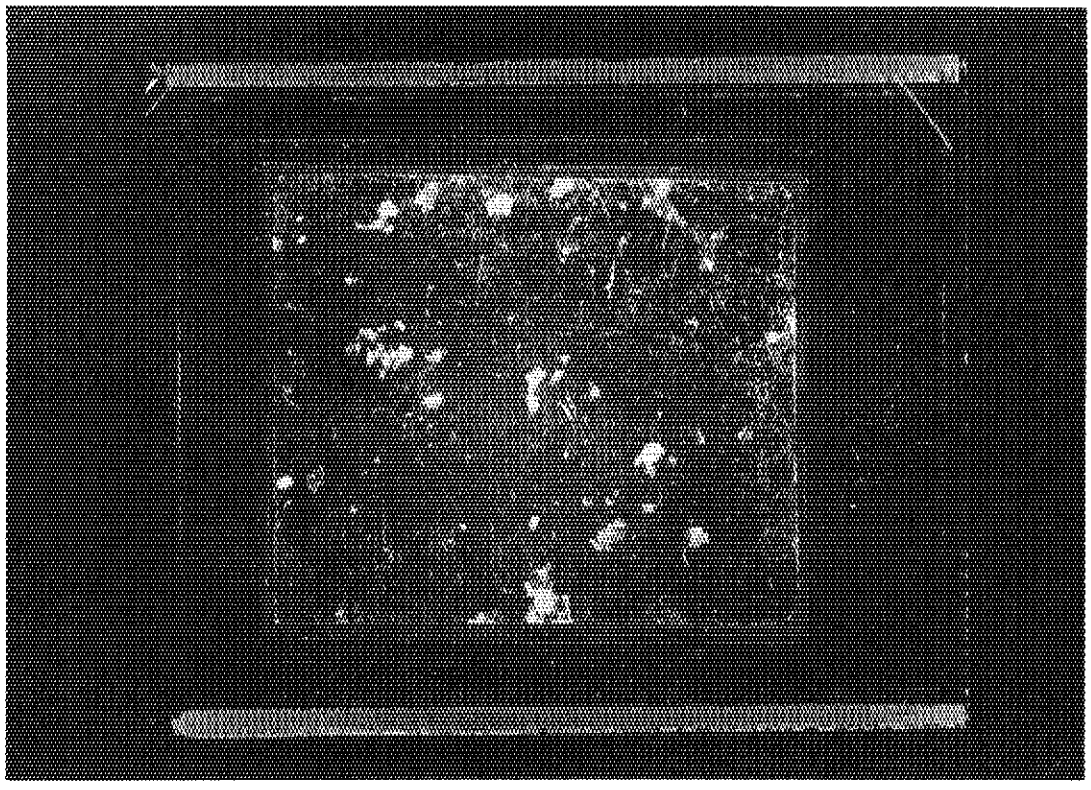

(b)

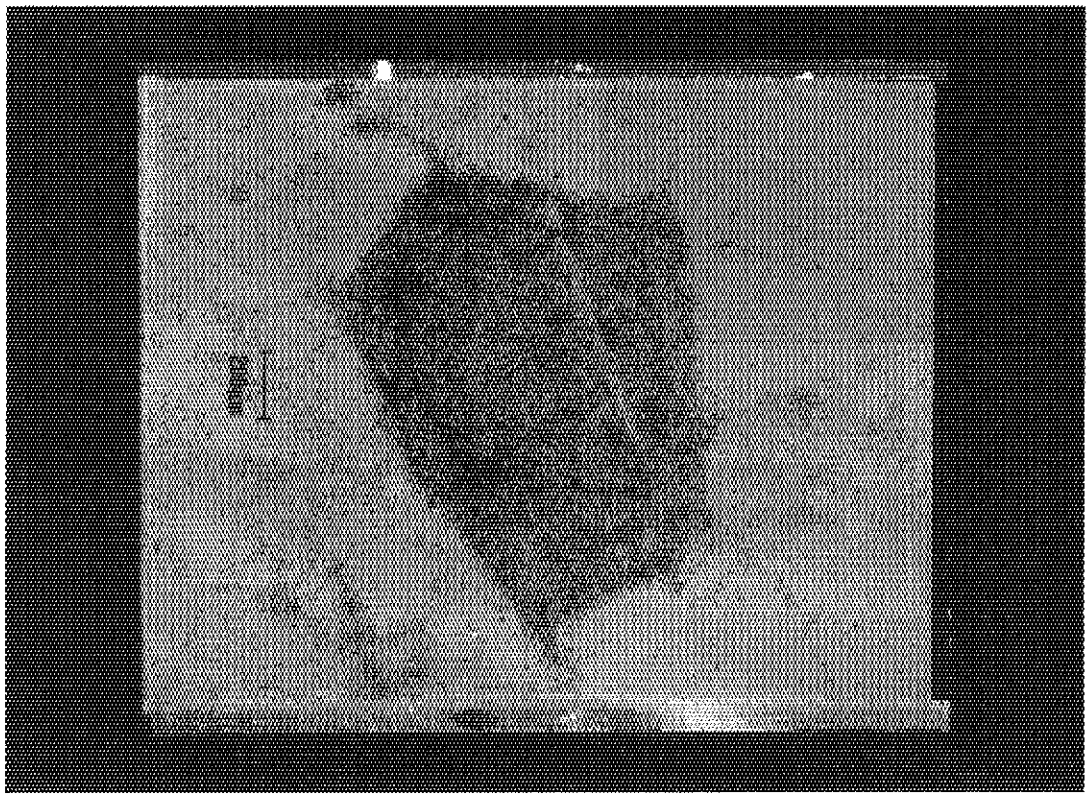

Fig. 2 Autoradiographs of ^{237}Np sorbed on the granite thin section
(a) low magnification photo; positive
(b) high magnification photo; negative

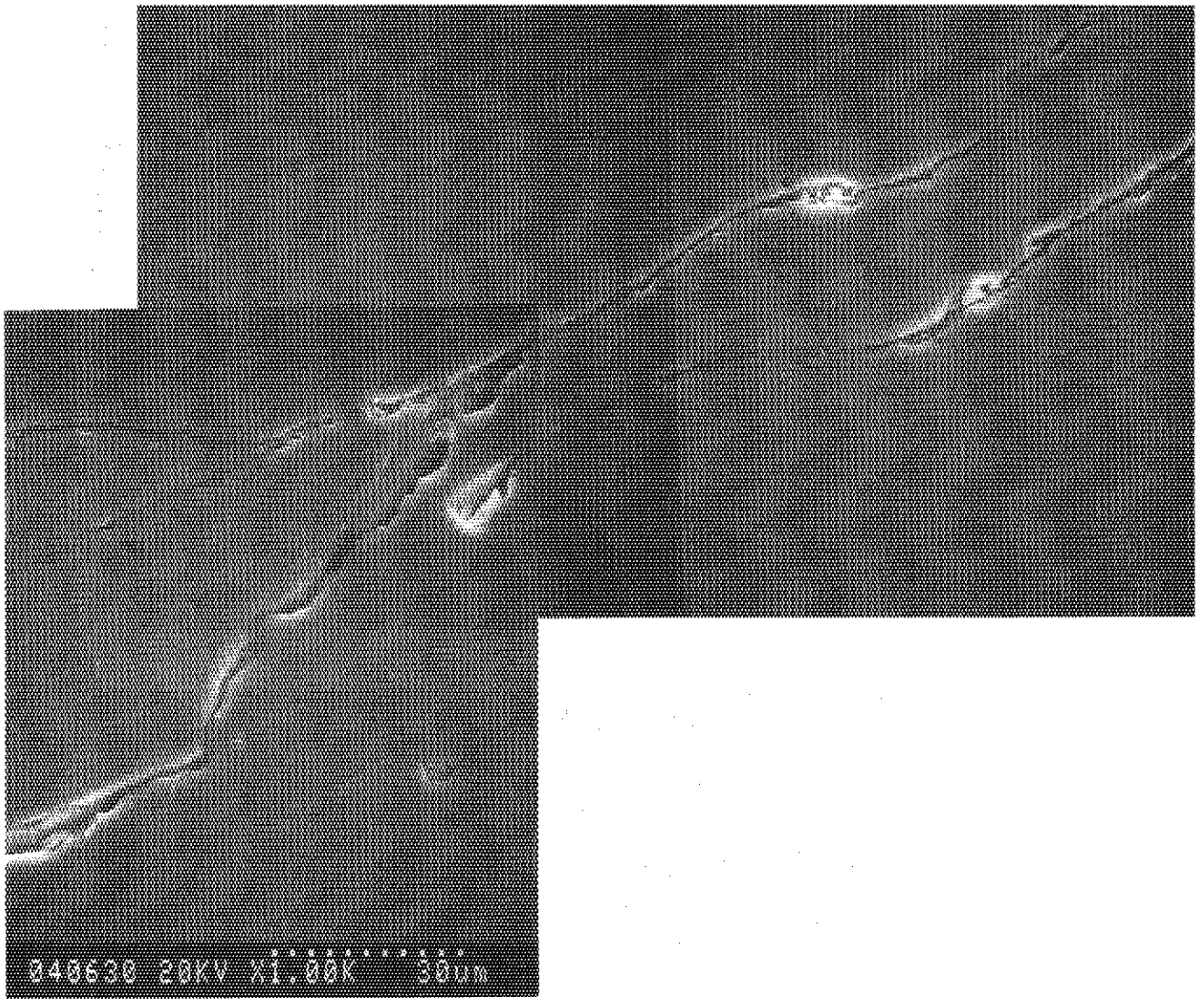

Fig. 3 Secondary electron image of grain boundaries among quartz grains.

(3) Behavior of iron during weathering of a granitic rock

T. Nagano

Weathering is a phenomenon that rocks are altered by surface water for a long period. In this study, weathered granitic rocks were analyzed with a special reference to behavior of iron during weathering. Granitic rock samples were collected from a cliff near Mizunuma Dam, Kita-ibarakishi, Ibarakiken, Japan. This cliff can be classified into three major weathering zones, A, B and C [1]. The weathering degree increases in the order of A, B and C.

X-ray powder diffractometry (XRD) reveals that the rocks are composed of four major mineral phases, namely quartz, biotite, microcline and albite and that the peak height of biotite decreases as the weathering degree increases. Quantitative XRD analysis using internal standard method permits the determination of biotite content in bulk rocks. The result is shown in Fig. 1. The biotite content clearly decreases as the weathering degree increases, and this fact can be understood by the increasing dissolution of biotite in a geological time scale. The decrease of biotite content in bulk rocks can be taken as an indicator of the weathering degree.

A rock sample from the highly weathered zone (C zone) appears more reddish and yellowish than that from less weathered zone (A zone) with the naked eye. Stereomicroscopic images of the samples from the three different weathering zones show that brown parts around biotites, which can be seen more widely in an image of the high-weathered rock, are origins of the reddish tone of color. Moreover, an analysis by scanning electron microscopy equipped with energy dispersive X-ray analyzer (SEM-DEX) shows that these brown parts contain only Fe among elements heavier than Na. These are then considered to be iron oxides or hydroxides.

The color of rock powders from each weathering zone was measured by means of diffuse reflection method [2]. The result is shown in Fig. 2. A weak broad peak in the wavelength of 480-500 nm region appears to increase its absorbance as the weathering degree increases. The peak areas of this region are calculated and shown in Fig. 3. In this figure, the peak area of C zone is takne as 1. The increase of the peak area of 480-500 nm region due to the weathering is now obvious. This peak can be considered to be due to iron-bearing oxides (hematite), hydroxides (goethite) or amorphous materials [3].

Based on the above results, the following hypothesis can explain the behavior of iron during the granite weathering: iron in biotite was dissolved into surface water and then precipitated as iron-bearing minerals around biotite. Since iron can be regarded as an indicator of behavior of a part of radionuclides which are often coprecipitated with iron hydroxides, this study provides some quantitative parameters, such as dissolution and precipitation rates, for the radionuclide behavior during low temperature water-rock interactions.

References

1. Kunori, S., Abe, M. and Saito, T., Study of weathering of granitic rocks(1), Butsuri-Tanko, Vol.24, No.1, 6-17, 1971.
2. Mamiya, M., Techniques of absorption spectroscopy; (2) Diffuse reflectance spectroscopy, Bunkokenkyu, Vol.25, No.2, 99-115, 1976.
3. Hofmeister, A.M. and Rossman, G.R., Determination of Fe^{3+} and Fe^{2+} concentrations in feldspar by optical absorption and EPR spectroscopy, Physics and Chemistry of Minerals, Vol.11, 213-224, 1984.

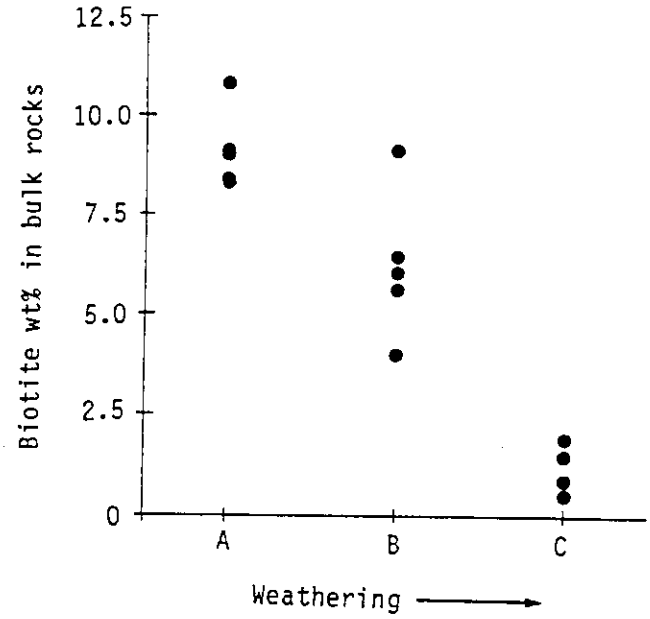

Fig. 1
Decrease of biotite content in weathered granitic rocks revealed by quantitative X-ray powder diffractometry.

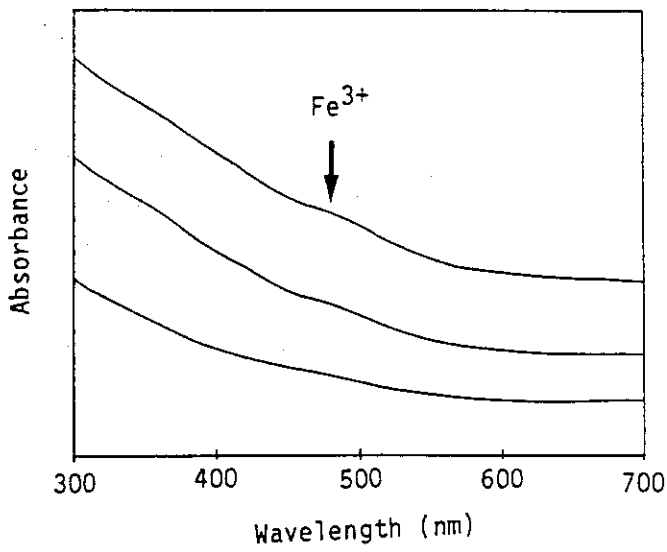

Fig. 2
Ultraviolet-Visible diffuse reflection spectra of bulk rock powders of weathered granitic rocks. A weak broad peak in 480-500 nm region increases following the weatheing. This peak is considered to be due to iron-bearing oxides, hydroxides or amorphous materials.

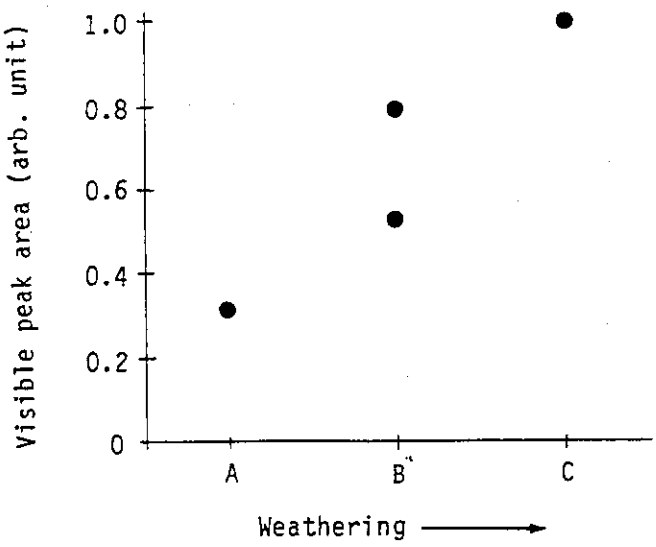

Fig. 3
Peak areas in 480-500 nm region of ultraviolet-visible spectra of powdered granitic rocks from A, B and C weathering zone. The area increases as the weathering degree increases.

(4) Field test (Borehole radar investigation)

R. Yamashita

Fracture zones are thoght to be main paths of radionuclide migration in crystaline rock masses. For the purpose of investigating locations and inclinations of fracture zones, the borehole radar measurement technique has been developed. Preliminary in-situ experiment was carried out at Inada quarry to estimate the possibility of this method.

Measuring system

There are two kinds of measurements using borehole radar. One is the crosshole measurement, another is the singlehole reflection measurement. The formar one was performed at the site. The schematic diagram of the crosshole measurement is shown in Fig. 1. Antennas of 80 MHz and 150 MHz were used.

Computed tomography

In crosshole measurements, a lot of paths covering the area surrounded by two boreholes are used. Travel time and attenuation of electromagnetic wave were determined from the recorded wave forms, and used as input data for tomography analysis. Reconstruction of the distribution of velocity and attenuation rate in surveyed area was made by means of computed tomography technique. Discretized equations for radar tomography are as follows.

$$Ti = Dij/Vj \tag{1}$$

$$\ln(Ai) = -Dij/Bj \tag{2}$$

where Ti : travel time measured at path-i
Vj : velocity of element-j
Ai : relative amplitude measured at path-i
Bj : skin depth of element-j
Dij : length of element-j crossed by path-i
i : path number
j : element number

The simultaneous equations are solved by ART (Algebraic Reconstruction Technique).

Experimental

Measurements were performed for four cross sections (B1-B2, B2-B3, B3-B1, L3-L4) (Fig. 2). The examined rock masses consists of granite and a vertical fracture zone was observed on the floor of the test chamber. One of the results of computed tomography analysis is shown in Fig. 3. It is hard to say that the fracture zone observed at the floor was successfully represented in the reconstructed picture. One of the reasons for this is that the reconstruction is difficult when a fracture zone has a small angle to the borehole axies and properties of rock do not have large variation along the boreholes. But as the result of the measurements, it was made clear that travel times and specific inductive capacity measured and calculated in the cross sections including the fracture zone were larger than those in the cross sections where there was no fracture zones.

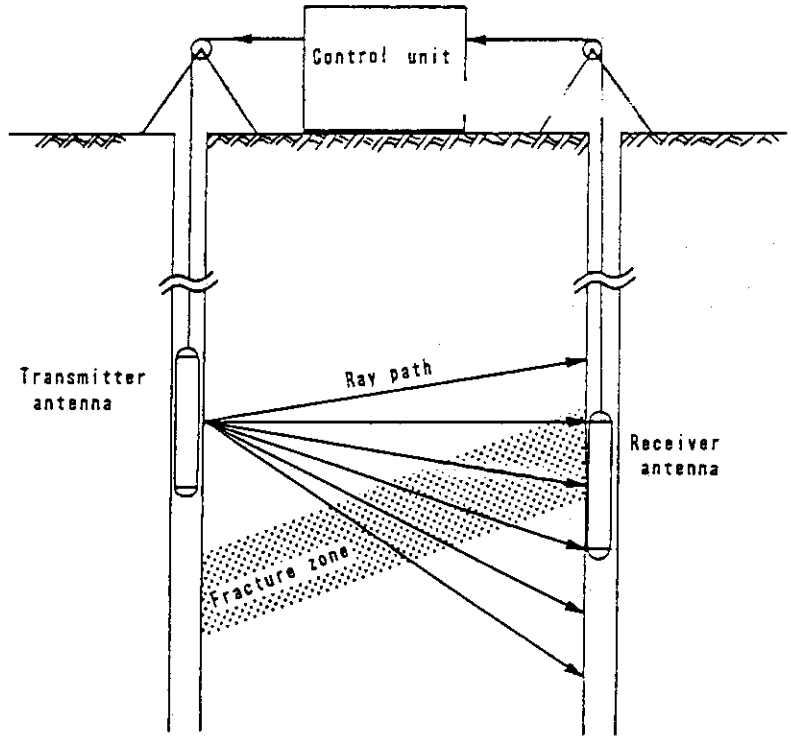

Fig. 1 Schematic diagram of the radar measurement.

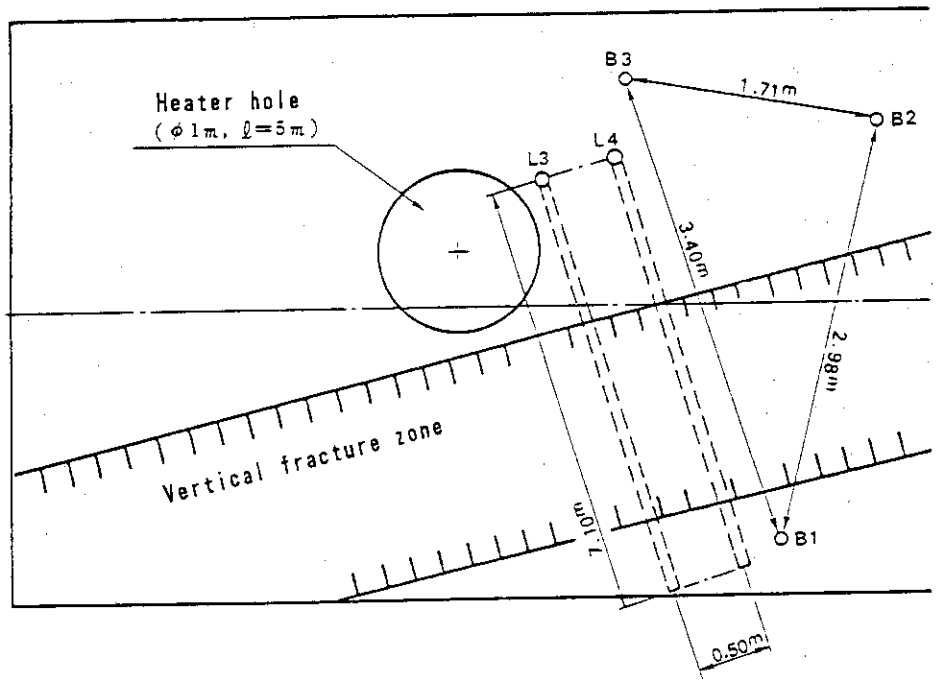

Fig. 2 Locations of boreholes used in the radar measurement.

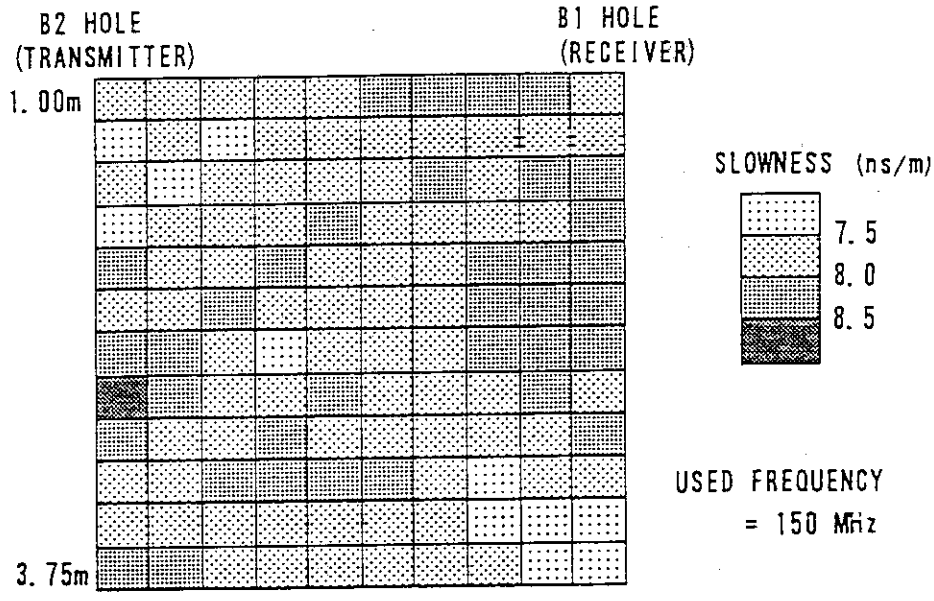

Fig. 3 Calculated result of slowness(1/Vj) for the section B1-B2.

(5) Consideration of Radionuclides Migration Model Based on Field Studies at Chalk River

H. Nakamura

Detailed information of past field program at CRNL about the radionuclides migration from low-level waste disposal area and glass block burial test sites, were transfered to JAERI based on the JAERI-AECL cooperation agreement. JAERI staffs visited CRNL to discuss the data in details. By reviewing the documents transfered to JAERI, the following important suggestions on the modelling of radionuclide migration are obtained:

① The mechanisms to make the leaching rate reduce with time are considered to be formation of insoluble protective surface layer depending on component of waste and/or groundwater rather than saturation of groundwater with glass components.

② As phenomena of adsorption of nuclides on solid phase of geosphere, there are irreversible reaction such as very slow reactions and mineralization rather than reversible reactions. For some nuclides, the irreversible reactions are dominant. Main minerals contributing to the irreversible reactions are iron oxyhydroxide and biotite-vermiculite for almost every nuclides.

③ As main species of radionuclides in solution, Tc, I, Ru and Sr are stable as ions prospected with thermochemical data, that is, Tc, I and Ru are anion and Sr is cation. Strongly adsorbing and easily precipitating nuclides seem to be mostly neutral or anionic chemical forms when they are stable in solution. The chemical species are mainly colloids and organic complexes. Microbiology contributes not only to the oxidation-reduction potential of groundwater, but also to the formation of colloids and organic complexes of easily adsorbing nuclides.

Considering the above suggestions, the migration mechanisms of nuclides in geosphere may be summarized as shown in Fig. 1. Most popular nuclide migration model for safety assessment in geological disposal is based on ion-exchange chromatography. Reversible Kd is used and only one Kd for one nuclide is used in general. The results of field investigations show that contribution of irreversible reactions, and neutral and anionic non-sorbing chemical forms can not be neglected.

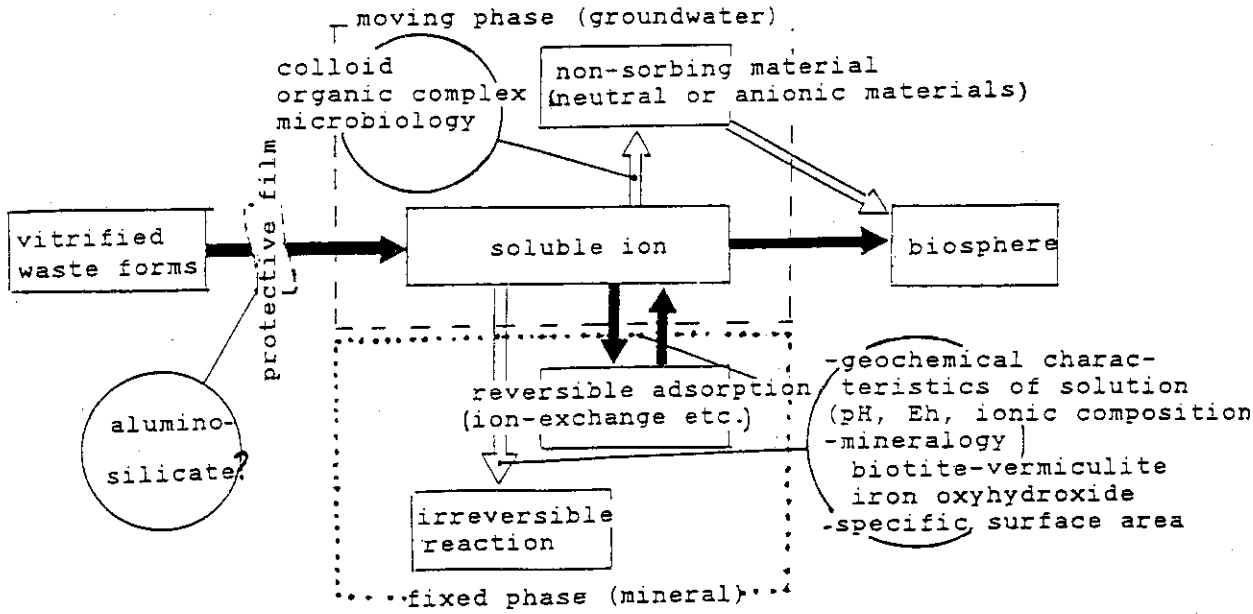

Fig. 1 Factors determming migration of nuclides in the geosphere

2.2 Natural Analogue

S. Nakashima

Application of natural phenomena to the safety evaluation of radioactive waste disposal has many approaches covering various disciplines. Among many aspects of this "natural analogue" study, a) elucidation of mechanisms of trace element migration-fixation processes in geosphere which might also work for waste radionuclides, and b) evaluation of their quantitative aspects in a geological time scale, are of primary importance (1).

Study of chemical forms of microphases in minerals and rocks, which are supposed to play an important role in radionuclide migration-fixation, is now in progress. Infrared microspectroscopy was first applied to minerals in order to study chemical states of water and its spatial distribution in minerals. A hydrated surface layer was detected on a red altered feldspar along paleo-water path, and this is considered to act as a water-rock interface permitting mass transfer.

Weathering degree of a granitic rock has been studied to pick up parameters which can be used to quantify low temperature water-rock interactions. The behavior of iron during weathering was hypothesized and this provides models for simulation experiments aiming the determination of kinetic parameters, such as dissolution and precipitation rate constants.

These studies give information on chemical forms of elements during water-rock interactions in a geological time scale and provide models for reaction paths to simulate long-term behavior of waste radionuclides in rocks.

(1) Infrared microspectroscopy of minerals as a tool for analyzing water-rock interactions

S. Nakashima

Fourier-transform infrared (IR) spectrometer equipped with IR microscope was used to analyze microscopic areas of minerals in the spectral range 4000 - 700 cm^{-1}. Among three methods tested (reflection, transmission-reflection, transmission), transmission spectra of rock thin sections (about 30 μm thick) give clear information on water in minerals (2).

Detailed mapping of 10 μm step on hydrous mineral inclusions in red altered feldspars (Fig. 1 and Fig. 2a) has been carried out in order to

verify the spatial resolution of IR microspectroscopy for water in minerals. Prehnite [$Ca_2(Al,Fe^{3+})_2Si_3O_{10}(OH)_2$] has a sharp OH peak at 3482 cm^{-1}, and its peak height was taken to show a 3-dimentional map as shown in Fig. 2b. This map should show spatial distribution of prehnite in this 120 × 140 μm area. In fact this IR mapping result coincides very well with the spatial distribution of prehnite identified under an optical microscope. The same IR mapping was done for chlorite [$(Mg,Al,Fe)_{12}(Si,Al)_8O_{20}(OH)_{16}$] by taking its OH peak maximum at 3400 cm^{-1} (Fig. 2c). The "L-shape" distribution of chlorite observed on this IR mapping is consistent with the optical distribution of this green mineral. These results suggest that IR micro-mapping by IR microspectroscopy can provide information on spatial distribution of different states of water in minerals in regions as small as 10 μm.

An application of IR microspectroscopy was made on a red altered granitic rock. Feldspars (now albite) are altered into reddish colors along fractures (now filled with prehnite) (Fig. 1 and Fig. 3a). Electron microscopy reveals that the reddish parts of feldspars corresponds to Na-Ca rich portions rather than K-rich ones, and iron minerals of about 0.5 μm are disseminated in Na-Ca rich portions of feldspars. These iron minerals (possibly hematite [Fe_2O_3] and goethite [FeO(OH)]) are considered to be responsible for the reddish color of feldspars.

IR transmission spectra on a thin section of these red feldspars indicate higher peak heights at 3622 cm^{-1} at the mineral surface (about 200 μm from the surface) than inner parts of the mineral (Fig. 3b). This IR peak is considered to be due to molecular water in feldspars and its intensity can be used to calculate water content by using reported molar absorption coefficients (3). The mineral surface is considered to contain about 0.6 wt% of molecular water compared with about 0.3 wt% in the inner parts.

The presence of chemically altered surface layers has long been assumed for leached minerals in the course of water-rock interactions and the diffusion of elements through these layers are assumed to be a rate-determining step of the mineral dissolution (Fig. 4). However, the presence of leached layer enough thick (10 - 100 nm at 25°C) to control the reaction rate has not been verified either by electron microscopy or X-ray photoelectron spectroscopy (XPS) (4). Recently, a resonant nuclear reaction (RNR) has been employed to do hydrogen depth profiling for dissolving minerals and glasses. This technique reveals the presence of surficial hydration layer

of 0.05 - 2 μm thick at around 70°C. The thickness of this layer might be much larger for higher temperatures. Based on this result, migration of molecular water into the surface has been hypothesized to be a key step in the dissolution kinetics (5, 6). However, RNR analysis only reveals the presence of hydrogen in the surface layer and cannot discriminate between hydrogen-containing species (H^+, H_3O^+, H_2O, OH^-). The speciation of hydrogen is possible under IR microspectroscopy as indicated above and so that the present results can be considered to be a first evidence of the presence of molecular water in the hydration laver.

Based on the present results of IR microspectroscopy, the red coloration of the granitic rock along fractures can be explained by the following hypothesis (Fig. 1): (a) diffusion of molecular water into feldspars and the formation of surficial hydration layers; (b) diffusion of iron through the hydrated surface layers of feldspars; (c) iron precipitation as iron hydroxides-oxides in microscopic cracks formed by the dissolution of Ca-rich molecules of feldspars, which are the most soluble portion among the constituents of the studied granitic rock.

These results provide bases to model the reaction paths and the rate-determining steps for the radionuclide migration-fixation during water-rock interactions (Fig. 4).

References

1. NAKASHIMA S. and NAKAMURA H. (1987). Mechnisms and quantitative evaluations of radionuclide fixation in rocks and sediments. In Natural Analogues in Radioactive Waste Disposal. (eds. B.COME and N.A.CHAPMAN), Graham and Trotman, Lancaster.
2. NAKASHIMA S. (1987). Infrared microspectroscopy of minerals: a new microphase characterization technique in earth sciences. NIHONDENSI News, 27, 1-2, 12-17.
3. HORMEISTER A.M. and ROSSMAN G.R. (1985). A model for irradiative coloration of smoky feldspar and the inhibiting influence of water. Phys. Chem. Minerals, 12, 324-332.
4. LASAGA A.C. (1984). Chemical kinetics of water-rock interactions. J. Geophys. Res., 89, B6, 4009-4025.
5. SMETS B.M.J. and LOMMEN T.P.A. (1983). The role of molecular water in the leaching of glass. Phys. Chem. Glasses, 24, 1, 35-36.
6. PETIT J-C., DELLA MEA G., DRAN J-C., SCHOTT J. and BERNER R.A. (1987). Mechanism of diopside dissolution from hydrogen depth profiling. Nature, 325, 6106, 705-707.

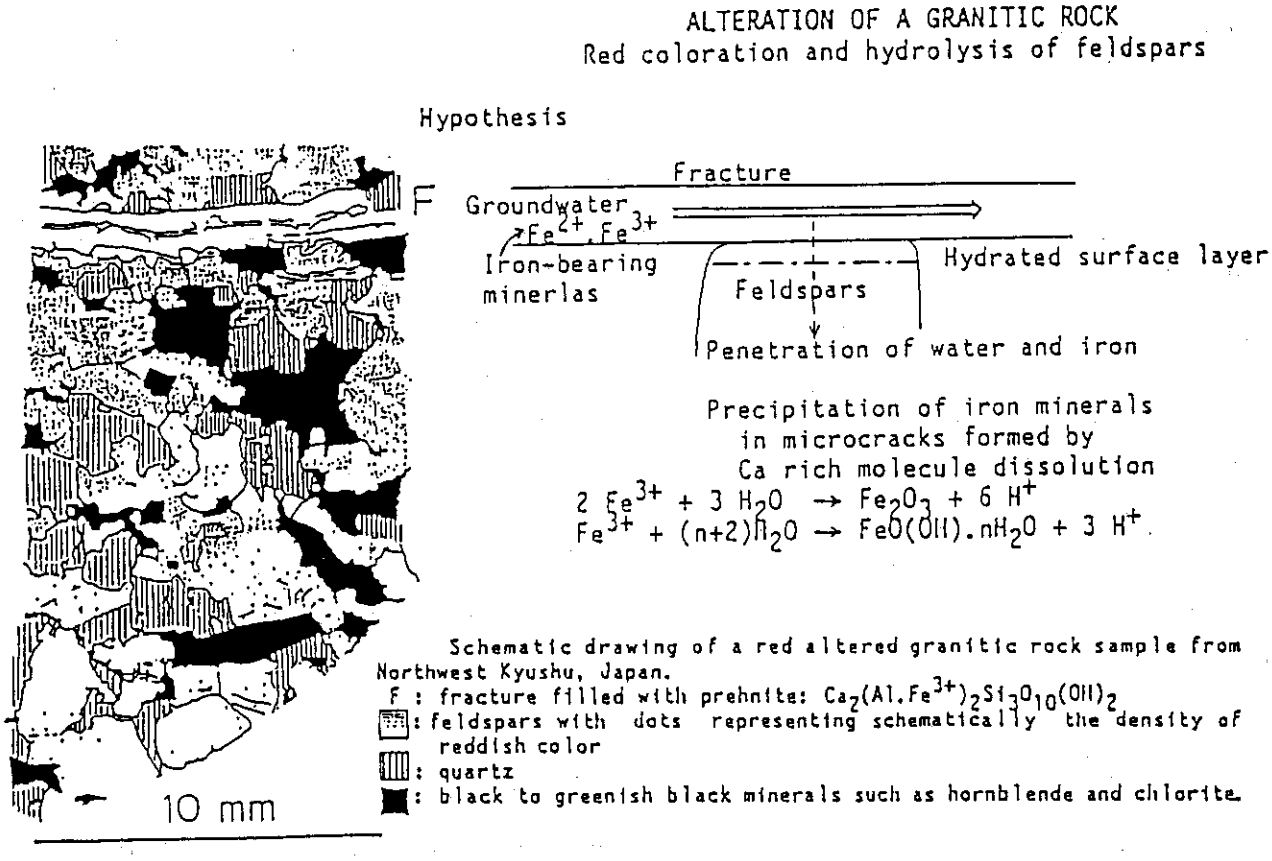

Fig. 1 Alteration of a granitic rock along fractures.

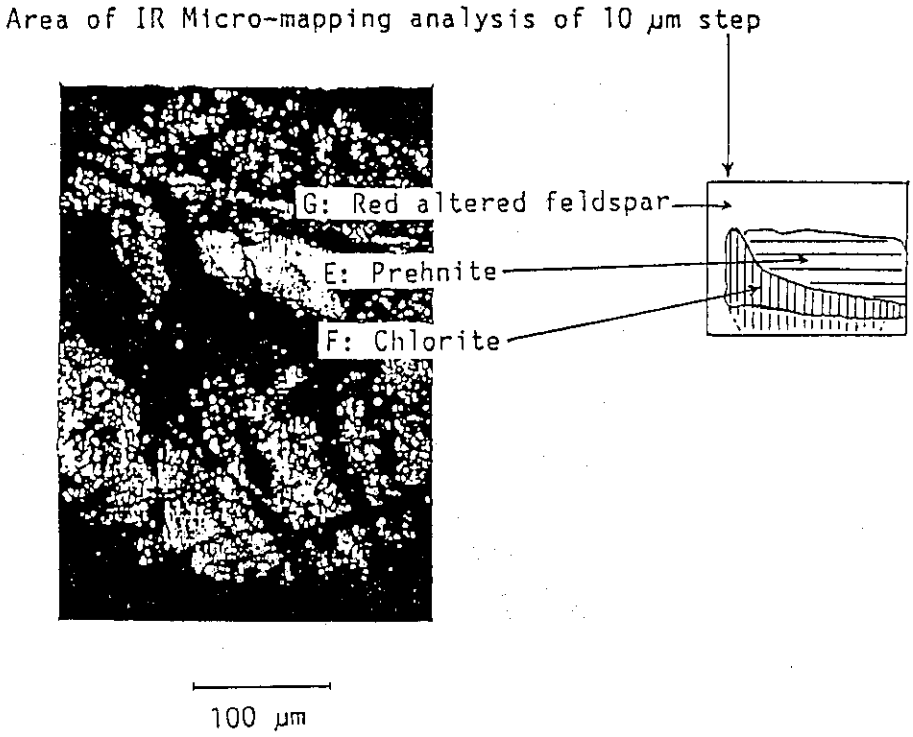

Fig. 2a Optical micrograph of hydrous mineral inclusions in a red altered feldspar.

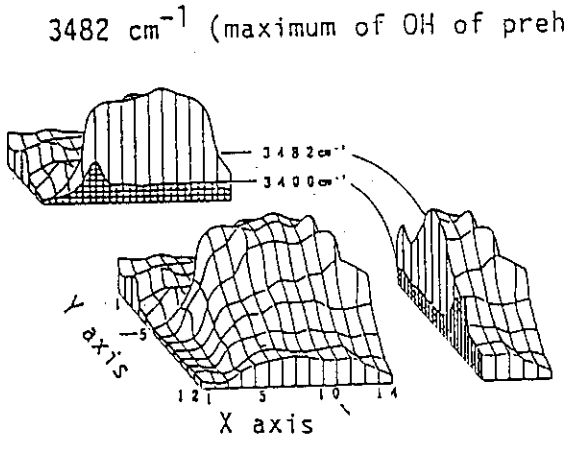

Fig. 2b
IR Peak height map at 3482 cm^{-1} for the hydrous mineral inclusions in a red altered feldspar (Transmission spectra of 10 μm area on a thin section). Contibutions of the peak at 3400 cm^{-1} are also indicated. This map coinsides with the spatial distribution of a prehnite crystal.

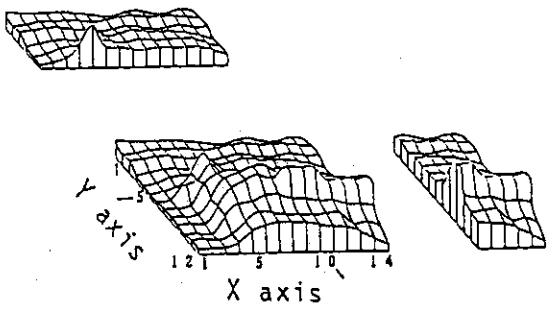

Fig. 2c
IR peak height map at 3400 cm^{-1} for the hydrous mineral inclusions in a red althered feldspar. This map coinsides with the spatial distribution of a chlorite crystal.

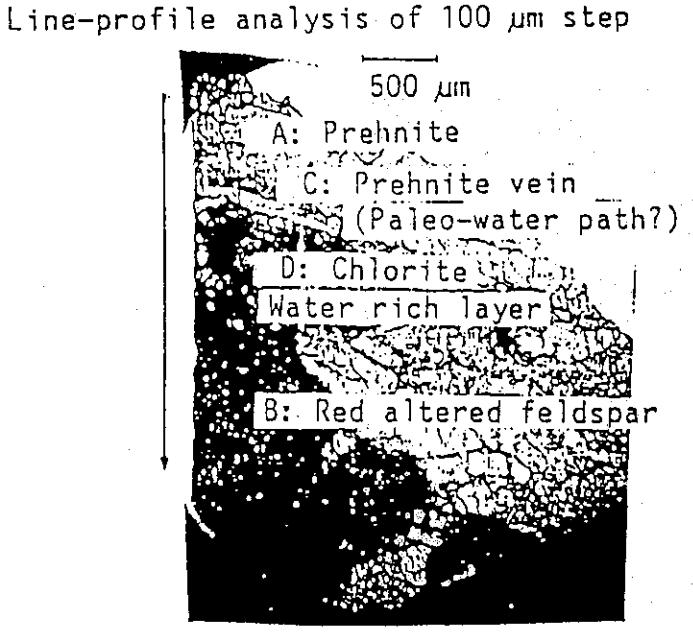

Fig. 3a Optical micrograph of a polished thin section of a red altered granitic rock.

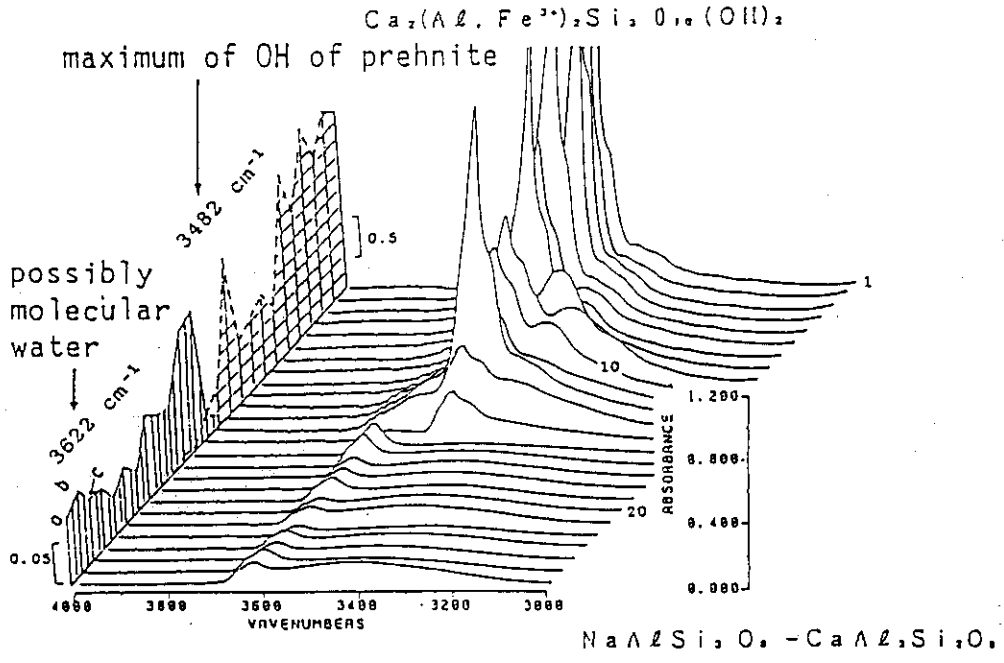

Fig. 3b Spectral results of line-profle analysis on a red altered granitic rock (transmission spectra on a thin section). Peak heights at 3622 cm^{-1} (possibly molecular water) and 3482 cm^{-1} (maximum of OH of prehnite) are projected on the left side.
The surface 200 μm layer of a red feldsdpar grain appears to be enriched in molecular water (tentatively about 0.6 wt%) than the inner part (about 0.3 wt%).

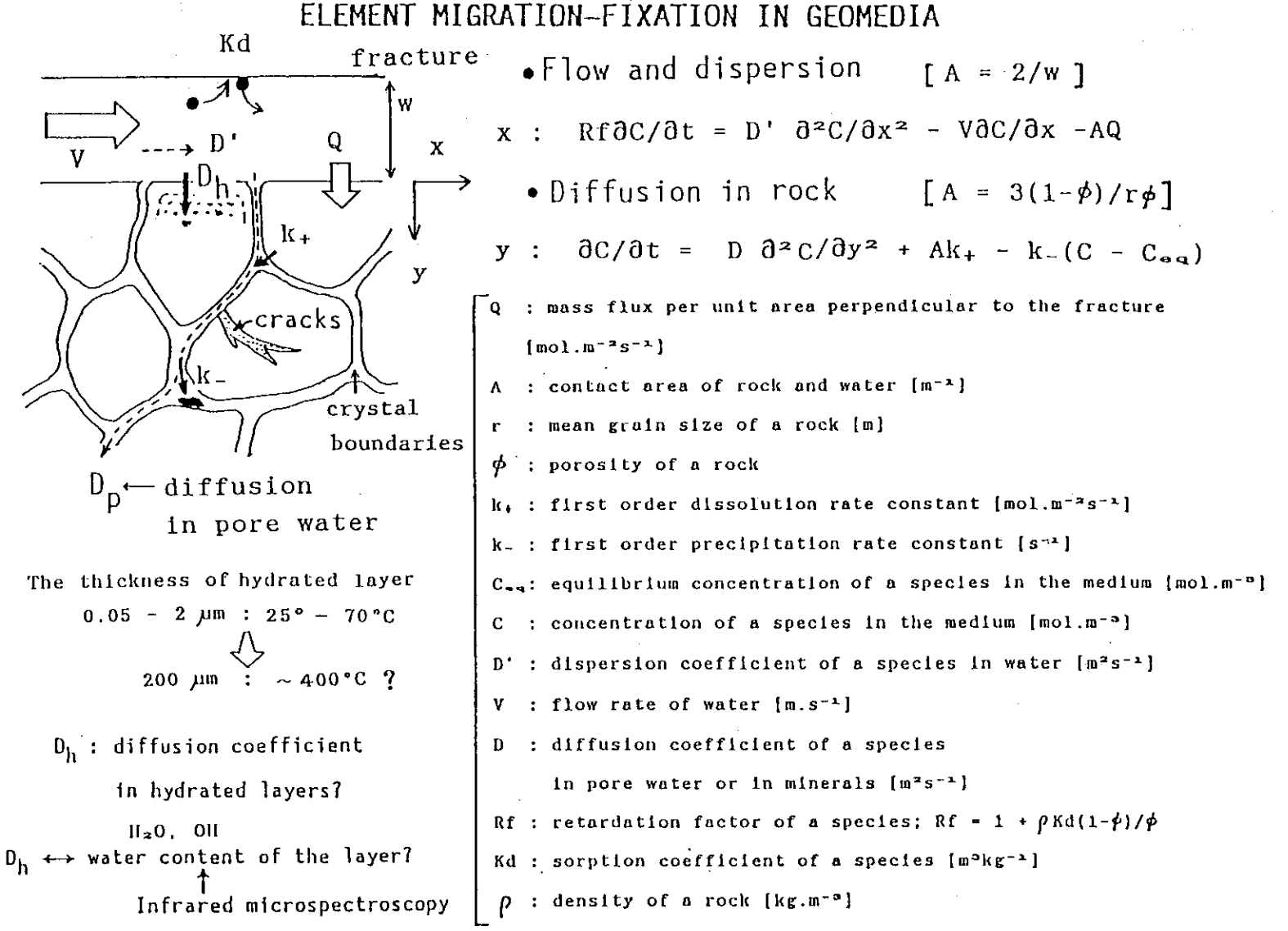

Fig. 4 A schematic model for the element migration-fixation in fractured rocks.

2.3 Safety Assessment

(1) Development safety assessment scenario for geological disposal

H. Nakamura

The first preliminary safety assessment of geological disposal system is planned in 1990 FY at JAERI. Scenario and data for the post-closure assessment have been selected from experimental data of our laboratory and informations from international cooperation programs. The pre-closure assessment has been discussed using informations from experts outside and investigations by contructed construction companies.

When the concept is decided, the scenario of assessment is selected according possible events and phenomena in the concept. Japanese Goverment has not selected any any candidate disposal site and concept of the facilities yet. Before discussing the safety assessment, dominant scenarios adverse the safety must be classified. The discussions are summarized for post- and pre-closure safety assessment.

1) Post-closure

Following critical values of parameters were discussed for classification of the scenario.

① The life of container

Potential hazard of the waste sharply decrease until 1,000 years with decay of ^{90}Sr and ^{137}Cs. During the following 10^6 years, it decrease very slowly. Then it is critical for evaluation of source term whether the life of container is longer than 1,000 years or not. This value becomes almost international consensus.

② Flow rate of groundwater in near field

The flux to geosphere of the radioactivity is divided into three regions as a function of water flow rate, by the leach rate, water access, and diffusion in the water. The respective critical flow rate depend on the disposal system in near field.

③ Flow rate of groundwater in far field

The nuclides migrate with water convection and diffusion in the pore water. The critical flow rate for diffusion dominant region can be calculated by the formula 4D/L approximately, where D is diffusion coefficient and L is distance of migration.

④ Migration time

It is critical whether the activity decays out during the migration or not. ^{90}Sr and ^{137}Cs should be decayed before the container is damaged. The thickness of buffer is possibly designed that diffusion time is enough for decay of these nuclides considering abnormal damage of the container. Even for long-lived nuclides such as ^{99}Tc and ^{237}Np, there is possibility to design the thickness of rock mass for their decay if the flow rate is slow enough for diffusion control region of migration.

A set of scenario was discussed as 1st draft in our group.

Base scenario

a) Contact of groundwater with package
b) Corrosion of overpack and leaching of the glass
c) Leaching of soluble nuclides at the same rate as the hydration rate of glass matrix
   Saturation of groundwater surrounding the glass with low soluble nuclides
d) Diffusion of nuclides in buffer material and rock mass near field
e) Dilution and migration with groundwater flow in fracture zone, diffusion into rock mass near the fracture zone
   Reverible adsorption, irreversible reactions such as precipitation and mineralization
f) Dilution with surface water; groundwater, river and/or sea water
g) Ingestion with drinking water and food
   Inhalation with dust

Other scenario

a) Slow change of water level by tectonic crustal movement (change of water flow rate)
b) Abnormal corrosion of overpack (change of container life)
c) New formation of faults (loss of diffusion dominant rock mass barrier)
d) Failure of shaft sealing (loss of natural barrier)
e) Deposition of nuclides at dicharge point (Reconcentration of radionuclides in biosphere)
f) Erosion of disposal pit at ground surface after long time tectonic movement (loss of all barriers after long period)

2) Pre-closure

The 5 year program of pre-closure safety assessment was started in 1986 FY. Many facilities handling nuclear fuel materials have been inspected by

national authority. The safety assessment methods and standards were almost completed, which will be applied to the disposal facility. However, we have a few experiences for the underground facilities. Accidents specific to the underground facilities have been examined, which include flooding, faults in shaft and fire accident. Flooding accidents were examined assuming several conceputual facilities.

The results were as following;

(i) Countermeasures for reducing damage

① Separation construction time and/or area from emplacement including transportation

② Preperation of reservation area for flooded water and pumping up system

③ Cautious pre-inspection of rock mass for characterization of hydrology

(ii) Results of the assessment

① There is no possibility of radiological contamination outside facility.

② The time is available for workers to evacuate.

It is posible to keep the retrievability.

Concepts of transportation system and ventilation system were designed for next year (1988) program, faults in shaft and fire accident examination.

(2) Model for safety assessment

H. Kimura, R. Yamashita

Numerical model of glass leaching

Computer code LEACH2DF was developed to quantify dissolution of nuclear waste glass. The dissolution model is described by the diffusion in the gel layer and glass matrix taking into account geochemical reactions between the glass-surface and liquid phase. The geochemical calculations are performed with computer code PHREEQE.[1] Boundaries of leachant-gel layer and gel layer-glass are treated with moving boundaries as shown as Fig. 1. The surface reactions of silica which is main component of glass matrix are considered as the representative of glass leaching mechanism. The reaction rate (dissolution flux from waste glass) $r_m(t)$ of H_4SiO_4 is given as follows:[2]

$$r_m(t) = k^+(1-IAP_{SiO_2}/k^*_{SiO_2}) \quad (1)$$

where IAP is the ion activity product of ($= aH_4SiO_2/(aH_2O)^2$ for the reaction $SiO_2 + 2H_2O = H_4SiO_4$), k^+ is rate constant and k^* is solubility product of SiO_2. Supersaturation is indicated by IAP/K > 1, whereas a solution below saturation shows values for IAP/K < 1. The diffusive transport equation is discretized by the Galerkin Finite Element Method and solved using Neumann type specified flux boundary condition (see eq.(1)).

HYDROCOIN study

HYDROCOIN (International project for studying groundwater hydrology modelling strategies) level-3 study deals with uncertainty and sensitivity analysis and compries seven cases. We calculated 3 cases (case 1, 3, 7) of level-3 study using 2D-SEEP and 3D-SEEP code.

In case 7 of level-3 studies, efficiency and accuracy of particle tracking algorythm are examined. As shown in Fig. 2, a single well discharging at a constant rate is located in a uniform flow field. (The well is located at (x,y) = (0,0), and the uniform flow field is given as head gradient is 0.01 in x direction.) The head and the velocity at each nodal point of finite element mesh are determined using the given analytical solution. Pathlines were calculated from the head field (head is given at each nodal point and velocities are calculated by the head gradients) and from the velocity field (velocity is given at each nodal point). Finite

element grids used were coarse grid (40 elements), medium grid (112 elements), and fine grid (364 elements). Error of trajectory, numerically calculated using coarse grid, from analytical trajectory for path no.7 is shown in Fig. 3. It is better to use the velocity field in the particle tracking calculation when the grid is coarse.

References

1) D.L. Parkhurst et al. Water-Resources Investigations 80-96, U.S. Geological Survey, Reston, Virginia, U.S.A. (1980)

2) B. Grambow, Final report Modelling of the corrosion of JSS-A Glass Phase IV of the JSS-Project, Hahn-Meitner-Institute, Berlin (1986)

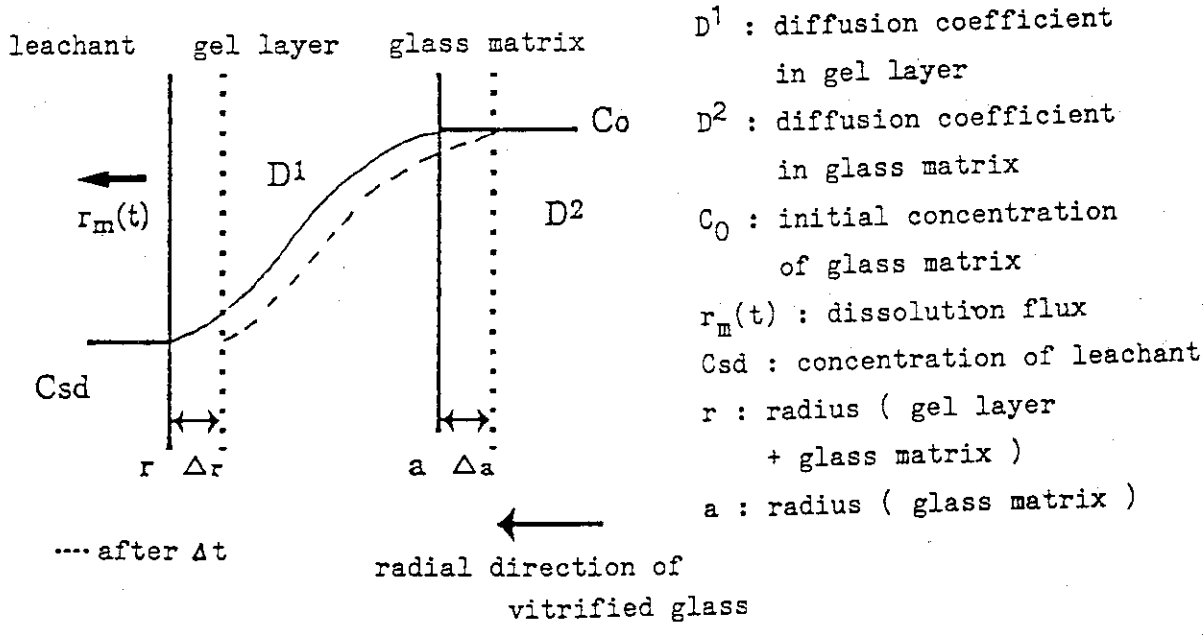

Fig. 1 Model of moving boundaries.

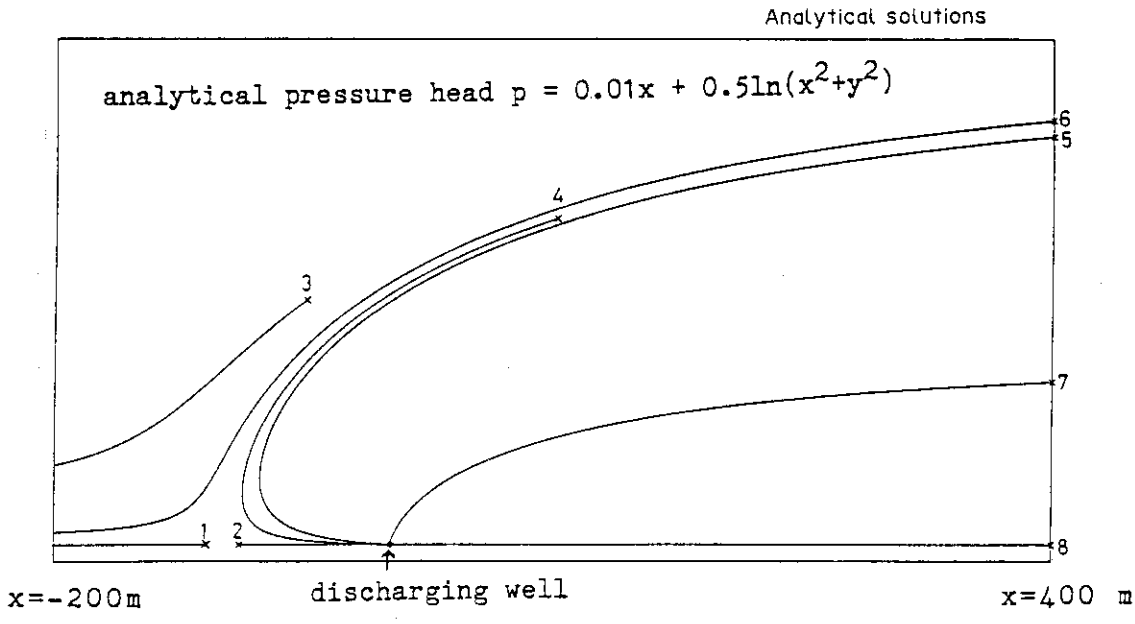

Fig. 2 Trajectories of particles released at eight points.

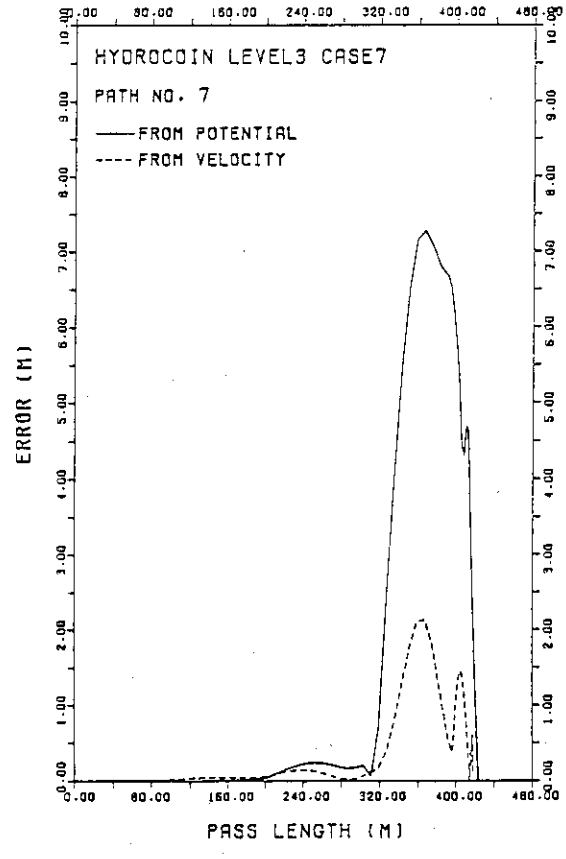

Fig. 3 Error of calculated path line along path No.7.

3. Hot Operation at WASTEF

S. Tashiro

The WASTEF (Waste Safety Testing Facility) has continued studies on the performance and long-term durability of HLW solidified forms and the related materials in storage and disposal conditions.

Actual high-level radioactive liquid waste was transported to WASTEF from the Tokai reprocessing plant of the Power Reactor and Nuclear Fuel Development Corporation and the safety examination using the actual waste was initiated on HLW materials. (Table 1)

Curium-244 doped Synroc was also produced at the hot cell of WASTEF and a accelerated alpha radiation stability test on Synroc started. It will end two years later at the 10^5 years equivalent aging of actual waste. (Table 2)

Besides the above two topics leachability tests using various radionuclides, accelerated alpha radiation stability test under beta and gamma irradiation on glass forms, and various activities supporting the safety examinations have been continued.

Table 1 Vitrified Form Production

Serial Number	Volume	Radionuclides in the Products	The Purpose of Production
H87008	1 ℓ		Preparation of actual waste test
H87009	0.5 ℓ		Preparation of actual waste test
H87010	0.5 ℓ		Preparation of actual waste test
H87012-1	0.25 ℓ	Cs-134, Cs-137 etc. (Total 146Ci)	Solidification test of actual waste
H87012-2	0.44 ℓ	Cs-134, Cs-137 etc. (Total 146Ci)	Solidification test of actual waste

Table 2 Synroc Production

Serial Number	Volume	Radionuclides in the Products	The Purpose of Production
S87001	3.14 mℓ	Cs-137 (2.17 mCi)	Performance test of the apparatus
S87002	3.14 mℓ	Cs-137 (2.17 mCi)	Performance test of the apparatus
S87003	3.14 mℓ	Cs-137 (2.17 mCi)	Performance test of the apparatus
S87004	3.14 mℓ	Cs-137 (2.17 mCi)	Performance test of the apparatus
S87005	3.14 mℓ	Cm-244 (13 Ci)	Alpha-radiation stability test
S87006	3.14 mℓ	Cm-244 (13 Ci)	Alpha-radiation stability test
S87007	3.14 mℓ	Cm-244 (13 Ci)	Alpha-radiation stability test
S87011	3.14 mℓ	Cm-244 (13 Ci)	Alpha-radiation stability test

(1) Transport of actual high-level liquid waste to WASTEF

N. Yamada

An accelerated alpha radiation stability test for the Power Reactor and Nuclear Fuel Development Corporation (PNC) grass smaples was planned with actual liquid waste under a collaboration between the Japan Atomic Energy Institute (JAERI) and the PNC on HLW Management. Prior to the test, the actual liquid waste of about 13 ℓ was transported using an approved packaging from the Reprocessing Plant of PNC to WASTEF of JAERI, on December 24th, 1987.

Details of the transport are summarized in the followings:

1) Packaging Used
   a) Name of Packaging: HLW-79Y-4T
      ("CENDRILLON" called by CEA France)
   b) Identification Mark of Package Design Approved: J/60/B(M) (Rev.1)
   c) Serial Number of Packaging Resistered: S1B60
   d) Outer Dimensions and Its Weight with skids:
      144 cm ϕ × 139 cm H (spherical)
      3,930 kg (nominal 4t)
   e) Drawings: See Fig. 1
2) Specifications of Contents Transported
   a) Content: HLW in solution of nitric acid
   b) Weight and Its Volume: 1.56 kg in liquid (about 13 ℓ containing small amounts of uranium and plutonium)
   c) Radioactivities: 3,736 Ci

      Major nuclides

Sr- 90	591 Ci
Cs-137	692 Ci
Pr-144	154 Ci
Am-241	7.3 Ci

   d) Heat Generation: 14 watt
3) Shipment Procedure Applied
   a) Transport Mode: Land Transport with a Truck of loading capacity 10 t
   b) Criteria of shipment: Exclusive Use (Full Load)
   c) Transport Route: Exclusive Line Constructed only for Nuclear Materials Transports between the Tokai Works of PNC and the Tokai Research Establishment of JAERI.

Under the witness of the Science and Technology Agency (STA) Technical Officials, applicable inspections were carried out to confirm that our

package and its content met the technical requirements provided in the Law.

The following inspection were required for the witness of officials:

a) visual appearance inspection,
b) lifting inspection,
c) weight measurement inspection,
d) surface contamination level inspection,
e) radiation dose rate inspection,
f) temperature measurement inspection,
g) leaktightness inspection,
h) pressure measurement inspection, and
i) radioactive contents inspection.

In above details of visual appearance inspection, fitting conditions of plugs, bolts and other devices were checked carefully in order to reconfirm no problem on leaktightness in transport and on other related functions.

In surface contamination level and radiation dose rate inspections, their results were negligible values in comparison with the background level and were accepted by the officials.

In leaktightness inspection, more times than scheduled were spent to stabilize a helium detector and its indicator before measurement and recording.

Presure measurement inspection required settlement of over 15 hrs. to achieve given pressure in the internal cavity and to reach to thermal equilibrium, therfore, it was necessary to make up the package containing the high-level liquid waste in the previous day of inspecting. And so the preparation of the packge were started the day before the shipment.

And then, additional inspections for the shipment method were also carried out by the Ministry of Transport (MOT) Official. Futher more, the Public Safety Commission of Ibaraki Prefecture superviced the safe transport, and the tranport was arranged with the Local Governments (prefectual and village), based on the Regional Agrement on Safe Operation of Nuclear Facilities between JAERI and the local Governments.

This transport of actual liquid waste included preparation and sending of empty packaging to PNC, loadind of actual liquid waste in the Reprocessing Plant, Shipping from PNC to JAERI and receiving at WASTEF, and therfore, the above mention of sequence was safety and carefully finished without any kind of trouble on December 23th to 24th.

As a result of many efforts of us for the transport the practice gave us many worthy experiences for the future plan.

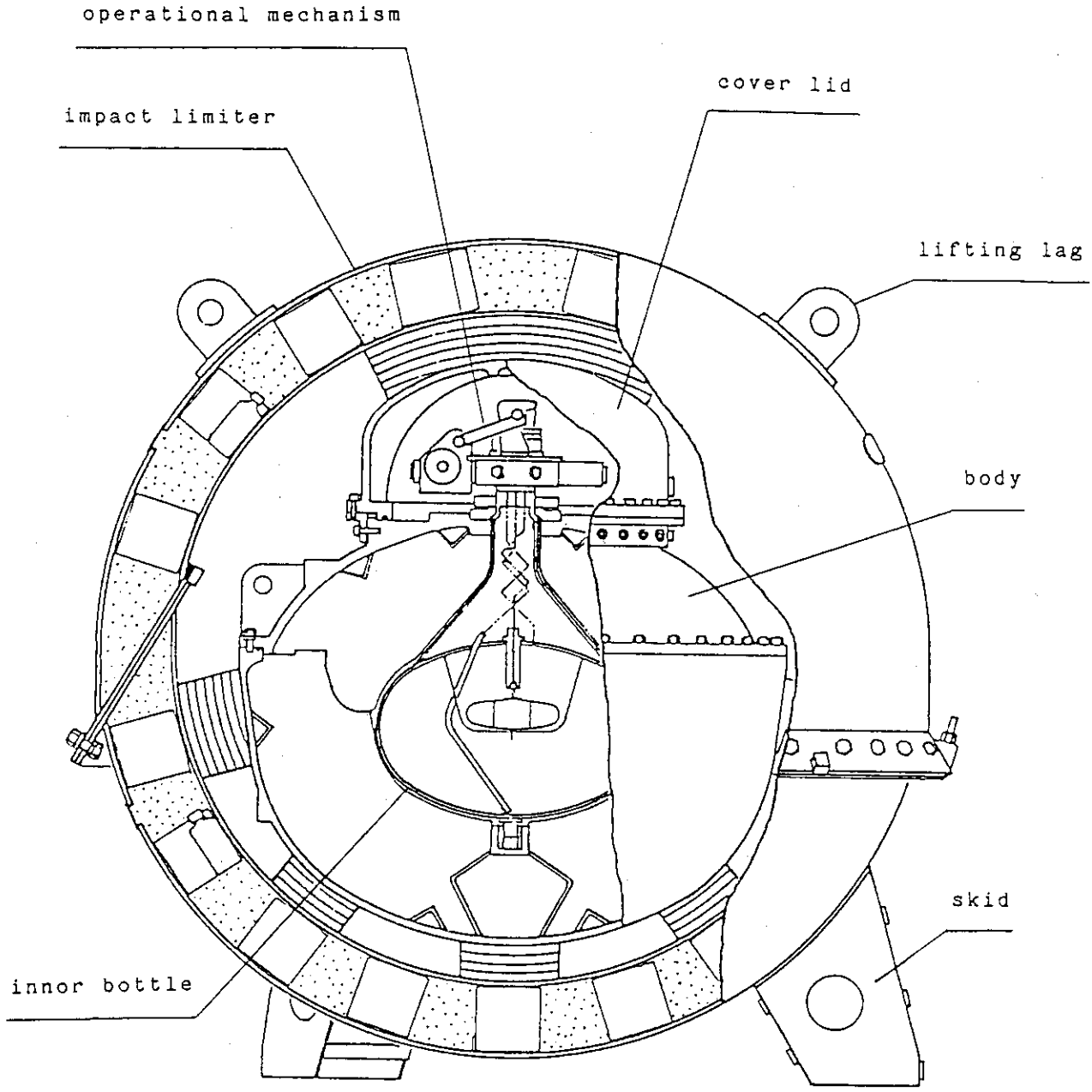

Fig. 1 Cross-section view of HLW-79Y-4T package

(2) Test plan with actual wastes

S. Tashiro

The first vitrification of actual wastes at WASTEF was carried out with one liter (292 Ci) of high radioactive liquid waste from the PNC Reprocessing Plant on Jan. 21, 1988. The full test scheme is given in Fig. 1.

The acidity, radioactivity, concentration of chemical elements and amount of total oxides in the liquid wastes were analyzed prior to the vitrification. The radioactivity of ^{137}Cs, ^{134}Cs, ^{106}Ru, ^{144}Ce, ^{154}Eu and ^{155}Eu was measured with a highpurity germanium (PHGe) coaxial detector, ^{242}Cm, ^{244}Cm and ^{241}Am with a silicon surface barrior detector, ^{241}Am with a HPGe planer type detector (LEPS), and gross alpha with 2 gas flow detector, respectively. The concentration of Na, Ni, Sr and Rh was analyzed with an atomic absorption spectroscopy and Fe, Cr, La, Nd, Zr and Mo with an inductively coupled plasma spectroscopy.

Final confirmation has been made for the performance of the vitrification apparatus by the first two runs of preliminary vitrification although it promises a good result by the production of more than 30 radioactive glass blocks. The products of the preliminary runs are to be used for preliminary tests of volatilization and leachability.

Main product of the actual waste will be crashed into granules and remolten with ^{244}Cm to provide test specimen for an accelerated alpha radiation stability test with actual waste.

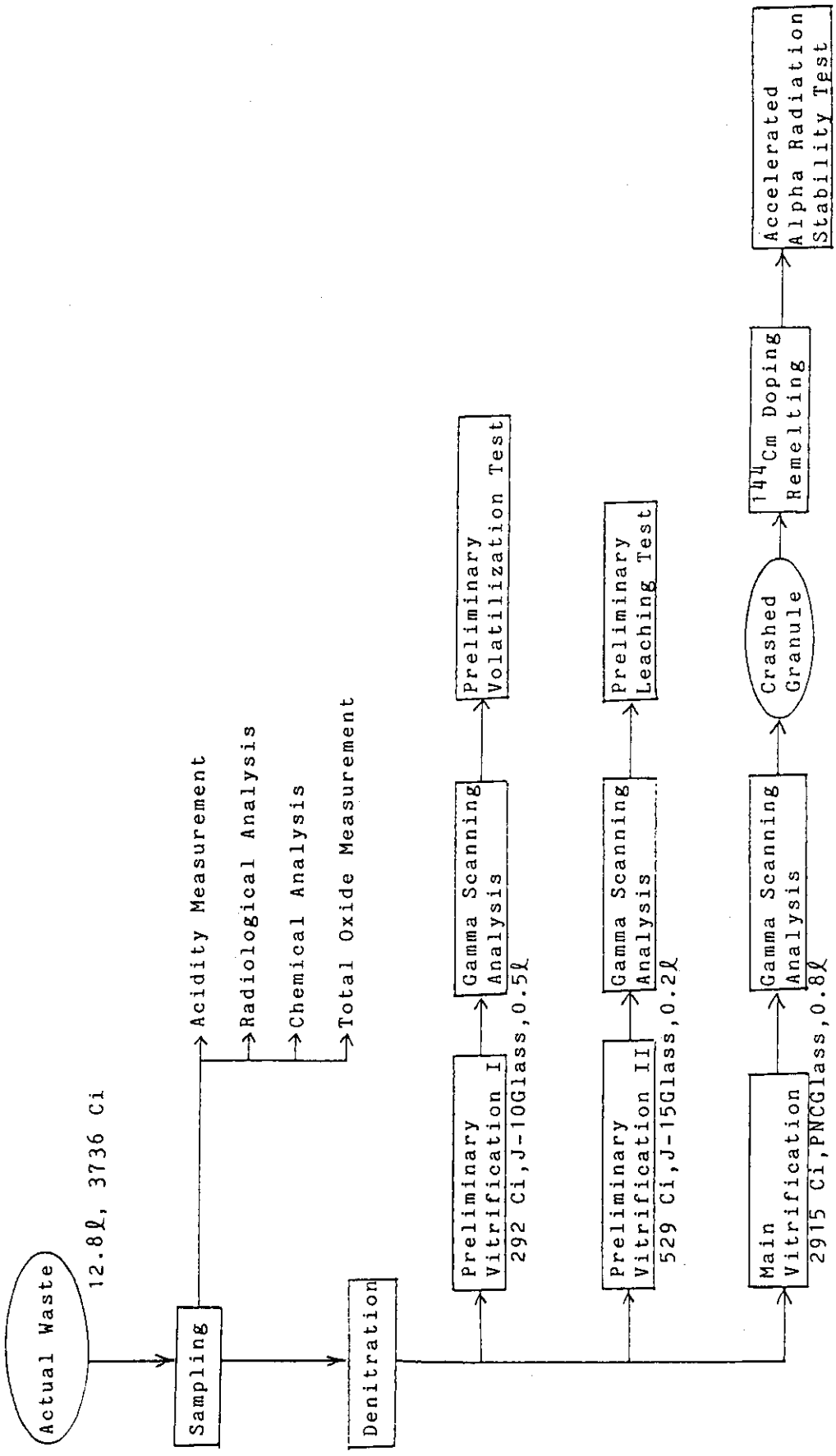

Fig. 1 Test scheme using actual wastes